Scholars' Mine

Doctoral Dissertations

Student Theses and Dissertations

Summer 2019

2X-Thru, 1X-Reflection, and Thru-Line de-embedding: Theory, sensitivity analysis, and error corrections

Bichen Chen

2X-THRU, 1X-REFLECTION, AND THRU-LINE DE-EMBEDDING: THEORY,

SENSITIVITY ANALYSIS, AND ERROR CORRECTIONS

by

BICHEN CHEN

A DISSERTATION

Presented to the Faculty of the Graduate School of the

MISSOURI UNIVERSITY OF SCIENCE AND TECHNOLOGY

In Partial Fulfillment of the Requirements for the Degree

DOCTOR OF PHILOSOPHY

in

ELECTRICAL ENGINEERING

2019

Approved by

Dr. Jun Fan, Advisor
Dr. James L. Drewniak
Dr. Daryl Beetner
Dr. David Pommerenke
Dr. Xiaoning Ye

PUBLICATION DISSERTATION OPTION

This dissertation consists of the following three articles which have been submitted for publication, or will be submitted for publication as follows:

Paper I: Pages 2-48, "2X-Thru De-embedding (2XTD) Technique: Error Analysis, Error Bounds and Error Reduction," are intended for submission to IEEE Transaction on Electromagnetic Compatibility.

Paper II: Pages 49-76, "A Novel Smart Fixture De-embedding (SFD) Method by Using 1X-Reflection Standard," have been accepted by IEEE Transaction on Electromagnetic Compatibility.

Paper III: Pages 77-103, "Thru-Line De-embedding (TLD), an Accurate and Simplified Fixture Removal Method with Self-validating Line Standard and De-embedding Error Quantification Mechanism," have been accepted by IEEE Transaction on Electromagnetic Compatibility.

ABSTRACT

Due to the simplicity of design and measurement, as well as the accuracy of results, the 2X-Thru de-embedding (2XTD), 1X-Reflection de-embedding (1XRD), and Thru-Line de-embedding (TLD) have been replaced the traditional de-embedding algorithms, such as TRL and SOLT. In this dissertation, theory of 2^n-port 2XTD, 1XRD, and TLD are completely derived first. The self-error reduction schemes is introduced to mitigate the de-embedding errors due to non-ideal manufacturing effects of non-zero mode conversion terms, as well as the asymmetric, and manufacturing variations. The validations are performed on both theory and self-error reduction through simulation and measurements cases. The 2X-Thru de-embedding (2XTD) is discussed in details. The prevailing 2X-Thru de-embedding (2XTD) requires much less calibration standards, yet still maintain the high accuracy of de-embedded results. Nevertheless every de-embedding method is based on the rigorous mathematical derivations, the manufacturing variations are inevitable. IEEE P370 committee provided the manufactured test coupons with golden standard to test the accuracy of different de-embedding methods when considering the manufacturing variations. Such manufacturing variations are propagated to the de-embedded results through the sensitivity of the test fixtures. The error reductions scheme in this section mitigates the de-embedded errors by correcting some of the manufacturing variations in the algorithm. This section will focus on the three kinds of manufacturing variations: 1) test fixture asymmetry; 2) the perturbations of the test fixtures in the calibration structure of 2X-Thru and de-embedding structure of Total; 3) the mode conversion terms due to the manufacturing variations.

ACKNOWLEDGMENTS

I would like to express my sincere gratitude to Dr. Jun Fan, my advisor, for accepting me into his group and for his teaching, instruction, warm encouragement on my research work, financial support to my study and direction for this thesis during my pursuit of the PhD degree.

I would like to thank Dr. James Drewniak for the encouragement on my study, helpful suggestions on my thesis and enlightening the way to the future.

I would like to thank Dr. Daryl Beetner for teaching in my courses, discussions related to my research and helpful suggestions during my PhD degree.

I would like to thank Dr. David Pommerenke for his enlightening to my research motion and teaching me great skills in doing research.

I would like to thank Dr. Xiaoning Ye for his insightful comments during the PhD degree.

I would also like to express my thanks to all the other faculty members and students in UMR/MST EMC lab for their team work and help in my research and coursework. It has been my great pleasure to work with you.

Finally, I would like to thank my family for their love, specifically my wife Lu and our little boy Ian for their unconditional support during my six years of graduate study.

TABLE OF CONTENTS

LIST OF ILLUSTRATIONS

PAPER III

LIST OF TABLES

SECTION

1. INTRODUCTION

De-embedding methods are fully derived and analyzed, to remove the fixture effects of the test coupons. A novel de-embedding methodology only using 1X-Reflection (1XRD) is adopted in the smart fixture de-embedding (SFD) tool. In the commercially available de-embedding methods, test fixtures are usually designed as reciprocal and passive to reduce the complexity of measurements and calculations. With such assumptions on the test fixtures, the proposed 1XRD SFD only requires one port measurement to perform the de-embedding. Compared with the classic TRL and SOLT, the 1XRD in this paper reduces the quantity of measurements drastically yet maintains the accuracy of results. With proper design, the 1X-Reflection SFD may overcome the typical inevitable errors in the TRL, SOLT, and 2XTD methods, such as fixture manufacturing variations.

Another de-embedding algorithm and procedure (TLD) that requires a zero-length thru and a non-zero length line is proposed. The TLD method is shown to have excellent correlation results to existing de-embedding algorithms, while having the advantages of being less complex in design (compared to TRL) and in algorithms (compared to 2XTD). It also provides a self-validating procedure to reveal the valid bandwidth of test fixtures and de-embedded results. In addition, the errors of test fixtures can be calculated, and error bounds can be applied to de-embedded results.

PAPER

I. 2X-THRU DE-EMBEDDING: THEORY, VALIDATION, AND ERROR CORRECTIONS

B.Chen

Department of Electrical Engineering

Missouri University of Science and Technology

Rolla, Missouri 65409–0050

Tel: 347–856–7895

Email: bcpr8@mst.edu

ABSTRACT

Accurate characterization of multi-port channels provides accurate electrical performance of high-speed parallel and serial links. The conventional numerical modeling and simulations only estimate the electrical behaviors, while the measurement truly quantify the electrical performance of the DUT. Due to design limitations, it commonly requires test fixtures to be inserted between the DUT and interface ports of measurement equipment. The discontinuities introduced by test fixtures are usually an unavoidable challenge for engineers. The fixture characterization procedure is the key step to achieve the accurate characterization of the test fixtures. Using the known electrical characterization of such text fixtures, de-embedding is able to rigorously remove the effects of these test fixtures, exposing the true performance of the device under test (DUT).

Keywords: De-embedding, 2X-Thru De-embedding, test fixtures, manufacturing variations, error reduction.

1. INTRODUCTION

Modeling equivalent lumped circuit [1]-[3] or equivalent networks [4]-[6] are two research mainstreams in de-embedding topic and recent output state-of-the-art results are dedicated to removing test fixtures by using both. Copious investigations of modeling equivalent lumped circuit are devoted in the application of on-wafer measurements, despite calibrations may performed, lumped fixtures into equivalent circuit are merely suitable for dedicate design and fabrication that deplete expensive wafer.

As the data rate increasing exponentially, to dislodge electrical large fixtures is ineluctable fashion in the de-embedding topic. The mathematical essential of electrical large fixture de-embedding is either through the ABCD matrix or T matrix. The ABCD or T matrix of DUT is calculated by the inverses of ABCD or T matrix of test fixtures multiply the ABCD or T matrix of the Total (Fixture + DUT + Fixture). Commercially available calibration and de-embedding techniques, such as the classic Thru-Reflect-Line (TRL), Load-Reflect-Match (LRM), Line-Reflect-Line (LRL), Thru-Reflect-Match (TRM) [7], and Short-Open-Load-Thru (SOLT) [8], as well as the novel 2XTD [9]-[12] related articles, are widely used in characterizing the electrical performance of DUT. TRL calibration is performed by using the zero length Thru, Reflect (short, or open), and Line standards, while LRM, LRL, and TRM are all derivatives of the TRL procedure. There are certain restrictions in the TRL calibration family, which include: 1) the characteristic impedance and propagation constant of the Thru and Line standards are required to be identical; 2)

broad-frequency coverage requires multiple Line standards; 3) the interconnects in the Thru, Reflect, and Line standards are assumed to be identical. The 2XTD dramatically reduces the complexity of fixture de-embedding by only using a symmetric designed zero length Thru standard, yet still maintains the accuracy of the de-embedded results.

Bockelman and Einsenstadt first elaborated mixed-mode S-Parameter (MMS) concept [13] in the year of 1995. And in 1997, they introduced a method to convert classical single-ended incident and reflection wave [14] to differential mode, common mode and mode conversions. Andrea Ferrero and Marco Pirola generalized mixed-mode s-parameters in [15]. Afterwards, plentiful of manuscripts have been applying mixed-mode concept in characterization and measurement for cascading networks of differential interconnections [16-18]. In the 4-port 2XTD, the mixed mode concept is adopted. Despite the mathematical expression of final de-embedding procedure is using the traditional single-ended representation, the fixture characterization procedure is performed on differential and common modes, respectively. The modal-based 2XTD requires balance designed test fixtures, that the differential and common modes are orthogonal to each other. For 2^n-port (n>2, and n is integer) S-parameters, not only are there modal conversions, but there are also near-end (NEXT) and far-end (FEXT) crosstalk terms in both the differential and common modes. Unlike the modal conversion, the FEXT and NEXT of the channel are very important in signal integrity performance quantification [19]-[20]. The high order mixed mode concept is proposed in this paper to include the NEXT and FEXT in the fixture characterization and de-embedding. Ideally, mode conversion terms are zero in a balance designed test fixture, but in reality, manufacturing variations causes these terms to be non-zero. Other manufacturing variations in the 2XTD are: 1) asymmetric of the zero length

Thru; 2) differences of fixtures in the zero length Thru and the fixtures in the Total. The 2XTD present in this paper is one of the accurate de-embedding methods in the de-embedding family, as all the three de-embedding errors due to the manufacturing variations are tackled. Such self-error reduction scheme is also suitable for the SOLT and TRL whenever there is manufacturing variations.

2. THEORY AND DERIVATION OF 2XTD

2.1. 2-PORT SINGLE-ENDED FIXTURE CHARACTERIZATION

The 2XTD was originally designed for the single-ended 2-port de-embedding applications. The 2XTD takes a symmetric designed zero length Thru, depicted in the Figure 1 (a) as the calibration standard. In addition to the symmetry, such calibration structure is inserted with a segment of transmission line to provide the gating point of the time domain manipulations. The gating point is the physical middle point of the 2X-Thru calibration standard, which divides the 2X-Thru into two identical 1X fixtures. Figure 1 (b) is the Total structure that the DUT is embedded into those two identical 1X fixtures.

(a)   (b)
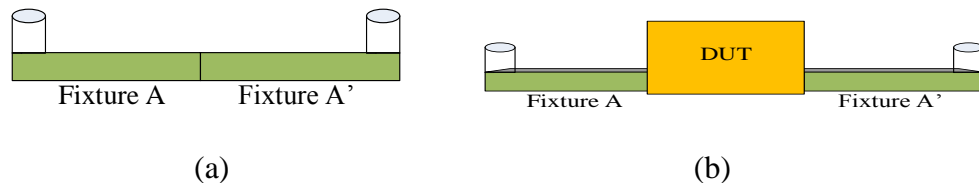
Figure 1. The topology of 2XTD: (a) 2X-Thru; (b) Total.

The fixture characterization in the 2XTD is the procedure to split the two 1X fixtures in the gating point. The de-embedding is to remove the characterized fixtures from the DUT. Because of symmetry, the fixture characterization is based on the classic 3-term error model, derived in [21]. In the 3-term error model (Figure 2), the e00 is the 'Directivity', the e11 is the 'Port Match', and the (e10e01) is the 'Tracking'. The a0, b0 and a1,b1 are incident and reflect wave at port 1 and port 2. Solving this 3-term error problem is to find linear relationship between the actual and measured reflection coefficients.
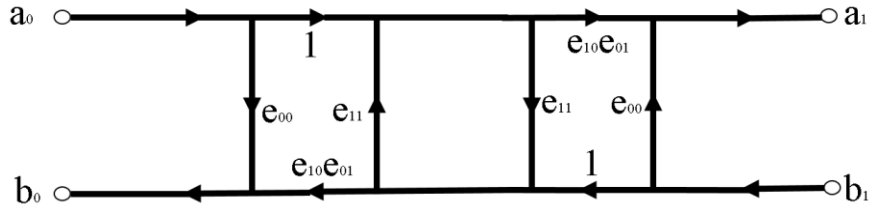
Figure 2. Signal flow chart of the 2X-Thru calibration standard.

The classic SOL method solve the three unknown errors by measuring three known independent standards, such as 'Short', 'Open', 'Load'. The measured and actual reflection coefficients are related as:

$$\Gamma_M = \frac{b_0}{a_0} = \frac{e_{00} - \Delta_e \Gamma_A}{1 - e_{11} \Gamma_A}$$

(1)

Where

$$\Delta_e = e_{00} e_{11} - (e_{10} e_{01})$$

Because the 2X-Thru calibration standard is symmetrically designed, the relationship between the 1X fixture and 2X-Thru fixture are described in (2) and (3). (2) and (3) also demonstrate the relationship between classic SOL and fixture characterization in the 2XTD:

$$S_{11}^{2X} + S_{21}^{2X} = e_{oo} + \frac{e_{10}e_{01}}{1-e_{11}} = S_{11}^{1X-Fixture} + \frac{S_{12}^{1X-Fixture} \times S_{21}^{1X-Fixture}}{1-S_{22}^{1X-Fixture}} = Open \tag{2}$$

$$S_{11}^{2X} - S_{21}^{2X} = e_{oo} + \frac{e_{10}e_{01}}{-1-e_{11}} = S_{11}^{1X-Fixture} + \frac{S_{12}^{1X-Fixture} \times S_{21}^{1X-Fixture}}{-1-S_{22}^{1X-Fixture}} = Short \tag{3}$$

The 'Load' of fixture characterization in 2XTD is calculated through the time domain waveform gating. The measured S_{11}^{2X} is convert to the TDR first, and followed by the time domain signal gating. The gated time domain signal is transferred back to the S-parameters, and performed re-normalization from transmission line characteristic impedance to the system characteristic impedance. An example on TDR of S_{11}^{2X} is depicted in the Figure 3 (a), and Figure 3 (b) is the gated time domain signal with the constant extrapolation after the gating point. Such time domain signal is required to be transferred back to the S-parameter, with re-normalization. The de-embedding procedure is by using transfer scattering parameters (T-parameters), the T network of the DUT is calculated as follows:

$$\left[T_{DUT}\right] = \left[T_{Fixture-A}\right]^{-1} \times \left[T_{Total}\right] \times \left[T_{Fixture-A'}\right]^{-1} \tag{4}$$

The transformation of S-parameters to T-parameters for a 4-port network is derived in [21], and The design criteria of 2XTD is well documented in [10].

(a)

(b)
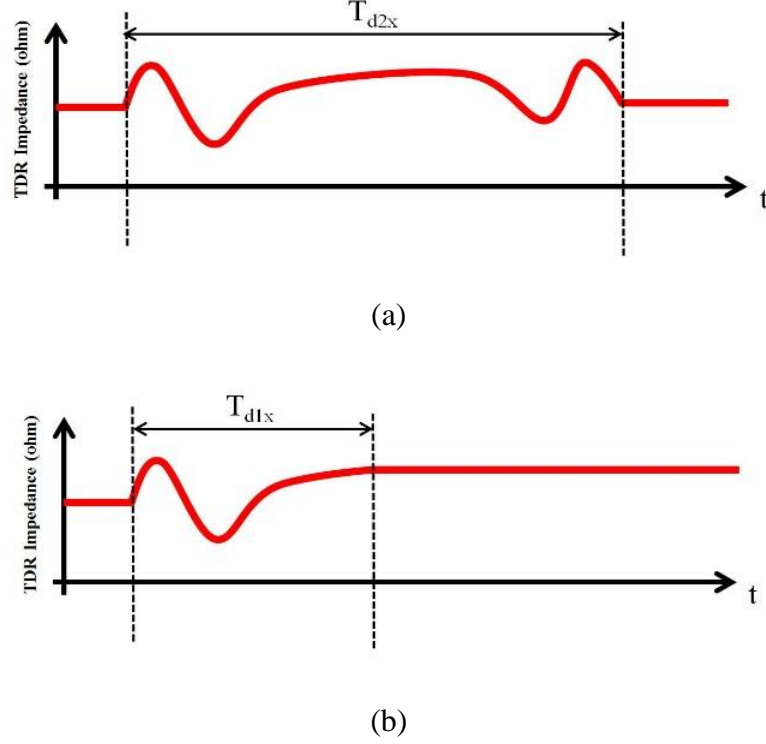
Figure 3. An example of TDR.

2.2. DESIGN REQUIREMENTS OF 2N-PORT 2XTD

The 4-port 2XTD is derived from 2-port 2XTD by using modal-based S-parameters. Beyond the requirement of symmetric design of 2X-Thru calibration standard, 4-port 2XTD also requires the balance designed fixtures. The single-ended S-parameters matrix of 4-port defined in (5) is transferred to the mixed-mode S-parameters matrix through (6):

$$\begin{bmatrix} b_1 \\ b_2 \\ b_3 \\ b_4 \end{bmatrix} = \begin{bmatrix} S_{11} & S_{12} & S_{13} & S_{14} \\ S_{21} & S_{22} & S_{23} & S_{24} \\ S_{31} & S_{32} & S_{33} & S_{34} \\ S_{41} & S_{42} & S_{43} & S_{44} \end{bmatrix} \times \begin{bmatrix} a_1 \\ a_2 \\ a_3 \\ a_4 \end{bmatrix}$$

(5)

$$\left[S_{mixed} \right] = [M] \times \left[S_{Single-ended} \right] \times [M]^{-1}$$

(6)

where

$$M = \frac{1}{\sqrt{2}} \begin{bmatrix} 1 & -1 & 0 & 0 \\ 0 & 0 & 1 & -1 \\ 1 & 1 & 0 & 0 \\ 0 & 0 & 1 & 1 \end{bmatrix}$$

(7)

The 'a' and 'b' in (5), with subscript notations, represent the incident and reflected waves at each port. Equation (8) is the mixed mode S-parameters representation of a 4-port network. The diagonal submatrices are the differential and common modes, while the off-diagonals are the mode conversion terms. Because of orthogonality in a balanced 4-port network design, modal-based fixture characterization in the 2XTD neglects the mode conversions and characterizes the differential and common modes separately, in the same fashion as 2-port 2XTD. After fixture characterization, 4-port single-ended 1X fixture will be acquired by using the reverse of Eq. (6). Eventually, the de-embedding is performed on the 4-port, by using Eq. (4). As a conclusion, the 4-port 2XTD requires the balanced design only in the fixtures, while the DUT could be an arbitrary 4-port network.

$$\begin{bmatrix} b_{d1} \\ b_{d2} \\ b_{c1} \\ b_{c2} \end{bmatrix} = \begin{bmatrix} S_{d1d1} & S_{d1d2} & 0 & 0 \\ S_{d2d1} & S_{d2d2} & 0 & 0 \\ 0 & 0 & S_{c1c1} & S_{c1c2} \\ 0 & 0 & S_{c2c1} & S_{c2c2} \end{bmatrix} \times \begin{bmatrix} a_{d1} \\ a_{d2} \\ a_{c1} \\ a_{c2} \end{bmatrix}$$

(8)

The 2^n-port single-ended network is defined in (9), with the first order mixed-mode given in (10), and the transfer matrix M given in (11).

$$\begin{bmatrix} b_1 \\ b_2 \\ . \\ . \\ b_{2^n-1} \\ b_{2^n} \end{bmatrix} = \begin{bmatrix} S_{11} & S_{12} & ... & S_{(1)(2^n-1)} & S_{(1)(2^n)} \\ S_{21} & S_{22} & ... & S_{(2)(2^n-1)} & S_{(2)(2^n)} \\ ... & ... & ... & ... & ... \\ S_{(2^n-1)(1)} & S_{(2^n-1)(2)} & ... & S_{(2^n-1)(2^n-1)} & S_{(2^n-1)(2^n)} \\ S_{(2^n)(1)} & S_{(2^n)(2)} & ... & S_{(2^n)(2^n-1)} & S_{(2^n)(2^n)} \end{bmatrix} \times \begin{bmatrix} a_1 \\ a_2 \\ . \\ . \\ a_{2^n-1} \\ a_{2^n} \end{bmatrix}$$

(9)

$$\begin{bmatrix} b_{d1} \\ . \\ b_{d(2^n-1)} \\ b_{d(2^n)} \\ b_{c1} \\ . \\ b_{c(2^n-1)} \\ b_{c(2^n)} \end{bmatrix} = \begin{bmatrix} S_{dd11} & \cdots & S_{dd(1)(2^n-1)} & S_{dd(1)(2^n)} & S_{dc11} & \cdots & S_{dc(1)(2^n-1)} & S_{dc(1)(2^n)} \\ \cdots & \cdots & \cdots & \cdots & \cdots & \cdots & \cdots & \cdots \\ S_{dd(2^n-1)(1)} & \cdots & S_{dd(2^n-1)(2^n-1)} & S_{dd(2^n-1)(2^n)} & S_{dc(2^n-1)(1)} & \cdots & S_{dc(2^n-1)(2^n-1)} & S_{dc(2^n-1)(2^n)} \\ S_{dd(2^n)(1)} & \cdots & S_{dd(2^n)(2^n-1)} & S_{dd(2^n)(2^n)} & S_{dc(2^n)(1)} & \cdots & S_{dc(2^n)(2^n-1)} & S_{dc(2^n)(2^n)} \\ S_{cd11} & \cdots & S_{cd(1)(2^n-1)} & S_{cd(1)(2^n)} & S_{cc11} & \cdots & S_{cc(1)(2^n-1)} & S_{cc(1)(2^n)} \\ \cdots & \cdots & \cdots & \cdots & \cdots & \cdots & \cdots & \cdots \\ S_{cd(2^n-1)(1)} & \cdots & S_{cd(2^n-1)(2^n-1)} & S_{cd(2^n-1)(2^n)} & S_{cc(2^n-1)(1)} & \cdots & S_{cc(2^n-1)(2^n-1)} & S_{cc(2^n-1)(2^n)} \\ S_{cd(2^n)(1)} & \cdots & S_{cd(2^n)(2^n-1)} & S_{cd(2^n)(2^n)} & S_{cc(2^n)(1)} & \cdots & S_{cc(2^n)(2^n-1)} & S_{cc(2^n)(2^n)} \end{bmatrix} \times \begin{bmatrix} a_{d1} \\ . \\ a_{d(2^n-1)} \\ a_{d(2^n)} \\ a_{c1} \\ . \\ a_{c(2^n-1)} \\ a_{c(2^n)} \end{bmatrix}$$

(10)

$$M = \frac{1}{\sqrt{2}} \begin{bmatrix} 1 & -1 & 0 & 0 & \cdots & \cdots & 0 & 0 \\ 0 & 0 & 1 & -1 & \cdots & \cdots & 0 & 0 \\ \cdots & \cdots & \cdots & \cdots & \cdots & \cdots & \cdots & \cdots \\ 0 & 0 & 0 & 0 & \cdots & \cdots & 1 & -1 \\ 1 & 1 & 0 & 0 & \cdots & \cdots & 0 & 0 \\ 0 & 0 & 1 & 1 & \cdots & \cdots & 0 & 0 \\ \cdots & \cdots & \cdots & \cdots & \cdots & \cdots & \cdots & \cdots \\ 0 & 0 & 0 & 0 & \cdots & \cdots & 1 & 1 \end{bmatrix}$$

(11)

The M is a $2^n \times 2^n$ matrix, in which the diagonal of above half 1 and -1, and the diagonal of below half are 1 and 1. An equation similar to Eq. (6) is used to transfer the 2n-port single-ended S-parameters matrix to the mixed-mode S-parameters matrix. However, the crosstalk terms in the differential and common modes of the first order 2n-port mixed-mode S-parameters matrix are not solvable in the fixture characterization procedure of the single-ended 2XTD as presented in the section A, because of the additional unknowns. Figure 4 (a) shows an example of 2^3-port 2X-Thru calibration standard in the mixed-mode representation. The differential and common mode submatrices in the 2^3-port mixed-mode S-parameters are analogous to the 2^2-port single-ended S-parameters, in which the FEXT and NEXT terms are not solvable in the single-ended 2XTD.

(a)

(b)
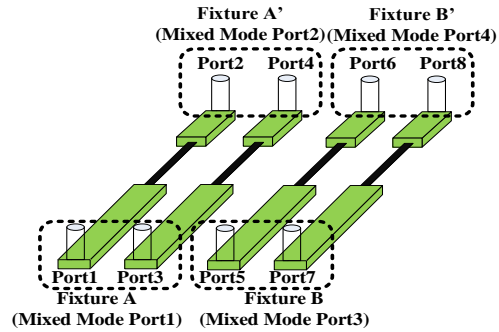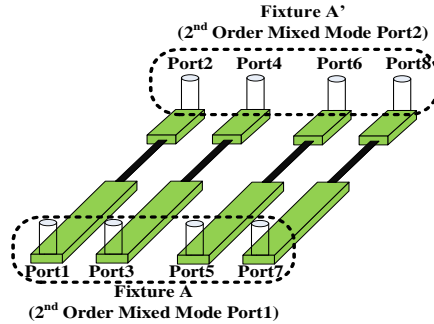
Figure 4. An example of 2X-Thru calibration standard of a 2^3-port network: (a) 1st order mixed-mode; (b) 2nd order mixed-mode.

In such 2^3-port example, by performing a procedure using Eq. (6) on differential mode and common mode S-parameters matrices from 1st mixed-mode separately, the 2nd order mixed-mode S-parameters matrix is acquired. The transfer matrix used on the differential and common modes is the same as the 'M' in the 22-port single-ended to mixed-mode transformation. The 2nd order mixed-mode 8-port S-parameters matrix is written in (12). Extend the same idea on the 2n-port network, n-1 times of transformation is required before applying the 2-port fixture characterization on 2(n-1) pairs of diagonal sub-matrices.

Rigorously, the (n-1) order transformation is only valid when the mode conversion terms in the (n-2) order mixed-mode are 0. The non-ideal mode conversion terms in the fixtures and corresponding treatment will be discussed in the next chapter.

$$\begin{bmatrix} b_{dd1} \\ b_{dd2} \\ b_{dc1} \\ b_{dc2} \\ b_{cd1} \\ b_{cd2} \\ b_{cc1} \\ b_{cc2} \end{bmatrix} = \begin{bmatrix} S_{dddd11} & S_{dddd12} & 0 & 0 & 0 & 0 & 0 & 0 \\ S_{dddd21} & S_{dddd22} & 0 & 0 & 0 & 0 & 0 & 0 \\ 0 & 0 & S_{ddcc11} & S_{ddcc12} & 0 & 0 & 0 & 0 \\ 0 & 0 & S_{ddcc21} & S_{ddcc22} & 0 & 0 & 0 & 0 \\ 0 & 0 & 0 & 0 & S_{ccdd11} & S_{ccdd12} & 0 & 0 \\ 0 & 0 & 0 & 0 & S_{ccdd21} & S_{ccdd22} & 0 & 0 \\ 0 & 0 & 0 & 0 & 0 & 0 & S_{cccc11} & S_{cccc12} \\ 0 & 0 & 0 & 0 & 0 & 0 & S_{cccc21} & S_{cccc22} \end{bmatrix} \times \begin{bmatrix} a_{dd1} \\ a_{dd2} \\ a_{dc1} \\ a_{dc1} \\ a_{cd1} \\ a_{cd2} \\ a_{cc1} \\ a_{cc2} \end{bmatrix} \tag{12}$$

The remaining 2n-port fixtures removing procedure is the same as the 4-port case, and the DUT is not necessarily in balanced design.

3. FULL-WAVE SIMULATION VALIDATION

A 2^3-port example in the full-wave simulation is used first to validate the derivations of the algorithm in the ideal scenario. The 2X-Thru calibration standard and 1X fixture are simulated independently in HFSS. The 2X-Thru calibration standard model has 4 transmission lines in the inner layer of a PCB, as depicted in Figure 5 (a). The length of the 2X-Thru (from port to port) is 650 mil. In addition, a 1X fixture with 325 mil length is also simulated. The simulated 1X fixture serves as the golden standard of validation.

(a)   (b)
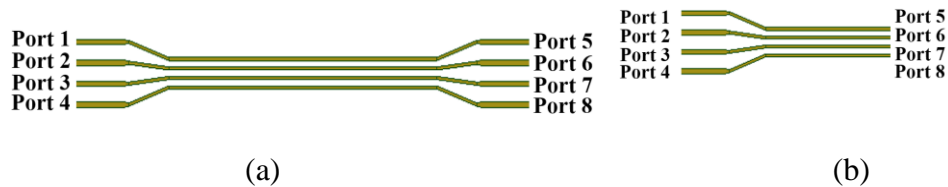
Figure 5. Full-wave simulation validation model: (a) 2X-Thru; (b) 1X-Thru.

The extracted |SDD11|, |SDD12|, |SDD13| (DDNEXT), and |SDD14| (DDFEXT) of the 1X-Thru fixture are selected to compare with the simulated 1X-Thru golden standard in Figure 6. The extracted 1X fixture has excellent agreement with the simulated golden standard.

(a)

(b)

(c)

(d)
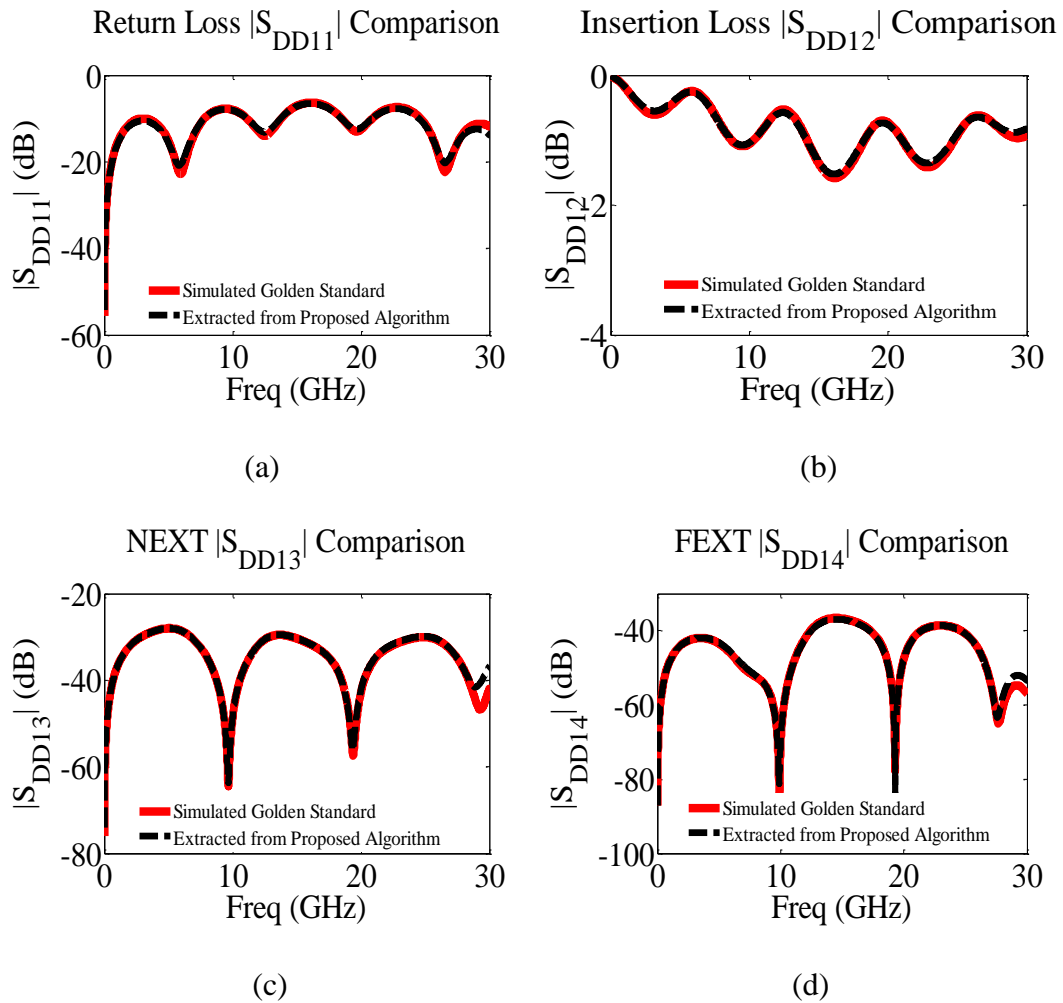
Figure 6. 1X-Thru comparison: (a) differential return loss |SDD11|; (b) differential insertion loss |SDD12|; (c) DDNEXT |SDD13|; (d) DDFEXT |SDD14|.

4. MODE CONVERSION CHARACTERIZATION OF 2N -PORT 2XTD

In the differential signaling, ideally, the phase differences between waveforms propagating on P/N pair is 180°, which keeps the energy in the odd mode only. However, if the phase differences is not exact 180°, some of the energy would convert from the odd mode to the even mode through mode conversions which are generated by the unbalance between P/N pair. Such phenomenon on a balanced designed 2n-port fixtures could be caused by the length differences, trace etching differences, proximity effects, and glass weave effect during the manufacturing process [21-24].

4.1. DERIVATIONS ON CONVERSION CHARACTERIZATION

In (18), the diagonal differential and common modes sub-matrices of 1X fixtures have already characterized by using 2n-port 2XTD. The typical errors from the asymmetry of 2X-Thru and fixture characteristic impedance variations are also treated with proper error reduction algorithms as written in the above sections. The off-diagonal sub-matrices are the mode conversion terms. In the published articles [26] on the 8-port differential s-parameter de-embedding, with enforced balanced design, the mode conversion terms are neglect. Despite the low level mode conversions may not create significant de-embedded errors, to complete the study, mode conversion terms because of the manufacturing are characterized. As a consequence, the de-embedded errors will be further reduced. The low level mode conversion characterization derivation is using the 2^2-port 2XTD as the example. The mode conversion characterizations in the higher order (n>2) of the mixed-

mode are easy to be extended. The reciprocal 22-port mixed-mode S-parameter matrix is

written as single-ended representation in Eq. (13):

$$
\begin{bmatrix} b_{d1} \\ b_{d2} \\ b_{c1} \\ b_{c2} \end{bmatrix} = \begin{bmatrix} S_{dd11} & S_{dd12} & S_{dc11} & S_{dc12} \\ S_{dd21} & S_{dd22} & S_{dd21} & S_{dd22} \\ S_{cd11} & S_{cd12} & S_{cc11} & S_{cc12} \\ S_{cd21} & S_{cd22} & S_{cc21} & S_{cc22} \end{bmatrix} \times \begin{bmatrix} a_{d1} \\ a_{d2} \\ a_{c1} \\ a_{c2} \end{bmatrix}
$$

$$
= \frac{1}{2} \times \begin{bmatrix} S_{11}-S_{13}-S_{31}+S_{33} & S_{12}-S_{14}-S_{32}+S_{34} & S_{11}+S_{13}-S_{31}-S_{33} & S_{12}+S_{14}-S_{32}-S_{34} \\ S_{21}-S_{23}-S_{41}+S_{43} & S_{22}-S_{24}-S_{42}+S_{44} & S_{21}+S_{23}-S_{41}-S_{43} & S_{22}+S_{24}-S_{42}-S_{44} \\ S_{11}-S_{13}+S_{31}-S_{33} & S_{12}-S_{14}+S_{32}-S_{34} & S_{11}+S_{13}+S_{31}+S_{33} & S_{12}+S_{14}+S_{32}+S_{34} \\ S_{21}-S_{23}+S_{41}-S_{43} & S_{22}-S_{24}+S_{42}-S_{44} & S_{21}+S_{23}+S_{41}+S_{43} & S_{22}+S_{24}+S_{42}+S_{44} \end{bmatrix} \times \begin{bmatrix} a_{d1} \\ a_{d2} \\ a_{c1} \\ a_{c2} \end{bmatrix}
$$

$$
(13)
$$

where

$$
S_{dc11} = S_{cd11} = \frac{1}{2} \times (S_{11} - S_{33})
$$

$$
(14\text{-}1)
$$

$$
S_{dc12} = S_{cd21} = \frac{1}{2} \times (S_{12} - S_{34} + (S_{14} - S_{32}))
$$

$$
(14\text{-}2)
$$

$$
S_{dc21} = S_{cd12} = \frac{1}{2} \times (S_{12} - S_{34} - (S_{14} - S_{32}))
$$

$$
(14\text{-}3)
$$

$$
S_{dc22} = S_{cd22} = \frac{1}{2} \times (S_{22} - S_{44})
$$

$$
(14\text{-}4)
$$

When characterize the S_{dc11} and S_{dc22} in the 1X fixtures, the single-ended

$S_{11}, S_{22}, S_{33}, S_{44}$ of 1X fixtures are required to be calculated first. Meanwhile, the S_{12}, S_{34}

of 1X fixture in (14-2) and (14-3) are also calculated. The calculation procedure is same as

the 2-port single-ended 2XTD when terminating the other 2 ports. The S_{14}, S_{23} of 1X

fixture are approximate as $\frac{1}{\Delta}$ of the S_{14}, S_{23} of the 2X fixture as the FEXT is proportional to

the length. So, $S_{14} - S_{23}$ of 1X fixture is calculated in (15).

$$\frac{1}{\Delta} = \frac{S_{14}^{1X} - S_{23}^{1X}}{S_{14}^{2X} - S_{23}^{2X}} = \frac{S_{14}^{1X} + S_{23}^{1X}}{S_{14}^{2X} + S_{23}^{2X}} \tag{15}$$

Where

$$\Delta = \frac{S_{cc}^{2X} - S_{dd}^{2X}}{S_{cc}^{1X} - S_{dd}^{1X}} \tag{16}$$

4.2. VALIDATIONS ON MODE CONVERSION CHARACTERIZATION

The mode conversion characterization is demonstrated by using an unbalanced but symmetric 2^2-port 2X-Thru, followed by the justification (mode conversion <-15dB at entire bandwidth) that TG1 proposed in the P370 committee. As drawn in Figure 7 (a), in the 2X-Thru, the lead-in portions on the top trace are 6.5 mil while on the bottom are 7.5 mil. The mode conversion terms of such 2X-Thru are listed in the Figure 7 (b).

(a)   (b)
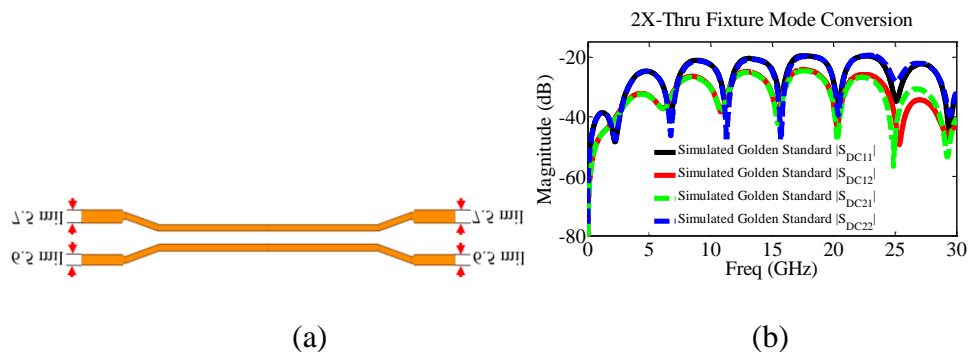
Figure 7. 2X-Thru with unbalanced design: (a) upper trace and lower trace has different width of lead-in portion; (b) mode conversion terms.

Such unbalanced 2X-Thru is still symmetric as the mode conversion is the focus in this section. The 1X fixture is also simulated to serve as the golden standard, and compare with the characterized mode conversion terms. In addition, the simulated differential and common modes golden standard are also compared with the characterized differential and common modes in this case to verify the correctness of characterization on these two major modes. Details of 1X fixture differential mode comparison are displayed in Figure 8 (e)-(g).
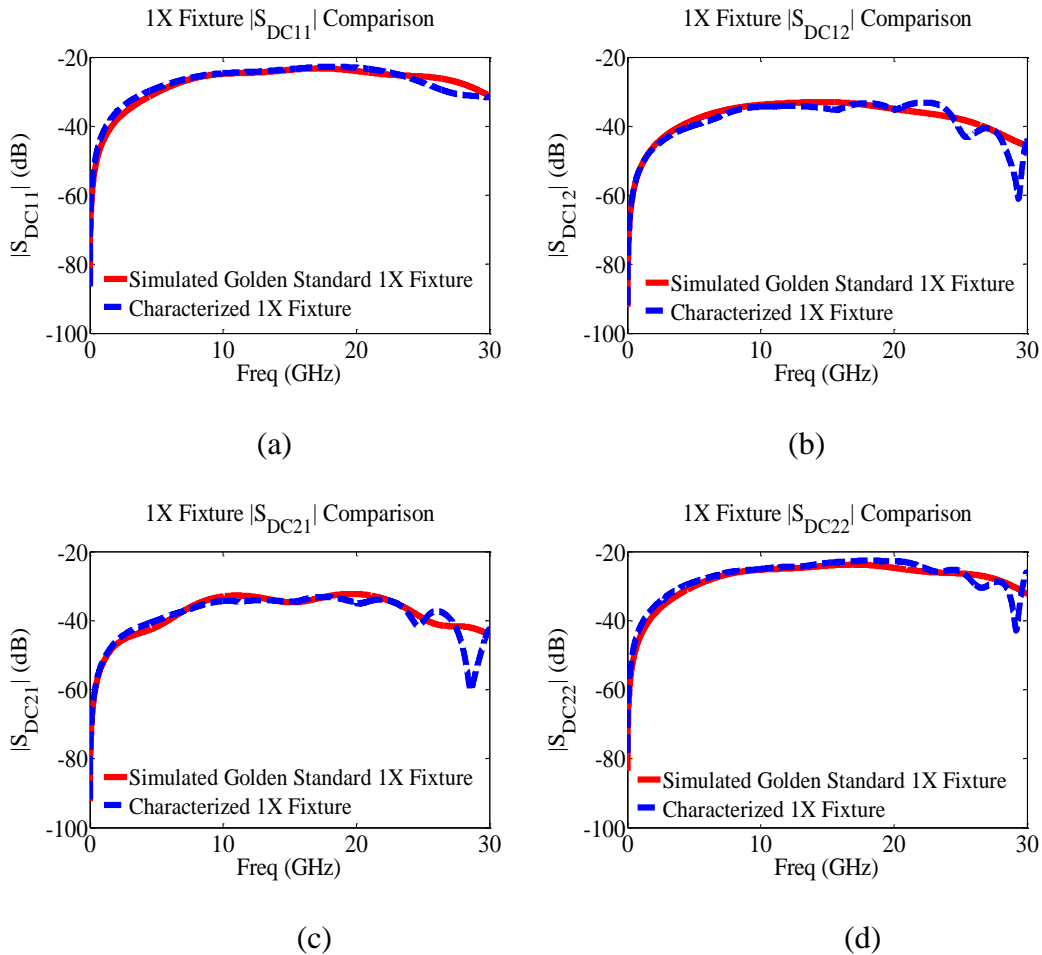
Figure 8. 1X fixture comparison: (a) |SDC11|; (b) |SDC12|; (c) |SDC21|; (d) |SDC22|;(e) |SDD11|;(f) |SDD21|;(g) |SDD22|.
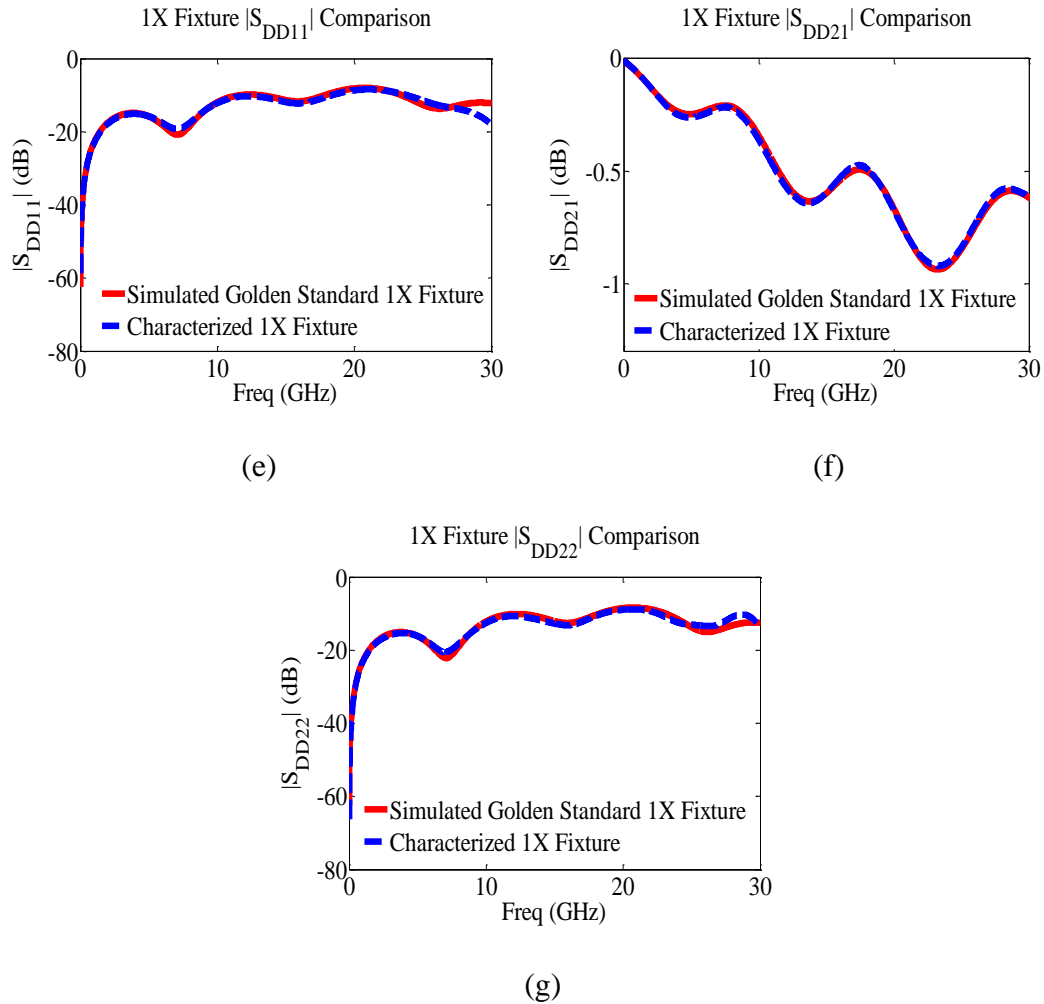
Figure 8. 1X fixture comparison: (a) |SDC11|; (b) |SDC12|; (c) |SDC21|; (d) |SDC22|;(e) |SDD11|;(f) |SDD21|;(g) |SDD22|. (cont.)

5. COMPARISON ON THE DE-EMBEDDED RESULTS

Conventionally, a single-ended 2X-Thru fixture is designed to remove the fixtures effects of multi-port de-embedding application. The actual fixtures attached to the DUT is designed as spread-out spider legs like shape is to decrease the crosstalk between different traces. When perform the de-embedding by using single-ended 2X-Thru, the crosstalk terms are ignored. There are two typical errors in such approach: 1) the crosstalk before

the trace fan-out area may not negligible at the high frequency; 2) Each trace in such spider legs like fixture may route differently. Rigorously, the 2X-Thru fixture design should be designed exactly as the fixtures attached to the DUT, as shown in Figure 9 (b). The multi-ports fixture characterization proposed in this paper by considering the crosstalk and mode conversion is suitable for such spider legs like 2X-Thru to acquire more accurate de-embedded results in the multi-port de-embedding. The multi-port 2X-Thru fixture in Figure 9 (b) has four differential ports (where P1 and P3 are one differential pair, P2 and P4 are another differential pair, and so on). The traces for the design are stripline routing with ground fillings on the same layer. Such 2X-Thru fixture is manufactured on the same test board with the Total structure in the Figure 9 (a).
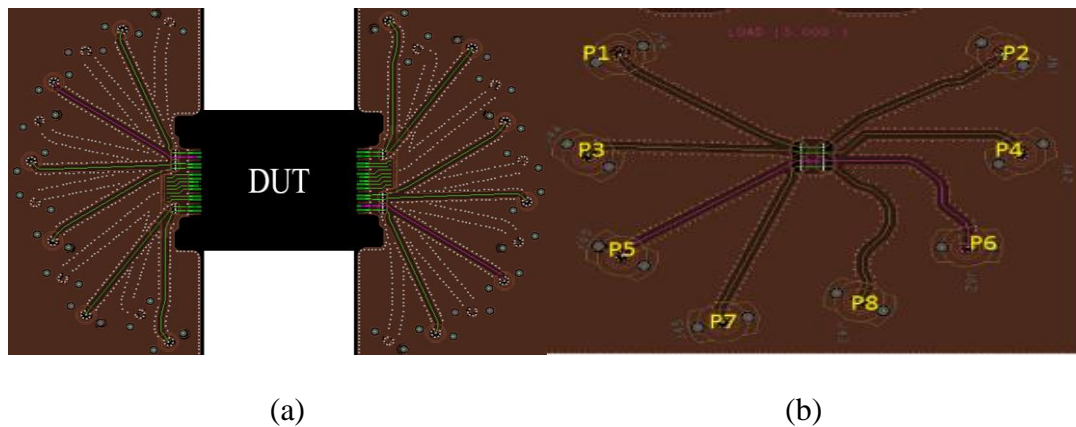
(a)   (b)

Figure 9. The layout and the manufactured test coupon: (a) Total (DUT embedded in between the fixtures) layout; (b) 2X-Thru fixture layout with exact spider legs like design as the Total; (c) manufactured Total.
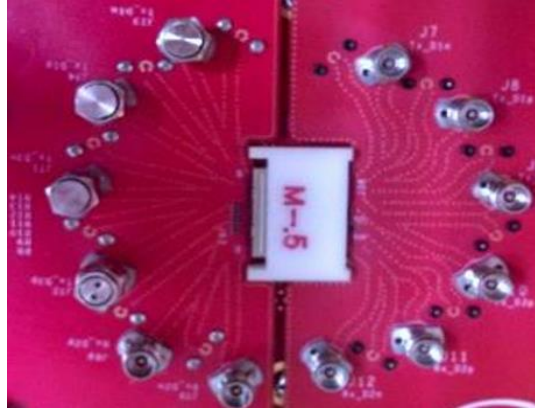
(c)

Figure 9. The layout and the manufactured test coupon: (a) Total (DUT embedded in between the fixtures) layout; (b) 2X-Thru fixture layout with exact spider legs like design as the Total; (c) manufactured Total.(cont.)

Because of the lack of a direct measurement of the 1X-Thru, and DUT, the full-wave models conducted from the layout are required. In the fixture characterization validation procedure, the 1X spider legs like fixtures from extraction of the proposed algorithm is compared with the direct simulation golden standard. Such spider legs like 2X-Thru full-wave model was cut into left 1X fixture and right 1X fixture due to the slight asymmetry in the 2X-Thru design.

The symmetry check and 1st order mode conversion are observed in Figure 10 (a) and (b). The symmetry check here is performed by comparing the percentage differences of return loss from left hand side and right hand side. For example, the asymmetric rate of port 1 and port 2, δ_1 is:

$$\delta_1 = 100 \times \left| \frac{S_{11} - S_{22}}{S_{11}} \right|$$

(17)
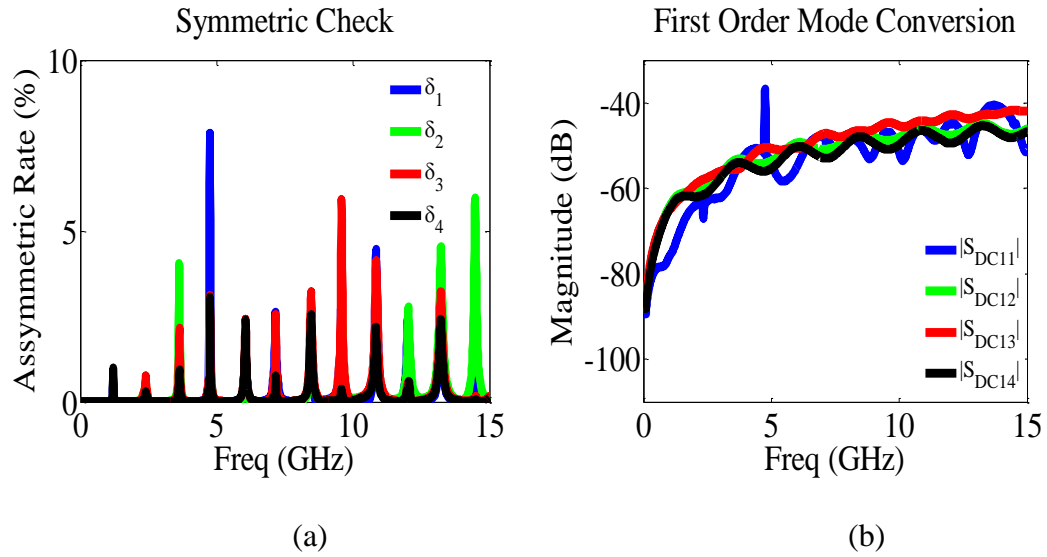
Figure 10. (a) Symmetric check; (b) 1st mode conversion check.

The δ_2, δ_3, and δ_4 in Figure 10 (a) are the asymmetric rates between port 3 and 4, port 5 and 6, and port 7 and 8, respectively. Overall, the asymmetric rate is lower than 8%, and 1st order mode conversion terms are below -40dB. The 1X fixture extraction procedure is also performed on the measurement data as well. A connector DUT was embedded into the manufactured fixtures, as shown in Figure 9 (c).

Figure 11 (a)-(h) drew the comparisons between left spider legs like 1X fixture from full-wave simulation golden standard, the 1X fixture of extraction from the multi-port 2X-Thru simulation and the 1X fixture of extraction from the multi-port 2X-Thru measurement.
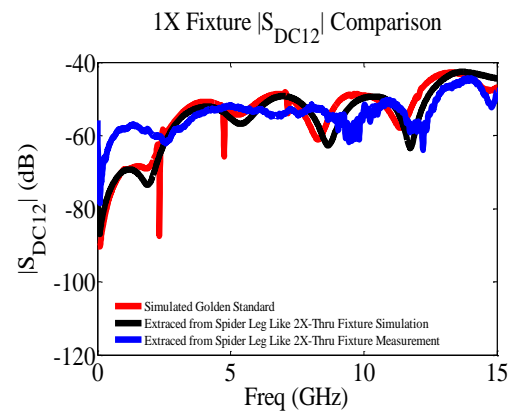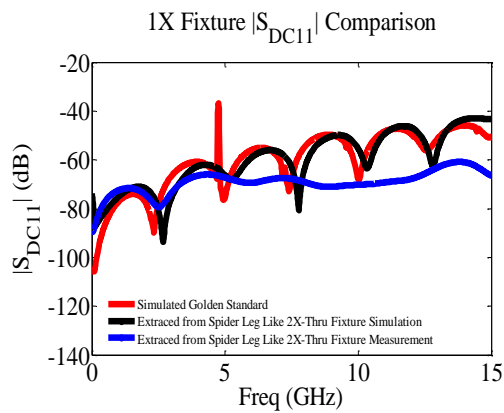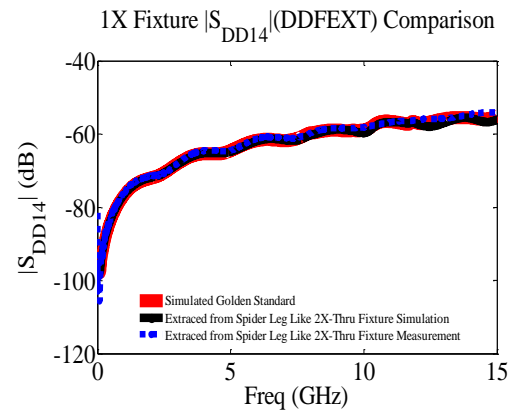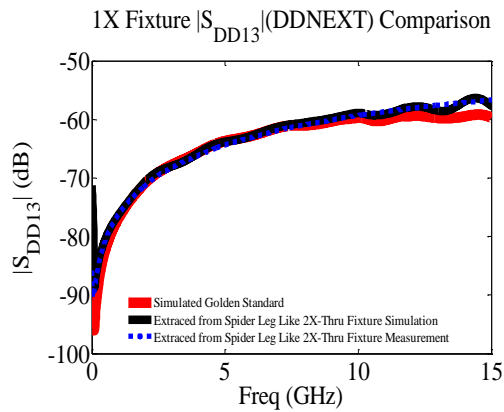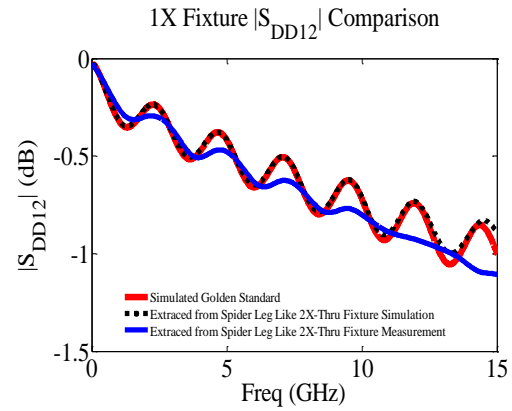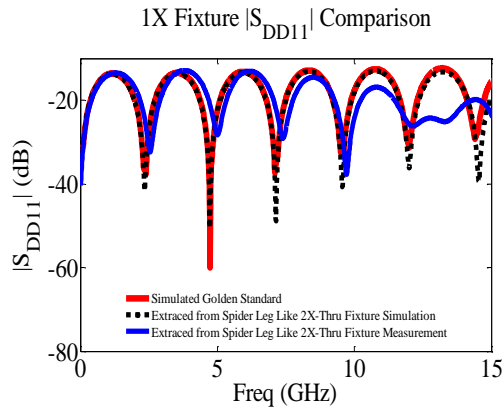
Figure 11. 1X fixture electrical performance comparisons: (a) |SDD11|; (b) |SDD12|; (c) |SDD13| (NEXT); (d) |SDD14| (FEXT); (e) |SDC11|;(f) |SDC12|;(g) |SDC13|;(h) |SDC14|.

1X Fixture |S_DC13| Comparison

1X Fixture |S_DC14| Comparison

(g) (h)
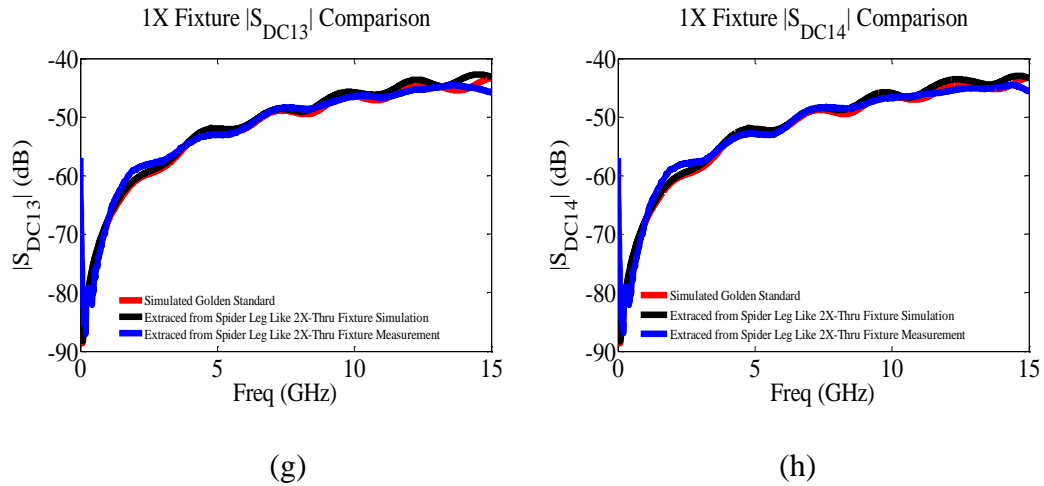
Figure 11. 1X fixture electrical performance comparisons: (a) |SDD11|; (b) |SDD12|; (c) |SDD13| (NEXT); (d) |SDD14| (FEXT); (e) |SDC11|;(f) |SDC12|;(g) |SDC13|;(h) |SDC14|.(cont.)

By observing the Figure 11 (a)-(h), the differential mode between the simulated golden standard and the results extracted from the multi-port 2X-Thru fixtures achieved great match, despite some asymmetry exist in such 2X-Thru. The asymmetry compensation is enforced in fixture characterization, and will be presented in a separate paper. The extracted mode conversion terms between the simulated golden standard and the extractions from 2X-Thru simulation also have great match in |SDC13| and |SDC14| but there are some small discrepancies in |SDC11| and |SDC12| because of the approximate made in (15). The measurement results somehow have slightly larger differences by comparing with the simulation golden standard is due to two major reasons: 1) the 1.8 mm connectors are not included in the full-wave models; 2) variations during the manufacturing process.

6. DESIGN GUIDES OF 2^N-PORT 2XTD

Any type of layer transition can cause a discontinuity. Such discontinuities are inevitable in fixture design and they cause the algorithm-related accuracy issue in the fixture characterization and de-embedding procedure [4]. Optimizations are necessary in designing to transitions in order to minimize the insertion and return losses of test fixtures. The transition optimizations include typical approaches such as a close to fan-out transmission line impedance via design, an optimal launch footprint, back drill of via stub, etc. In general, the statistic studies prioritize the approaches that give the best optimization performance in specific designs [13]-[14]. In [4], sensitivity analysis on a 2-port de-embedding example was well studied. Comparisons were conducted between the fixtures with and without transition optimization in both full-wave simulation and measurement scenarios. The conclusion is the fixture designs with optimization is much less sensitive in the 2XTD, and have better de-embedding accuracies. The transition optimizations in [4] are also suitable for fixture designs of 8-port 2XTD application.

The 2XTD (and other 2X-thru method) has length requirement for the transmission line between discontinuities, as the algorithm depends on time domain information. Transmission line behavior should be dominant at the middle point of the 2X-Thru's TDR response [15]. Figure 12. (a) and (b) give good and bad examples of TDR response of 2X-Thru fixtures. The characteristic impedance of the transmission line between discontinuities is 46 Ohm and the length of the transmission line in Figure 9 (a) is 800 mil, while in (b) it is 250 mil. Obviously, the TDR response in Figure 12 (b) does not reflect the actual information of the transmission line.
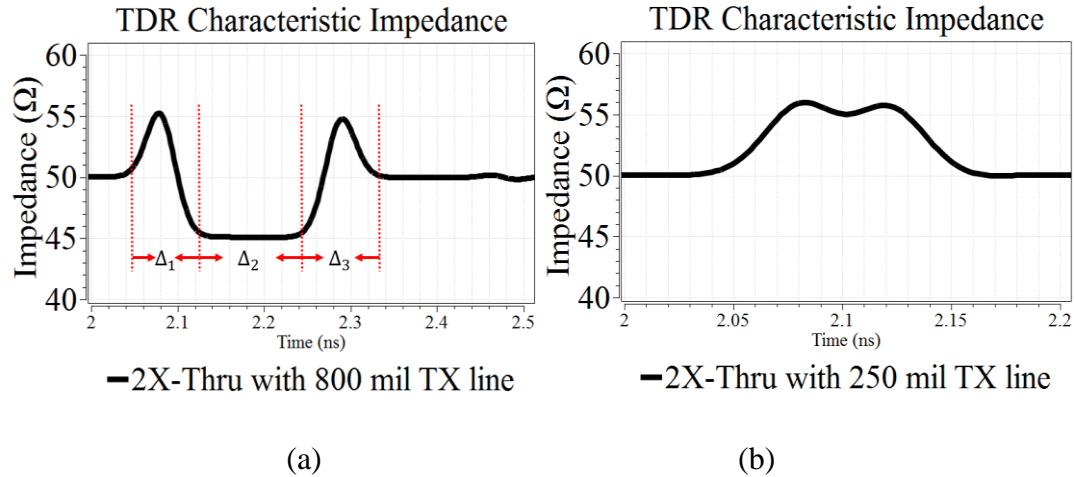
Figure 12. 2X-Thru TDR Characteristic impedance: (a) 800 mil transmission line between two discontinuities; (b) 250 mil transmission line between two discontinuities.

For engineering practice, the length of the transmission line should be equal or larger than the summation of discontinuities' lengths. In Figure 12 (a):

$$\Delta_2 \geq \Delta_1 + \Delta_3$$

(18)

Passivity means a system does not generate energy. The rule of passivity in the 2-port 2X Thru de-embedding is discussed in [20] and defined in (19).

$$\left| \frac{S_{11}^{2X}}{S_{21}^{2X}} \right| = \left| \frac{S_{22}^{2X}}{S_{21}^{2X}} \right| < 1$$

(19)

In the 2n-port 2XTD application, the equation in (19) is extended to S-parameters of (nth-1) order mixed mode 2X-Thru. Take the 8-port application as an example, the passivity rule in differential-differential mode is:

$$\left| \frac{S_{DDdd11}^{2X}}{S_{DDdd21}^{2X}} \right| = \left| \frac{S_{DDdd22}^{2X}}{S_{DDdd21}^{2X}} \right| < 1$$

(20)

The couplings and small extend mode conversion are characterized by using the proposed methodology in this work. The multi-port 2X-Thru designed as Figure 5. (a) became realistic to remove the multi-port fixture effect. The small extend of unbalance in the multi-port 2X-Thru is assumed from the manufacturing. In the designing, a good balanced and symmetric multi-port 2X-Thru design is still favorable to acquire the de-embedded results with high accuracy.

7. MATHEMATICAL DERIVATIONS OF ERROR REDUCTIONS IN 2XTD

7.1. ERROR REDUCTION 1 OF 2XTD: ASYMMETRY

As demonstrated in [22], 2XTD is based on the assumption of symmetric 2X-Thru fixture standard. The asymmetry in the manufactured 2X-Thru calibration standard may from the characteristic impedance variations along transmission line, the back drilling tolerance, connectors yield variations, etc. The error reduction of the asymmetry assumes the return losses on the left and right half of the 2X-Thru dominate the differences, while insertion losses remain the same. Figure 13. illustrates the signal flow chart of a single-ended 2-port 2X -Thru calibration standard with the asymmetry assumption.
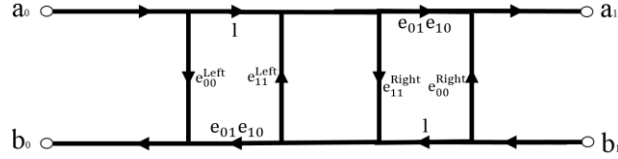
Figure 13. Signal flow chart of 2X-Thru calibration standard with asymmetric structure.

There are five unknowns in this asymmetry models. The $S_{11}^{1X-Left}$ and $S_{22}^{1X-Right}$ are calculated from the time domain gating method with the renormalization on left and right sides, respectively. Eq. (21) to Eq. (22) solve the $S_{11}^{1X-Right}$, $S_{22}^{1X-Right}$, and S_{21}^{1X} ($S_{21}^{1X} = S_{12}^{1X}$).

$$S_{11}^{1x-right} = \frac{S_{11}^{2x} - S_{11}^{1x-left}}{S_{21}^{2x}} \tag{21}$$

$$S_{22}^{1x-left} = \frac{S_{22}^{2x} - S_{22}^{1x-right}}{S_{21}^{2x}} \tag{22}$$

$$S_{21}^{1x} \times S_{12}^{1x} =$$
$$S_{21}^{2x} - \frac{(S_{11}^{1x-left} - S_{11}^{2x})(S_{22}^{1x-right} - S_{22}^{2x})}{S_{21}^{2x}} \tag{23}$$

A full-wave model with some extent of asymmetry is conducted to serve as the validation purpose of the error reduction 1 on the 2XTD. The golden standard is the direct simulations of 1X fixtures, is compared with the results from fixture characterization procedure with and without such asymmetry compensation treatment. The Figure 14 (a) shows the full-wave model of a 2^2-port 2X-Thru (850 mil) with asymmetric design. The lead-in traces at the left hand side has a 6.5 mils width, while the right hand side is 9.5 mils.

(b) and (c) of Figure 14 are showing the $|S_{DD11}|$ and $|S_{DD22}|$ comparisons and the TDR impedance of such 2X-Thru fixture. In such case, the differences of differential characteristic impedance is about $\pm10\%$, which is on the maximum-end of the manufacturing tolerance.
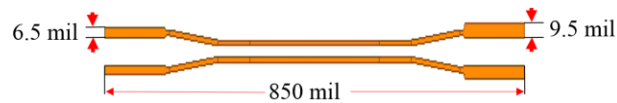
(a)
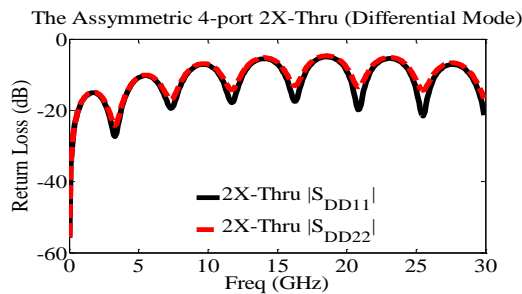
(b)
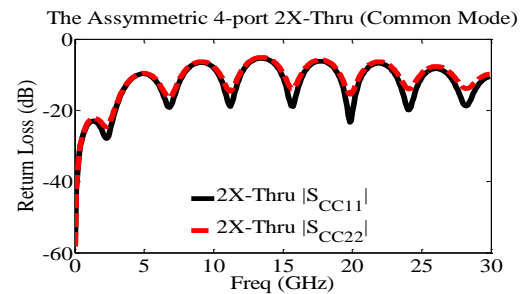
(c)
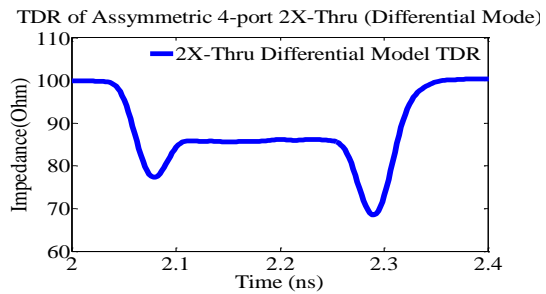
(e)
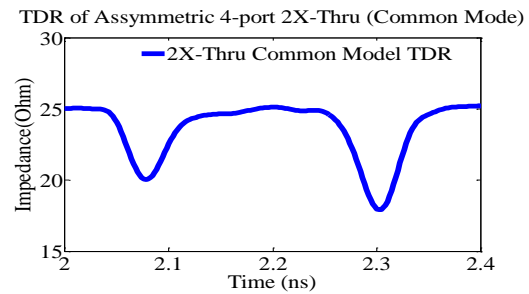
(f)

Figure 14.The asymmetric 2^2-port 2X-Thru: (a) full-wave models; (b) $|S_{DD11}|$ and $|S_{DD22}|$ comparison; (c) $|S_{DD11}|$ and $|S_{DD22}|$ comparison; (d) differential mode TDR impedance comparison; (e) common mode TDR impedance comparison.

The characterized 1X fixtures with and without error reduction on such asymmetric 2X-Thru calibration standard are compared with the simulated golden standard in the Figure 15. Both differential mode and common mode results indicate that much better agreement is achieved when the error reduction on the asymmetry is enforced. According to the assumption that the return losses in the modal-based s-parameters are treated differently in the left and right 1X fixture, while the insertion losses are remaining the same. Herein, compare with the golden standard, the extracted error reduced return losses only have little discrepancies, but there are still some error residues in the error reduced insertion losses.

(a)   (b)

Figure 15. Fixture characterization result comparisons: (a) |SDD11| of left 1X fixture; (b) |SDD22| of left 1X fixture; (c) |SDD11| of right 1X fixture; (d) |SDD22| of right 1X fixture;(e) |SDD21| of 1X fixture; f) |SCC11| of left 1X fixture; (g) |SCC22| of left 1X fixture; (h) |SCC11| of right 1X fixture; (i) |SCC22| of right 1X fixture;(j) |SCC21| of 1X fixture.
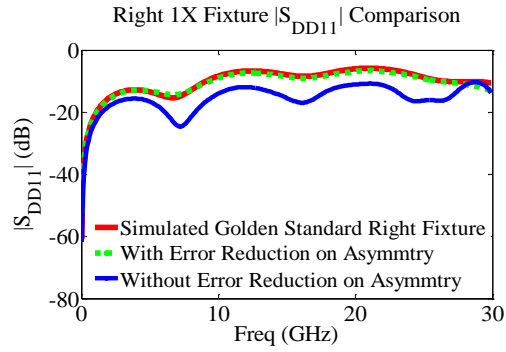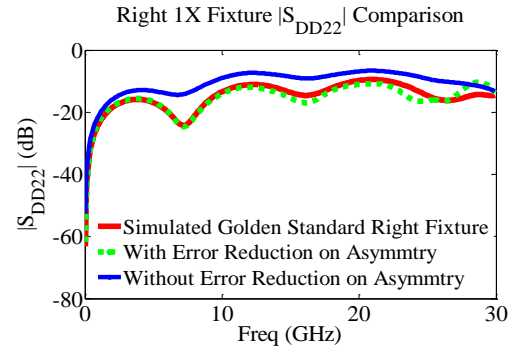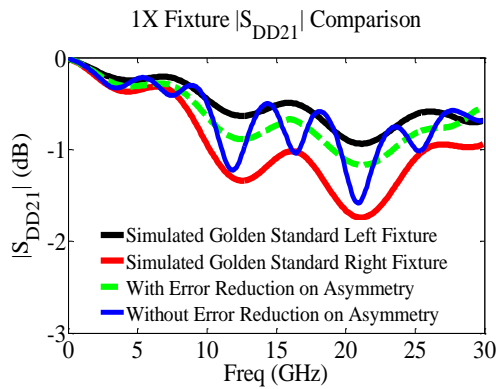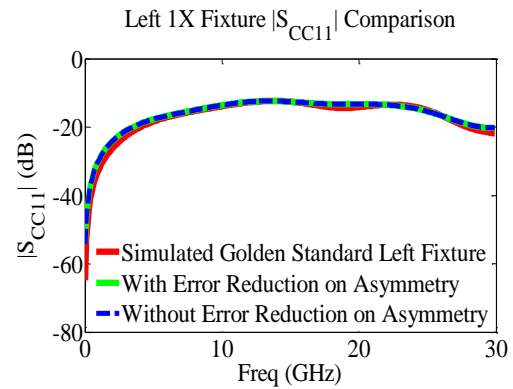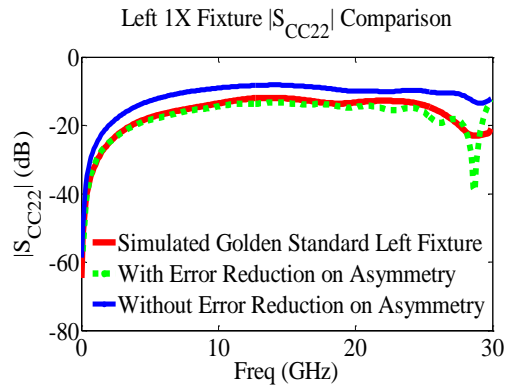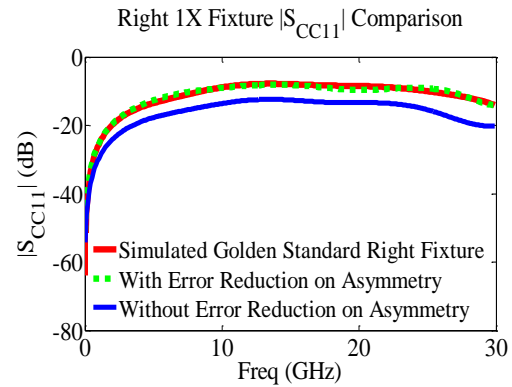
Figure 15. Fixture characterization result comparisons: (a) |SDD11| of left 1X fixture; (b) |SDD22| of left 1X fixture; (c) |SDD11| of right 1X fixture; (d) |SDD22| of right 1X fixture;(e) |SDD21| of 1X fixture; f) |SCC11| of left 1X fixture; (g) |SCC22| of left 1X fixture; (h) |SCC11| of right 1X fixture; (i) |SCC22| of right 1X fixture;(j) |SCC21| of 1X fixture. (cont.)

Figure 15. Fixture characterization result comparisons: (a) |SDD11| of left 1X fixture; (b) |SDD22| of left 1X fixture; (c) |SDD11| of right 1X fixture; (d) |SDD22| of right 1X fixture;(e) |SDD21| of 1X fixture; f) |SCC11| of left 1X fixture; (g) |SCC22| of left 1X fixture; (h) |SCC11| of right 1X fixture; (i) |SCC22| of right 1X fixture;(j) |SCC21| of 1X fixture. (cont.)

7.2. ERROR REDUCTION 2 OF 2XTD: FIXTURE VARIATIONS

Every de-embedding algorithm requires the fixtures in the calibration standards ought to be exactly same as the fixtures in the Total. However, the fixture variation is ineluctable during the manufacturing process. In the TRL, the effect of characteristic impedance variations of transmission lines among calibration standards is analyzed in [23]. In [23], author found that the impedance variations between Thru and Lines impact the calibration constants, c/a and b in the TRL equation. In the SOLT, beyond the impedance variations in the discontinuities and transmission lines, it is very difficult to fabricate accurate broadband 'short' and 'load' standards on PCBs. The 2XTD transfers the 'short', 'open', and 'load' to the wideband 2X-Thru calibration standard in the mathematical derivation [24], so the impedance change governs the 1X fixtures variations.

The error reduction on the 1X fixture impedance variations corrects the

$S_{11}^{1X-Left}, S_{22}^{1X-Right}, S_{22}^{1X-Leftt}$, and $S_{11}^{1X-Right}$ in the time domain waveforms. The

correction of $S_{11}^{1X-Left}$ and $S_{22}^{1X-Right}$ are gating the time domain waveforms from the

Total structure by using the reference gating points on the 2X-Thru.
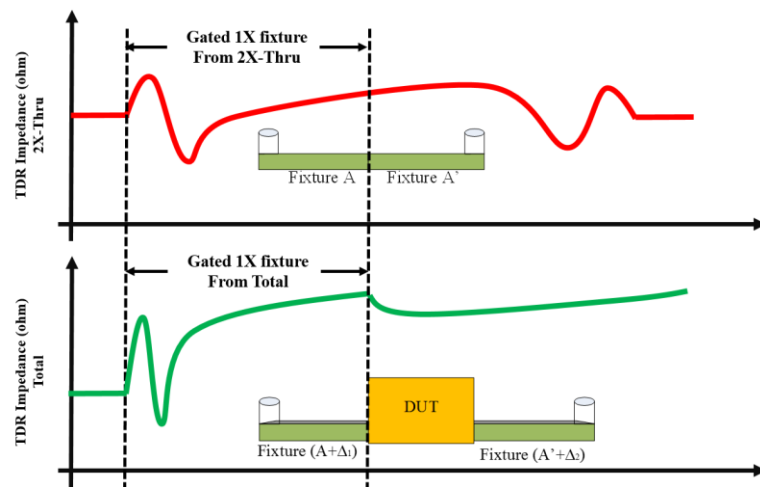
Figure 16. Corrected $S_{11}^{1X-Left}$ is gated from the Total structure.

Figure 16 provided an example that is showing the corrected $S_{11}^{1X-Left}$ is gated

from the left part of Total structure by referencing the same time index as the center of the

2X-Thru . By using the same idea, the corrected $S_{22}^{1X-Right}$ is acquired from the right hand

side of the Total structure. Constant extrapolations are required on the gated time domain

waveforms before perform the re-normalization and further calculations. The correction

of $S_{22}^{1X-Left}$ and $S_{11}^{1X-Right}$ are described in details as below, take the $S_{22}^{1X-Left}$ as example:

- Get the TDR impedance of original calculated $S_{22}^{1X-Left}$;

- Mark the delay of 1X fixture as Td, calculate the TDR impedance differences of original calculated and corrected $S_{11}^{1X-Left}$;

- Divide the TDR impedance differences from step (2) into n segments ($n = T_{total}/T_d$), and reverse the TDR impedance differences in each time segment;

- Add the reversed TDR impedance differences back to the TDR impedance from step 1 to get the corrected TDR impedance of $S_{22}^{1X-Left}$;

- Transfer the corrected TDR impedance of $S_{22}^{1X-Left}$ back to the s-parameter.

The $S_{21}^{1X-Left}$ and $S_{21}^{1X-Right}$ are also assumed the same in the 1X fixture variation error reduction procedure. The error quantification after the error reduction will estimate the final de-embedded upper and lower errors bounds due to estimated magnitude errors in the $S_{21}^{1X-Left}$ and $S_{21}^{1X-Right}$.

The error reduction on the fixture variations example of validation takes advantage of a symmetric 2X-Thru in the Figure 17 (a). In additional, a 500 mil, 100 Ohm differential transmission line DUT is inserted in between the left and right 1X fixtures, depicted in the Figure 17 (b). The widths on the lead-in traces at the left and right sides of the Total structure are 7.5 mil. The differential mode and common mode TDR characteristic impedances of 2X-Thru and Total are depicted in the Figure 17 (c) and (d), in which the fixtures are marked in the green dash box. A separate 500 mil differential transmission line DUT with 100 Ohm differential characteristic impedance is simulated independently as the golden standard of comparison. The symmetric 2X-Thru employed here is to avoid

the errors due to the asymmetry of 2X-Thru fixtures, and to identify the error reduction effect on the fixture variations between the 2X-Thru and the Total only. Such fixture variations satisfies the Class C fixture designing rules that work group 1 (WG1) of IEEE P370 committee proposed in [20]. The WG1 in the IEEE P370 committee discovered that the fixtures strongly influences the quality of the de-embedding results, and decided the ± 10% is the maximum characteristic impedance differences between the 2X-Thru and Total that any de-embedding algorithm can handle. The error reduction solution on such fixture variations issue follows the rule of maximum impedance variations that P370 proposed and further improves the de-embedding accuracies.
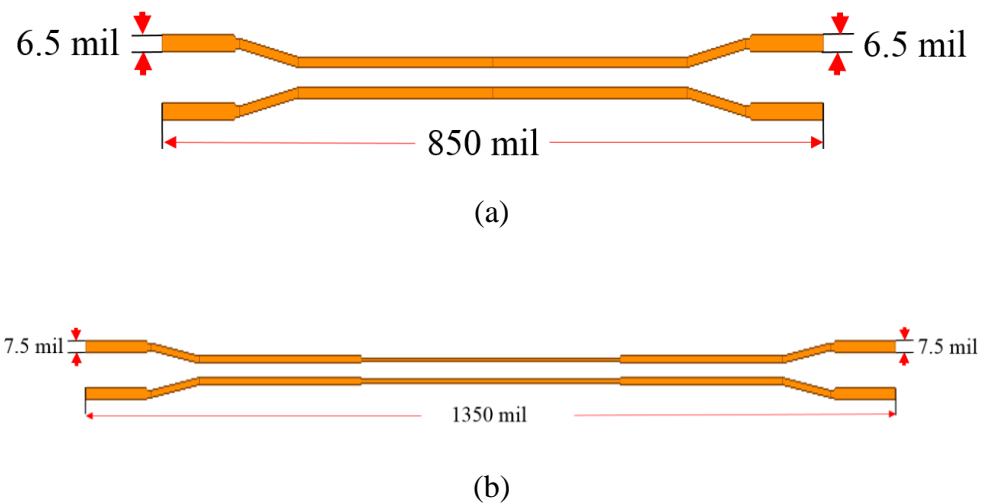
(a)

(b)

Figure 17. Fixture impedance variations between 2X-Thru and Total: (a) 850 mil symmetric 2X-Thru; (b) 1350 mil Total with the impedance variations at lead-in traces;(c) 5 Ohm differential characteristic impedance differences at lead-in traces of fixtures; (d) 1.5 Ohm common characteristic impedance differences at lead-in traces of fixtures.
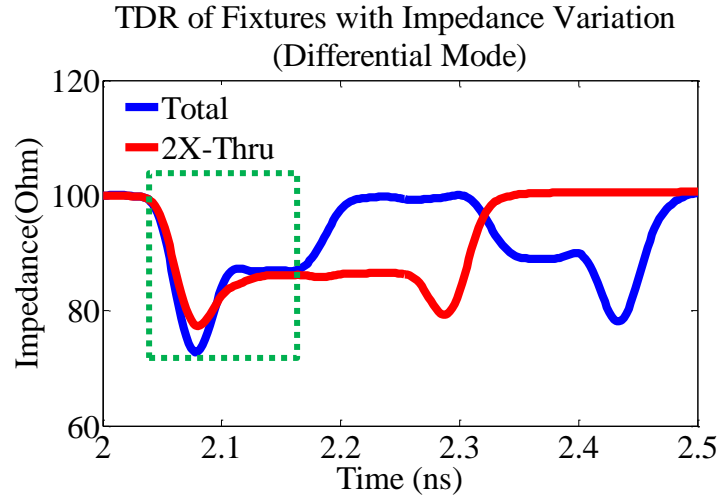
(c)
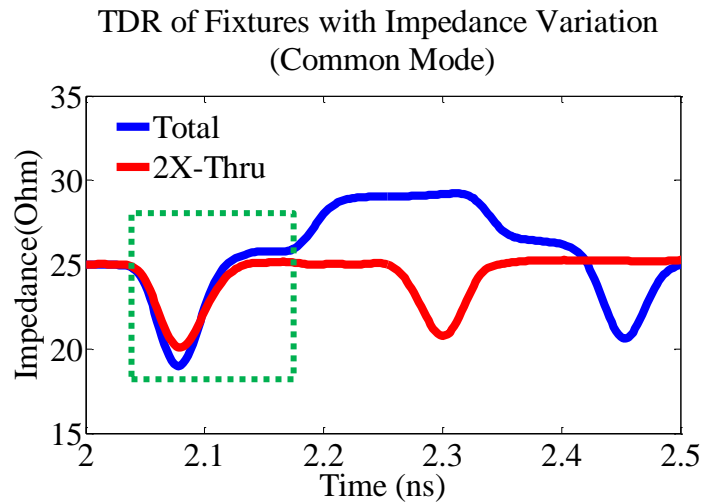
(d)

Figure 17. Fixture impedance variations between 2X-Thru and Total: (a) 850 mil symmetric 2X-Thru; (b) 1350 mil Total with the impedance variations at lead-in traces;(c) 5 Ohm differential characteristic impedance differences at lead-in traces of fixtures; (d) 1.5 Ohm common characteristic impedance differences at lead-in traces of fixtures.(cont.)

Both differential and common modes s-parameters and TDR characteristic impedances of DUT are compared in the Figure 18. Obviously, with the error correction

on the fixture variations, the de-embedded results have drastically improvement on the accuracy. The TDR characteristic impedances of the DUT comparison indicates that without the error reduction on the fixture variation, the de-embedded results are none causal.
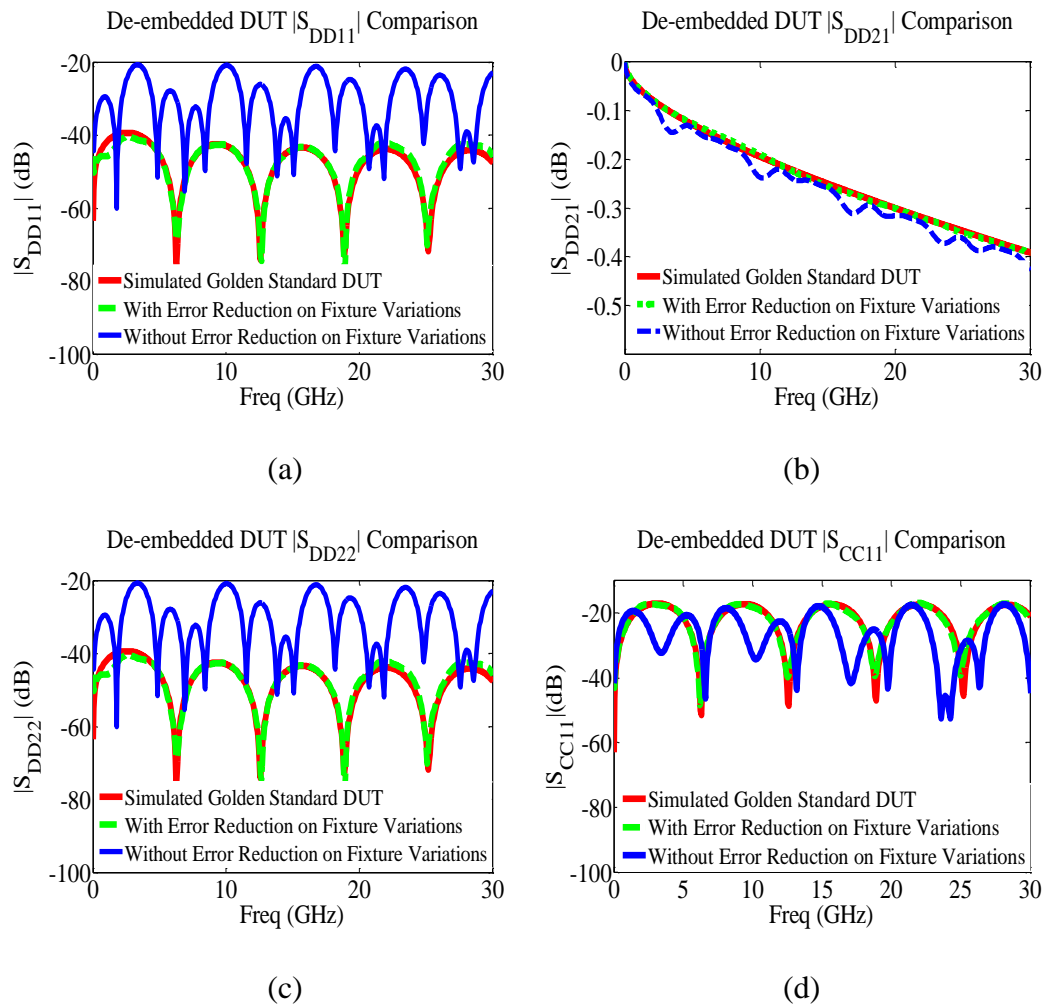
Figure 18. DUT comparisons between golden standard and de-embedded results: (a) |SDD11|; (b) |SDD21|; (c) |SDD22|; (d) |SCC11|;: (e) |SCC21|; (f) |SCC22|;(g) differential mode TDR characteristic impedance; (h) common mode TDR characteristic impedance.

De-embedded DUT $|S_{CC21}|$ Comparison

De-embedded DUT $|S_{CC22}|$ Comparison

(e)

(f)

TDR of Fixtures Comparison (Differential Mode)

TDR of Fixtures Comparison (Common Mode)

(g)

(h)
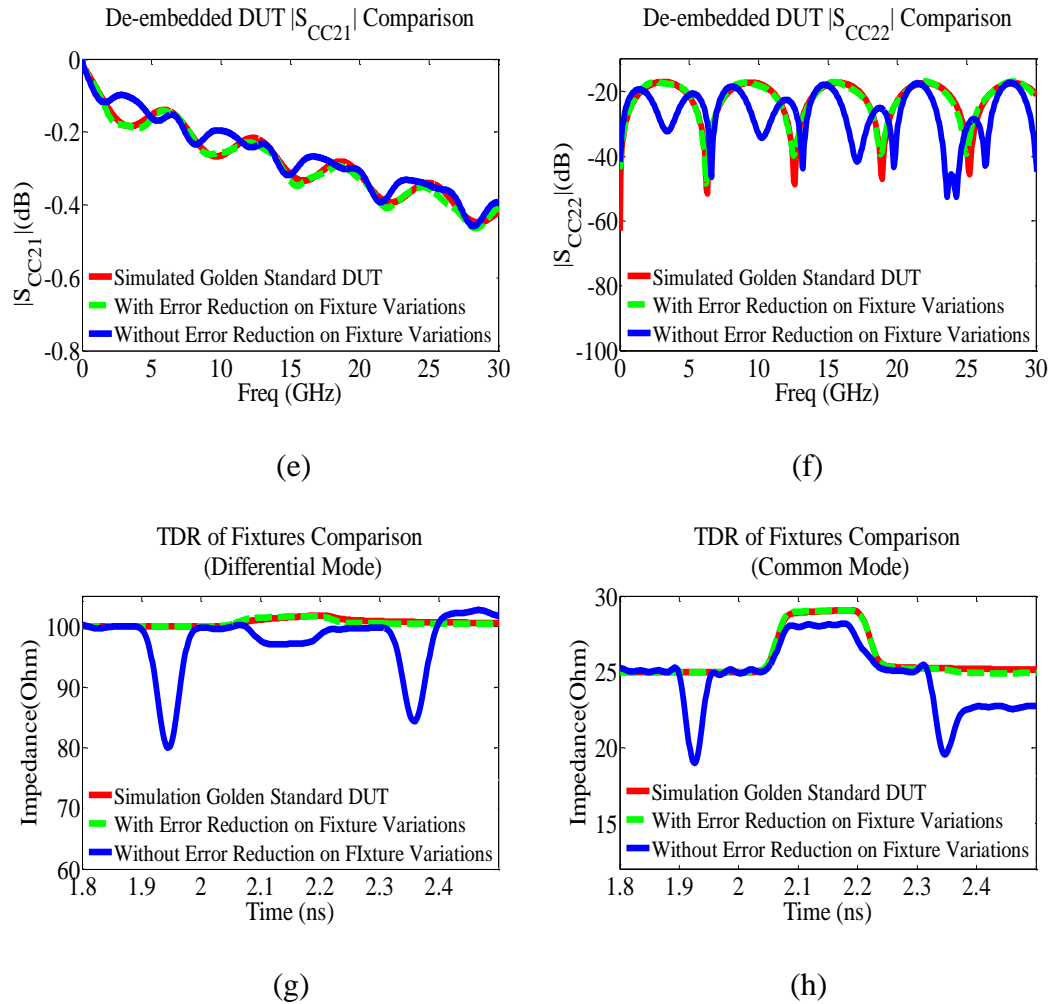
Figure 18. DUT comparisons between golden standard and de-embedded results: (a) |SDD11|; (b) |SDD21|; (c) |SDD22|; (d) |SCC11|;: (e) |SCC21|; (f) |SCC22|;(g) differential mode TDR characteristic impedance; (h) common mode TDR characteristic impedance.(cont.)

7.3. SENSITIVITY STUDY OF 2XTD AFTER ERROR REDUCTIONS

The usefulness of any de-embedding method depends in part on the accuracy and reliability of its output. However as discussed in above chapters, the precision s-parameters on the 2X-Thru and the Total are very rarely if ever available, the de-embedded s-

parameters of the DUT are subject to imprecision through the sensitivity coefficients in the de-embedding procedure. The local sensitivity assesses the sensitivity of a model response by locally varying the values of input factors. Such sensitivity is often evaluated through gradients or partial derivatives of the output functions at these factor values. In [25], the numerical and analytical sensitivity are compared and validated on the general fixture de-embedding. In addition, author provided the comparison of sensitivity coefficients with and without signal integrity optimizations. As a consequence, the design with fully optimizations on the signal integrity has much lower sensitivity coefficients The local sensitivity coefficient of the de-embedded embedded $|S_{21}^{\text{DUT}}|$, associated with $S_{11}^{1X-Left}$, is defined in Eq. (24), and calculated numerically in (25) and (26) for the first order and second order, respectively:

$$Sensitivity(S_{21}^{DUT}, S_{11}^{1X-Left}) = \left| \frac{\partial S_{21}^{DUT}}{\partial S_{11}^{1X-Left}} \right|_{X^0} \tag{24}$$

$$\frac{\partial S_{21}^{DUT}}{\partial S_{11}^{1X-Left}} \approx \frac{S_{21}^{DUT}(S_{11}^{1X-Left} + \Delta x) - S_{21}^{DUT}(S_{11}^{1X-Left})}{\Delta x} \tag{25}$$

$$\frac{\partial^2 S_{21}^{DUT}}{\partial (S_{11}^{1X-Left})^2} \approx \frac{S_{21}^{DUT}(S_{11}^{1X-Left} + \Delta x) + S_{21}^{DUT}(S_{11}^{1X-Left} - \Delta x) - 2S_{21}^{DUT}(S_{11}^{1X-Left})}{\Delta x^2}$$

$$\tag{26}$$

The small de-embedded errors can also be estimated through the sensitivity coefficients. It assumes that $\Delta x = |\Delta x| e^{j\phi}$ is a small complex number. Approximated errors for finite differences (25) and (26) are $O(|\Delta|)$ and $O(|\Delta|^2)$. Basically, the first-order and second-order errors for de-embedded $|S_{21}^{\text{DUT}}|$ is approximated as:

$$\Delta S_{21}^{DUT} = ((\frac{\partial S_{21}^{DUT}}{\partial S_{11}^{1X-Left}} + \frac{\partial^2 S_{21}^{DUT}}{\partial (S_{11}^{1X-Left})^2}) \times \Delta S_{11}^{1X-Left} + 2 \times (\frac{\partial S_{21}^{DUT}}{\partial S_{12}^{1X-Left}} + \frac{\partial^2 S_{21}^{DUT}}{\partial (S_{12}^{1X-Left})^2}) \times \Delta S_{12}^{1X-Left}$$

$$+ (\frac{\partial S_{21}^{DUT}}{\partial S_{22}^{1X-Left}} + \frac{\partial^2 S_{21}^{DUT}}{\partial (S_{22}^{1X-Left})^2}) \times \Delta S_{22}^{1X-Left}) + ((\frac{\partial S_{21}^{DUT}}{\partial S_{11}^{1X-Right}} + \frac{\partial^2 S_{21}^{DUT}}{\partial (S_{11}^{1X-Right})^2}) \times \Delta S_{11}^{1X-Right}$$

$$+ 2 \times (\frac{\partial S_{12}^{DUT}}{\partial S_{12}^{1X-Right}} + \frac{\partial^2 S_{21}^{DUT}}{\partial (S_{12}^{1X-Right})^2}) \times \Delta S_{12}^{1X-Right} + (\frac{\partial S_{21}^{DUT}}{\partial S_{22}^{1X-Right}} + \frac{\partial^2 S_{21}^{DUT}}{\partial (S_{22}^{1X-Right})^2}) \times \Delta S_{22}^{1X-Right})$$

$$(27)$$

In addition, the $S_{12}^{1X}, S_{21}^{1X}, S_{22}^{1X-Left},$ **and** $S_{11}^{1X-Right}$ are depend on the $S_{11}^{1X-Left}$ and $S_{22}^{1X-Right}$. Herein, the Eq. (27) is rewritten as Eq. (28), where all the partial derivatives are calculated numerically.

$$\Delta S_{21}^{DUT} = ((\frac{\partial S_{21}^{DUT}}{\partial S_{11}^{1X-Left}} + \frac{\partial^2 S_{21}^{DUT}}{\partial (S_{11}^{1X-Left})^2}) + 2 \times (\frac{\partial S_{12}^{DUT}}{\partial S_{12}^{1X-Left}} \times \frac{\partial S_{12}^{1X-Left}}{\partial S_{11}^{1X-Left}} + \frac{\partial^2 S_{21}^{DUT}}{\partial (S_{12}^{1X-Left})^2} \times \frac{\partial^2 S_{12}^{1X-Left}}{\partial (S_{11}^{1X-Left})^2})$$

$$+ (\frac{\partial S_{21}^{DUT}}{\partial S_{22}^{1X-Left}} \times \frac{\partial S_{22}^{1X-Left}}{\partial S_{11}^{1X-Left}} + \frac{\partial^2 S_{21}^{DUT}}{\partial (S_{22}^{1X-Left})^2} \times \frac{\partial^2 S_{22}^{1X-Left}}{\partial (S_{11}^{1X-Left})^2})) \times \Delta S_{11}^{1X-Left}$$

$$+ ((\frac{\partial S_{21}^{DUT}}{\partial S_{22}^{1X-Right}} + \frac{\partial^2 S_{21}^{DUT}}{\partial (S_{22}^{1X-Right})^2}) + 2 \times (\frac{\partial S_{12}^{DUT}}{\partial S_{12}^{1X-Right}} \times \frac{\partial S_{12}^{1X-Right}}{\partial S_{22}^{1X-Right}} + \frac{\partial^2 S_{21}^{DUT}}{\partial (S_{12}^{1X-Right})^2} \times \frac{\partial^2 S_{12}^{1X-Right}}{\partial (S_{22}^{1X-Right})^2})$$

$$+ (\frac{\partial S_{21}^{DUT}}{\partial S_{22}^{1X-Right}} \times \frac{\partial S_{22}^{1X-Right}}{\partial S_{22}^{1X-Right}} + \frac{\partial^2 S_{21}^{DUT}}{\partial (S_{22}^{1X-Right})^2} \times \frac{\partial^2 S_{22}^{1X-Right}}{\partial (S_{22}^{1X-Right})^2})) \times \Delta S_{22}^{1X-Right}$$

$$(28)$$

The complex errors in the de-embedded results, take S_{21}^{DUT} as an example, are associated with the sensitivity coefficients as well as the errors in the $S_{11}^{1X-Left}$ and $S_{22}^{1X-Right}$. The errors of the $S_{11}^{1X-Left}$ and $S_{22}^{1X-Right}$ are mitigated in the second error reduction procedure, thus the dominate residual errors are the deterministic errors from the 2XTD algorithm itself. Such deterministic errors are unknown in this stage.

8. ERROR BOUNDS OF SINGLE-ENDED 2XTD AFTER ERROR REDUCTIONS

The error bounds evaluate the maximum and minimum magnitude of the de-embedded results. The calculation procedure is also associated with the fixture characterization algorithms. In [26] and [27], authors applied such idea on the TLD and

general fixture de-embedding respectively. In the error bounds calculation of TLD, the

$e^{-\gamma l}$ magnitude error are calculated by comparing the extracted value with the fitted value.

With a 360° sweeping in the complex plane, the complex errors of $e^{-\gamma l}$ with all

possibilities are constructed. In the [27], the error in the fixtures is assumed to be a

frequency independent constant value, which may not the fixture error function in a

realistic case.

After the error reductions of asymmetry and the fixtures impedance variations, the

remaining errors due to the manufacturing variations only exist in the insertion losses of

the left and right fixtures. If the network of the 1X fixture is losses, then there is no real

power can be delivered to the network. So in a losses network,

$$\sum_{k=1}^{N} S_{ki} S_{kj}^{*} = \delta_{ij}$$

(29)

Where $\delta_{ij} = 1$ if $i = j$ and $\delta_{ij} = 0$ if $\neq j$. In a two-port single-ended lossless

network, it means:

$$| S_{11}^{1X-Left} |^2 + | S_{12}^{1X-Left} |^2 = 1$$

(30)

In the test fixtures on a PCB with certain extend of loss, the left-hand side of Eq.

(30) is less than 1. By assuming the total loss of the 1X fixtures in the 2X-Thru and in the

Total are same, the magnitude error of $S_{12}^{1X-Left}$ is calculated in (31).

$$| \Delta S_{12}^{1X-Left} | = abs(\sqrt{| S_{11}^{1X-Left-Uncorrected} |^2 + | S_{12}^{1X-Left-Uncorrected} |^2 - | S_{11}^{1X-Left-Corrected} |^2}) - | S_{12}^{1X-Left-Uncorrected} |$$

(31)

The following error bounds calculation procedures are same as the [20]. The 2X-

Thru and Total in the Figure 19 (a) and (b) are used to examine the error bounds with and

without enforcing the error reductions. Such example is performed on the |SDD21| for simplicity, the rest s-parameters and their error bounds have similar observations as the |SDD21|. The main purpose of error reductions is to mitigate the errors from the manufacturing variations. After the error reductions, the error bounds are supposed to be tighter, which further indicates the higher accuracy of de-embedded results with enforced error reductions. The comparisons results in the Figure 19 (a) and (b) fully meet the expectations.

(a)

(b)

(c)

(d)
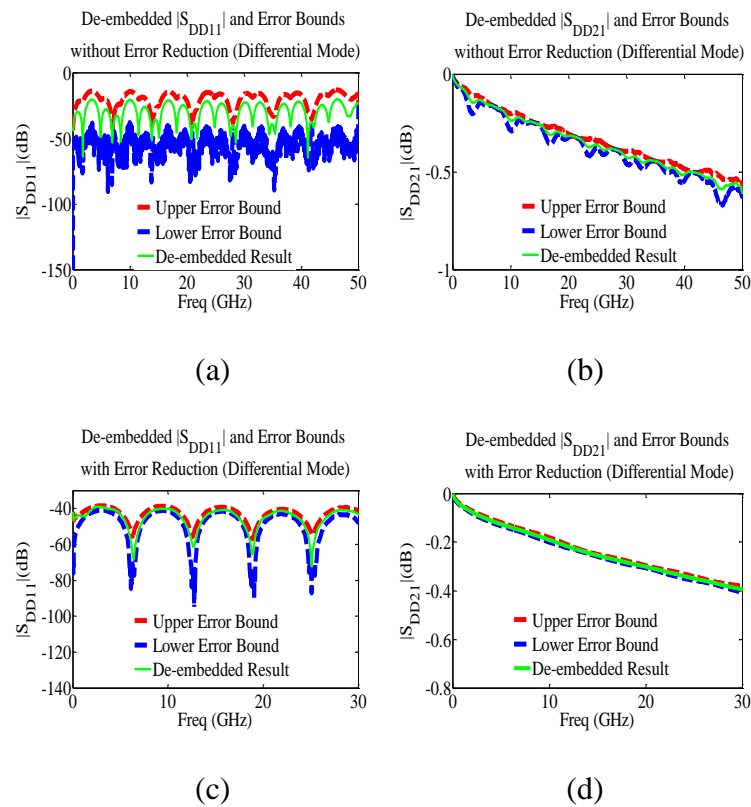
Figure 19. Differential mode de-embedded results and the error bounds: (a) |SDD11|without enforcing the error reductions; (b) |SDD21|without enforcing the error reductions; (c) |SDD11| with enforcing the error reductions; (c) |SDD21| with enforcing the error reductions.

9. VALIDATION OF ERROR REDUCTION AND SENSITIVITY

In the measurement validation, the manufactured Plug and Play (PP) test coupons from the WG 1 of IEEE P370 de-embedding committee are adopted to emphasize the importance of error reductions. These test coupons include two types of DUT. DUT 1 is an 11cm long microstrip line with a female connector and a female to male adaptor at each side, and the DUT 2 is an 11cm long waveguide structure with a female connector and a female to male adaptor at each side.
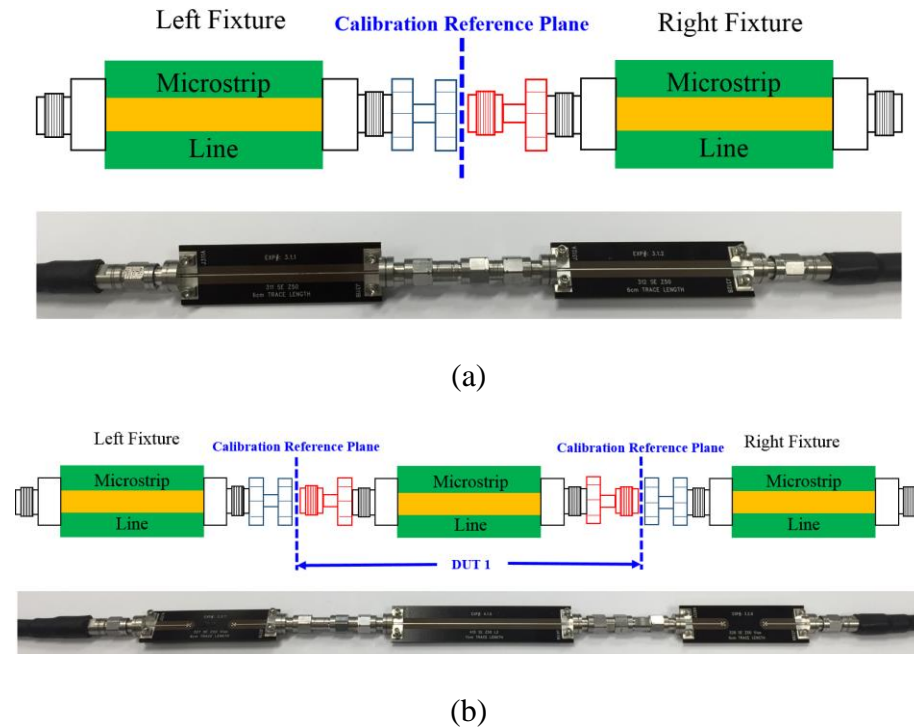
(a)

(b)

Figure 20. The manufactured Plug and Play test coupons from the IEEE P370, WG 1: (a) 2X-Thru with some extends of asymmetry; (b) DUT 1 embedded in the Total with some extends of fixture variations; (c) DUT 2 embedded in the Total with some extends of fixture variations; (d) names and symbols of connector and adaptors in the schematic; (e) the measurement setups.
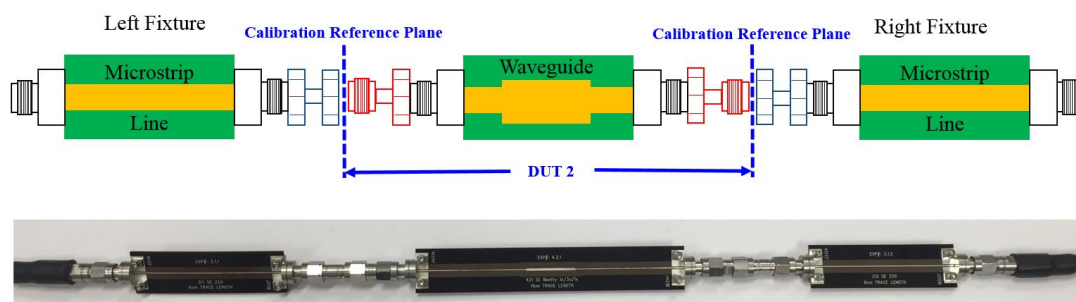
(c)
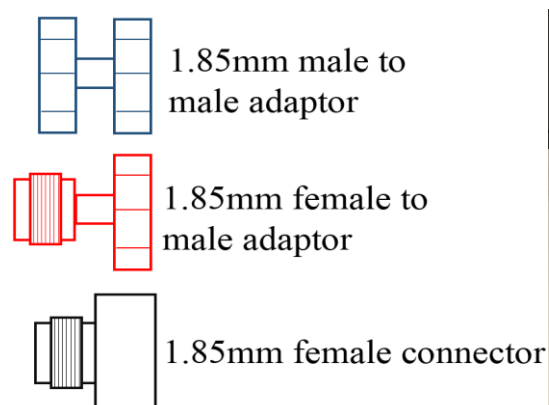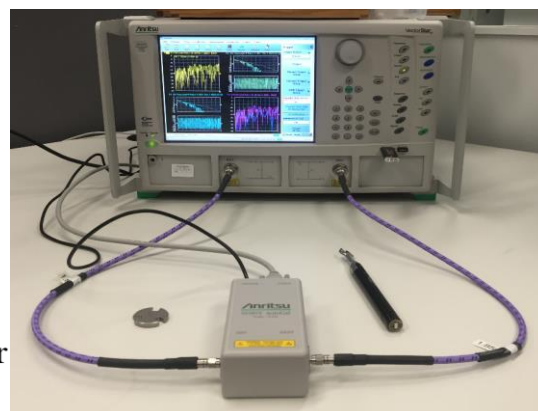
(d)   (e)

Figure 20. The manufactured Plug and Play test coupons from the IEEE P370,
WG 1: (a) 2X-Thru with some extends of asymmetry; (b) DUT 1 embedded in the Total
with some extends of fixture variations; (c) DUT 2 embedded in the Total with some
extends of fixture variations; (d) names and symbols of connector and adaptors in the
schematic; (e) the measurement setups. (cont.)

The DUT 1 and DUT 2 are embedded in the Total structures, demonstrated in the

Figure 20 (b) and (c). The 2X-Thru structure is drawn Figure 20 (a), in which left and right

fixtures are not perfectly symmetric to the calibration line. Such asymmetry is intentionally

induced by using the male to male and female to male adaptors to connect them in the 2X-

Thru. In addition, the fixture variations are implemented through using different right

fixture topology. Figure 20 (d) are the names of the connector and adaptors symbols used

in the drawing schematics. The female connectors are 1.85 mm edge mounted, and all adaptors are also 1.85 mm. The 2XTD with and without error reductions are performed on the Total 1 and Total 2 to expose the electrical performances of DUT 1 and DUT 2, respectively. The golden standards in the comparisons are the direct measurement of DUT 1 and DUT 2, as they are attached with 1.85 mm female coaxial connectors.

(a)

(b)

(c)

(d)

Figure 21. DUT comparisons on the IEEE P370 test coupons between golden standard and de-embedded results: (a) |S11| of DUT 1; (b) |S21| of DUT 1; (c) |S22| of DUT 1; (d) |S11| of DUT 2; (e) |S21| of DUT 2; (f) |S22| of DUT 2;(g) TDR characteristic impedance of DUT 2; (h) TDR characteristic impedance of DUT 2.

De-embedded DUT 2 |S_{21}| Comparison

De-embedded DUT 2 |S_{22}| Comparison

(e)

(f)

TDR Characteristic Impedance Comparison of DUT 1

TDR Characteristic Impedance Comparison of DUT 2

(g)

(h)
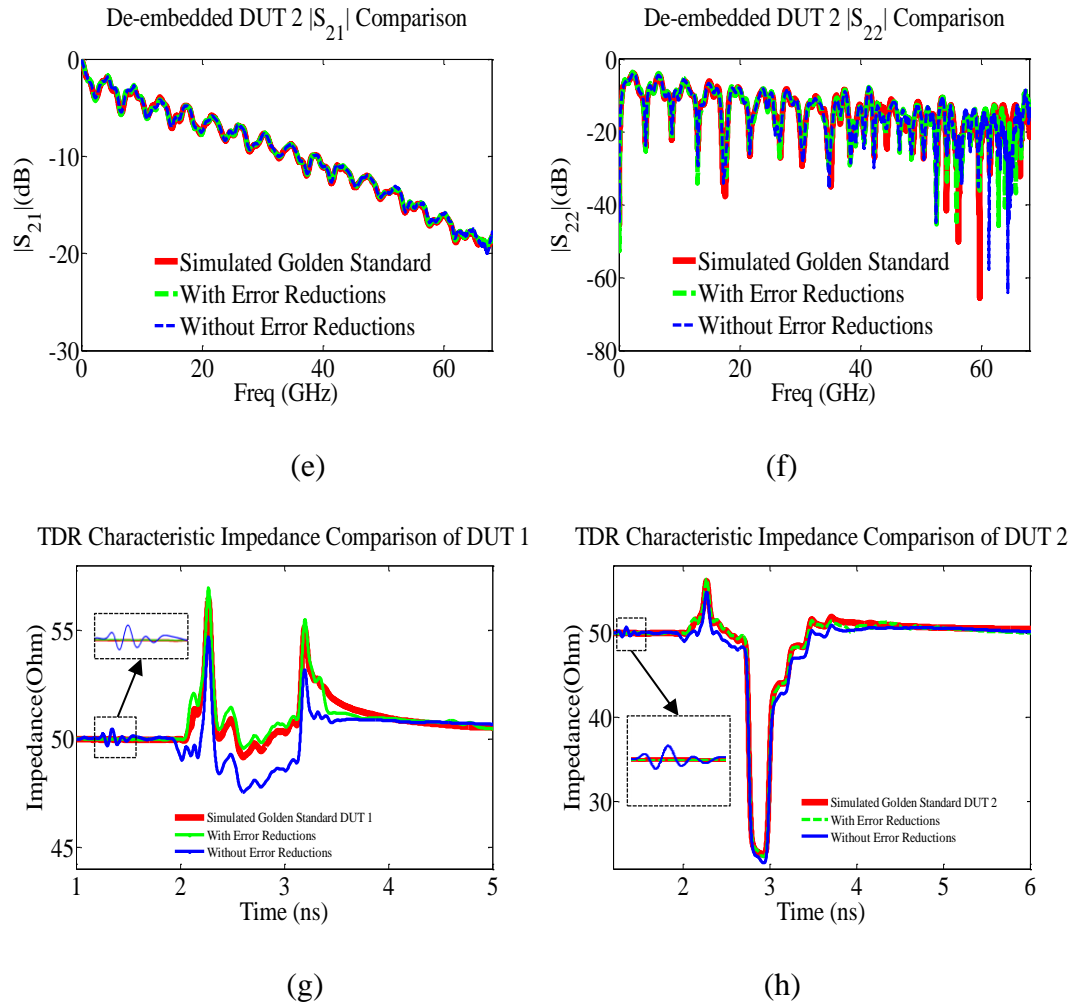
Figure 21. DUT comparisons on the IEEE P370 test coupons between golden standard and de-embedded results: (a) |S11| of DUT 1; (b) |S21| of DUT 1; (c) |S22| of DUT 1; (d) |S11| of DUT 2; (e) |S21| of DUT 2; (f) |S22| of DUT 2;(g) TDR characteristic impedance of DUT 2; (h) TDR characteristic impedance of DUT 2.(cont.)

The comparisons between the de-embedded S-parameters and the measurement golden standards may not be easily to distinguish the advantage of the error reductions. However, in the TDR comparisons of both DUT 1 and DUT 2, without the error reductions, larger discrepancies exist between the de-embedded result and the golden standard in both

cases. Furthermore, as zoomed out in the (g) and (h) of Figure 21, the non-causal effects

happened on both TDRs without error reductions.

REFERENCES

J. Song, F. Ling, G. Flynn, W. Blood, and E. Demircan., "A De-embedding Technique for Interconnects," in *Electronic Performance Electronic packaging*, 2001, pp.129-132.

Luuk F. Tiemeijer, R .J. Havens., " A Calibrated Lumped-Element De- embedding Technique for On-Wafer RF Characterization of High-Quality Inductors and High-Speed Transistors," in *IEEE Trans. On Electron Devices*, vol. 50, pp.822-829, March 2003.

A. Mangan, S.P. Voinigescu, M. Yang, and M. Tazkauanu., " De-embedding Transmission Line Measurement for Accurate Modeling of IC Designs," in *IEEE Trans. On Electron Devices*, vol. 53, pp.235-241,Feb. 2006.

R. Lane., "De-embedding Device Scattering Parameters," *Microwave Journal*, vol. 27, pp. 149-156, Aug. 1984.

G. F. Engen, "Calibration technique for automated network analyzers with application to adapter evaluation," *IEEE Trans. Microwave Theory and Technology*, vol. 22, pp. 1255–1260, Dec. 1974.

R. W. Beatty, G. F. Engen, and W. J. Anson., "Measurement of Reflections and Losses of Waveguide Joints and Connectors Using Microwave Reflect-meter Techniques." *IRE Trans. Instrum*., vol. 9, no. 2, pp. 219–226, Sep.1960.

Lingyun Ye, Caixia Li, Xinglin Sun, Shuai Jin, Bichen Chen, Xiaoning Ye, Jun Fan., "Thru-Reflect-Line Calibration Technique: Error Analysis for Characteristic Impedance Variations in the Line Standards," *IEEE Transactions on Electromagnetic Compatibility*, vol.PP, Dec. 2016.

H. Cho and D. Burk, "A three step method for the de-embedding of high frequency S-parameters measurements," in *IEEE Trans. Electron Devices*, vol. 38, pp. 1371–1375, June 1991

Bichen Chen, Xiaoning Ye, Bill Samaras,Jun Fan, "A Novel De-Embedding Method Suitable for Transmission-Line Measurement," *IEEE Asia-Pacific Symposium on Electromagnetic Compatibility,* May 25-29, 2015

Bichen Chen, Mikheil Tsiklauri, Chunyu Wu, Shuai Jin, Jun Fan, Xiaoning Ye, Bill Samaras., "Analytical and numerical sensitivity analyses of fixtures de-embedding," in *Electromagnetic Compatibility (EMC), 2016 IEEE International Symposium.*

Chunyu Wu, Bichen Chen, Tsiklauri Mikheil, Xiaoning Ye, Jun Fan., " error bounds analysis of de-embedded results in 2x Thru de-embedding methods" in *Electromagnetic Compatibility (EMC),* 2017 *IEEE International Symposium.*

Xiaoning Ye, Jun Fan, Bichen Chen, James L. Drewniak, Qinghua Bill Chen, "accurate characterization of pcb transmission lines for high speed interconnect" in *2015 Asia-Pacific Symposium on Electromagnetic Compatibility (APEMC).*

D. E. Bockelman and W. R. Eisenstadt., "Combined differential and common-mode scattering parameters: Theory and simulation," *IEEE Trans. Microwave Theory and Technology*, vol. 43, no. 7, pp. 1530–1539, Jul. 1995

David E.Bockelman., "Pure-Mode network Analyzer for On-Wafer Measurements of Mixed-Mode S-Parameters of Differential Circuits" *IEEE Trans. Microwave Theory and Technology*, Vol. 45, No.7, pp.1071-1077, July 1997.

A. Ferrero and M. Pirola., "Generalized mixed-mode S- parameters *IEEE Trans. Microwave Theory and Technology*, vol. 54, no. 1, pp. 458–463, Jan.2006.

W. Fan., "Mixed-Mode S-Parameter Characterization of Differential Structures" *5th Electronic Packaging Technology Conference*, Maui, Hawaii, July 2003, pp. 533-537.

K.M. Ho, K. Vaz, and M. Caggiano, "Scattering Parameter Characterization of Differential Four-port Networks Using a Two-port Vector Network Analyzer," in *Proc. 2005 Electron. Components Technol. Conf.,*2005, pp.1846–1853.

A. G. Chiariello, A. Maffucci, G. Miano, F. Villone, and W. Zamboni,"A Transmission Line Model for Full-wave Analysis of Mixed-mode Propagation," *IEEE Trans. Adv. Packag.*, vol. 31, no. 2, pp. 275–284 ,May2008.

Bichen Chen, Muqi Ouyang, Shaohui Yong, Yansheng Wang,Yadong Bai,Yan Zhou, Jun Fan., "Integrated Crosstalk Noise (ICN) Analysis among Multiple Differential BGA and Via Pairs by Using Design of Experiments (DoE) Method," in *Electromagnetic Compatibility (EMC), 2017 IEEE International Symposium.*

Bichen Chen, Junda Wang, Ying S.Cao, Muqi Ouyang, Yansheng Wang, Shuai Jin, Xusheng Liu, Xiping Peng, Jun Fan, "Differential Integrated Crosstalk Noise (ICN) Mitigation in the Pin Field Area of SerDes Channel, " *Electromagnetic Compatibility (EMC), 2018 IEEE International Symposium.*

Stephen H. Hall; Howard L. Heck, "Appendix B: FourPort Conversions between T and S Parameters," in Advanced Signal Integrity for High-Speed Digital Designs ,Wiley-IEEE Press, 2009, pp.641-643

II. A NOVEL SMART FIXTURE DE-EMBEDDING (SFD) METHOD BY USING 1X-REFLECTION CALIBRATION STANDARD

B.Chen

Department of Electrical Engineering

Missouri University of Science and Technology

Rolla, Missouri 65409–0050

Tel: 347–856–7895

Email: bcpr8@mst.edu

ABSTRACT

With successively growing operating frequency and shrinking device size, accurate S-parameter measurements are quintessential in designing and verifying characterizations of these devices. Because of measurement features, demanding devices under test (DUT) are customarily embedded into test fixtures to allow pre-requisite interfaces for measurement probes via interconnects. Therefore, de-embedding is an indispensable process for obtaining requested S-parameters of the targeted DUT, in which a typical example is modern multiple vector network analyzers (VNA) to perform calibration by removing unnecessary test fixtures. Modeling equivalent lumped circuit [1]-[2] and equivalent networks [3]-[4] are two research mainstreams in the previous de-embedding topic. Recent output state-of-the-art de-embedding methods focused on reducing the complexity of calibrations, yet maintaining the accuracy of results.

1. INTRUDUCTION

Commercially available calibration and de-embedding techniques, such as the classic thru-reflect-line (TRL), load-reflect-match (LRM), line-reflect-line (LRL), thru-reflect-match (TRM) [5], and short-open-load-thru (SOLT)[6], as well as the novel 2X-thru[42]-[45] are widely used in characterizing electrical performances of devices under test (DUTs).

The comprehensive SOLT, in which the classic 12-term error model is applied, uses short, open, load, and thru as the calibration standards. It requires a 'thru' connection or a network which S-parameters must completely be known. If a reciprocal, but unknown two-port network replaces the known 'thru', such a model is reduced to a seven-term error one. Furthermore, if the fixtures are designed as reciprocal and passive, a three-error term model is conducted to solve the unknowns in the test fixtures. The test fixtures in SOLT standards are assumed to be exactly the same as those in the total structure in which the DUT is embedded.

TRL calibration uses the zero length thru, reflect (short, or open), and line standards to remove the test fixtures, while LRM, LRL, and TRM are the derivatives of TRL. There are also certain restrictions in the TRL calibration family, which include: 1) characteristic impedances and propagation constants among the thru and line standards are required to be identical; 2) broad-frequency coverage requires multiple line standards; 3) the interconnects in the thru, reflect, and line standards are assumed to be identical.

The prevailing 2X-thru method dramatically reduces the complexity of fixture de-embedding by using a zero length thru standard only. The 2X-thru method relies on very practical assumptions, such as symmetric and reciprocal 2X-thru fixtures. By taking advantage of the time-domain channel characterization (TCC), the 2X-thru method acquires one of the unknowns from time domain. Despite the simplicity of the method, the disadvantages of 2X-thru include: 1) asymmetry of 2X-thru; 2) fixtures differences due to the manufacturing variations.

The proposed 1X-Reflection SFD in this paper addresses the issues mentioned above by utilizing the 1X-reflection terminated with either open or short to accurately remove the reciprocal and passive fixture effects. Compared to traditional TRL, the 1X-reflection SFD also significantly reduces the number of calibration structures, yet maintains the accuracy of de-embedded results without multiple line standards. Compared with 2X-thru SFD, the calibration pattern in the 1X-reflection SFD only requires a half-length of the 2X-thru. The overall advantage of 1X-reflection SFD is extremely suitable for applications with limited design space, and applications with high manufacturing variations or de-embedding sensitivities [7]-[8]. In addition, the multi-port 1X-reflection SFD is based on the mixed-mode S-parameters (MMS) concept, to de-embed the test fixtures in the even and odd modes separately.

2. 1X-REFLECTION SFD THEORY

By connecting one end to the coaxial port of vector network analyzer (VNA), while terminating the other end either open or short, the 1X-reflection SFD requires the reflection measurement only as depicted in Figure 1.
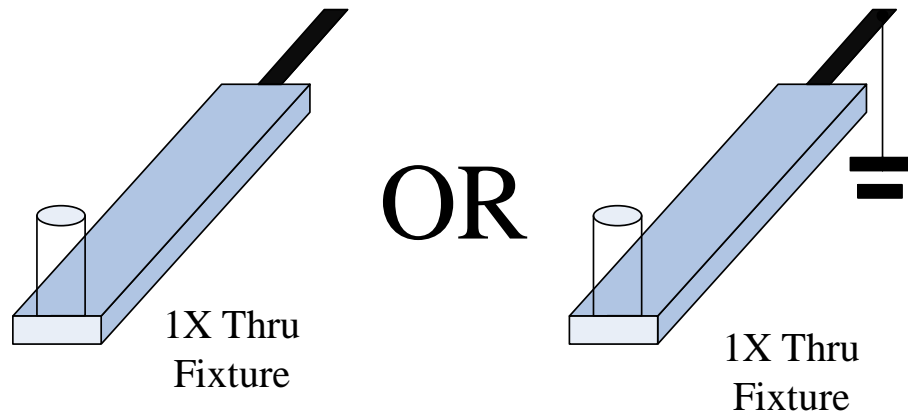
Figure 1. 1X-Reflection SFD calibration patterns.

The 1X-reflection SFD assumes that fixtures are reciprocal and passive, which reduces the number of unknowns to only three.

2.1. ONE-PORT, 3-TERM ERROR MODEL

The 1X-reflection SFD algorithm is derived from the three-term error model (shown in Figure 2 (a)). As mentioned in the introduction, the 3-term error model is simplified from the 12-term model (shown in Figure 2 (b)) by assuming the fixture is reciprocal and passive, crosstalk leakage term is zero, and neither forward nor reverse flow changes the port match condition [9].

(a)

(b)
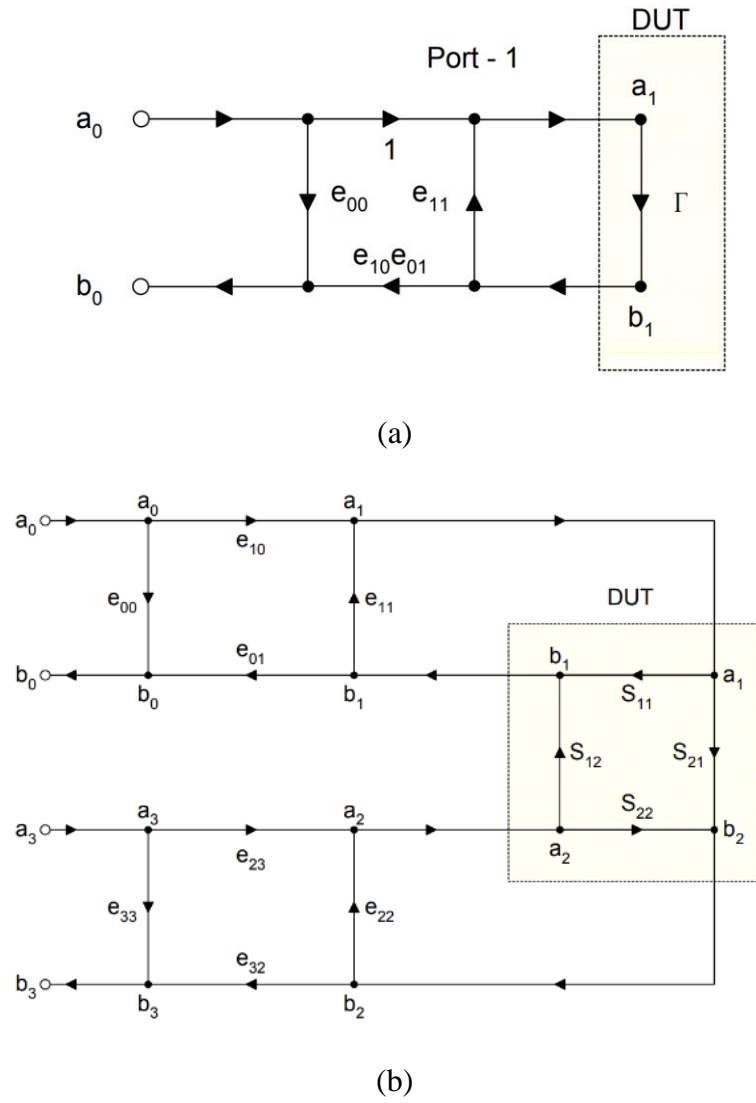
Figure 2. Flow graph of error models: (a) one-port three-term error; (b) two-port 12-term error.

In the one-port, three-term error model, the e_{00} is the directivity, the e_{11} is the port match, and the ($e_{10}e_{01}$) is the tracking. Solving the one-port, three-term error problem is to find the linear relationship between the actual and measured reflection coefficients. The three unknown errors are determined by measuring three known independent standards,

such as 'short', 'open', 'load'. The measured and actual reflection coefficients are related

as:

$$\Gamma_M = \frac{b_0}{a_0} = \frac{e_{00} - \Delta_e \Gamma_A}{1 - e_{11} \Gamma_A} \qquad (1)$$

Where

$$\Delta_e = e_{00} e_{11} - (e_{10} e_{01}) \qquad (2)$$

The linear form of (1) is characterized as:

$$e_{00} + \Gamma_M \Gamma_A e_{11} - \Gamma_A \Delta_e = \Gamma_M \qquad (3)$$

Despite the ideal coefficients of Γ_A for 'open', 'short', and 'load' are 1,-1,and 0, the

manufacturing process usually adds parasitic, variations, and uncertainties to these

standards. Rigorously, when solving one-port SOL in (3), all the non-ideal effects should

be considered individually on each standard due to the randomness in the manufacturing

process.

2.2. TIME DOMAIN CHANNEL CHARACTERIZATION

In the 1X-reflection SFD, the 'open' or 'short' standard provides only one linear

equation. Thus, two additional independent linear equations are necessary to characterize

the electrical performance of the test fixtures. The general procedure of additional

equations acquisition is performed by TCCR and depicted in Figure 3.

```
┌─────────────────────────────────────┐
│      Reflection s-parameters         │
│    to TDR waveform transformation    │
└─────────────────────────────────────┘
                  ⇓
┌─────────────────────────────────────┐
│         Additional TDR               │
│      waveforms reconstruction        │
└─────────────────────────────────────┘
                  ⇓
┌─────────────────────────────────────┐
│      Additional TDR waveforms        │
│    to s-parameters transformation    │
└─────────────────────────────────────┘
```
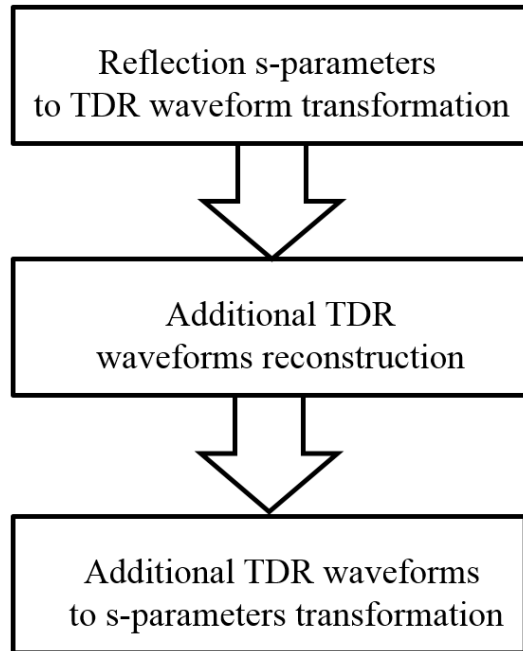
Figure 3. Flowchart of TCCR procedure.

There are two ways of finding time-domain responses from frequency characteristics. One is inverse discrete Fourier transform (IDFT) and the other is complex pole fitting with direct time-domain computation. IDFT is the commonly used method to acquire the TDR from return loss. However, the drawback of IDFT is when over sampling, the wrong steady state is reached; yet when the down sampling causality issue appears at the TDR response, without performing improvements on the IDFT method, the TCCR procedure introduces errors. The improvements include rotating the non-causal portion of time domain response and appending to the right end. The second approach is to fit a sample of the frequency-domain function and are represented in a form of rational fraction expansion (RFE), that the coefficients and poles of the summands are complex conjugate pairs:

$$H(s) = H_\infty + \sum_{m=1}^{M} \frac{A_m}{1 + \dfrac{s}{a_m}} \tag{4}$$

Thus, the unit step response is:

$$a(t) = [H_\infty + \sum_{m=1}^{M} A_m - \sum_{m=1}^{M} A_m e^{-\alpha_m t}] \, for \quad t \geq 0 \tag{5}$$

The RFE has the advantage due to it is a complete and causal representation of a linear system. Generally, the TDR waveform consists an incident wave $V^+(t)$, and a reflected wave $V^-(t)$ in the time domain as (6):

$$V_{TDR} = V^+(t) + V^-(t) \tag{6}$$

The typical TDR responses of the same 1X fixture terminated with open, short, and load are plotted in Figure 4 (a). To mimic the actual scenario, the 1X-reflection fixture is designed as a 1-inch transmission line cascaded with discontinuities as shown in Figure 4 (b).

(a)   (b)
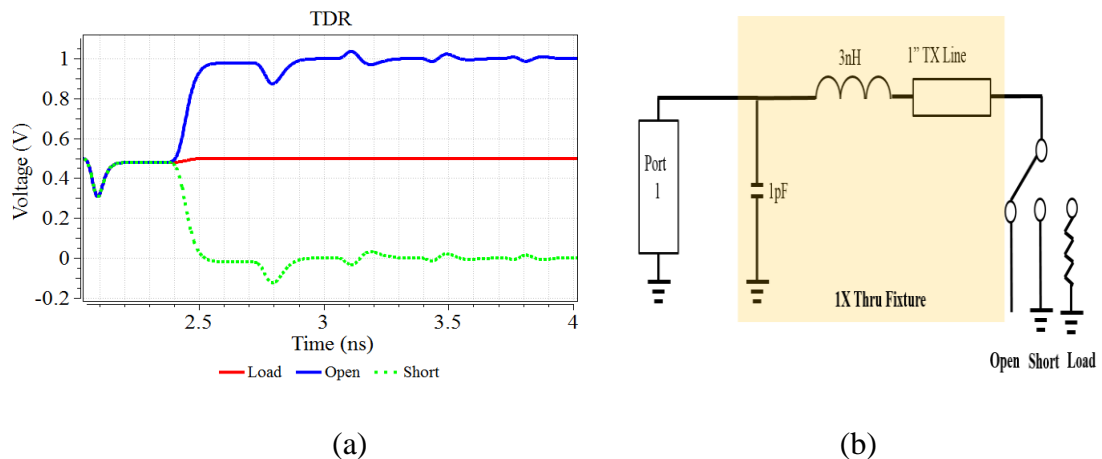
Figure 4. An example of TDR response from s-parameter input: (a) 1X-reflection TDR response with SOL terminations; (b) the corresponding 1X-reflection circuit diagram.

Despite the ideal voltages of open, short, and load TDR are V_{TDR}, 0, and 0.5 V_{TDR}, due to the discontinuities, the multiple reflections propagate into the responses as Figure 4 (a) illustrates. The time domain responses before T_d are same in each termination but behave differently after T_d. The required termination in the 1X-reflection SFD is either open or short, while the other two standards are calculated from TCCR. Table 1 demonstrates the details of reconstructing short from open, and the reversed procedure (where n=0,1,2,3…). The load reconstruction from open or Short is performed by three steps: 1) cutting the TDR wave form at T_d; 2) extending the transmission line by assuming the matched impedance at port 2; 3) renormalizing the port impedance at the port 2 side. The full S-parameter matrix of 1X-thru is acquired after the TCCR procedure.

Table 1. Time domain waveform reconstruction between open and short

	Open→Short	Short →Open
0~T_d	Keep the same	Keep the same
(2n+1)T_d~(2n+2)T_d	Flip the Open, and minus 1	Flip the Short, and plus 1
(2n+2)T_d~(2n+3)T_d	Open minus 1	Short plus 1

2.3. 1X-REFLECTION DESIGN CRITERIA

Discontinuity elements such as BGA and Vias are inevitable in the 1X fixture designs. However, the proposed method does not allow the open or short directly terminated discontinuities, which is a similar requirement of the 2X-thru de-embedding method [44]. A segment of transmission line is required in between the discontinuities

and terminations as depicted in Figure 5 (a), otherwise errors will be introduced in the

TCCR procedure.
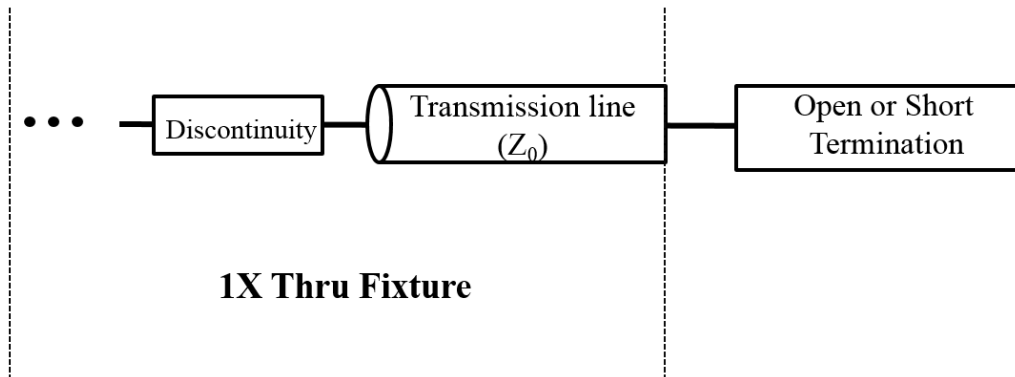
(a)
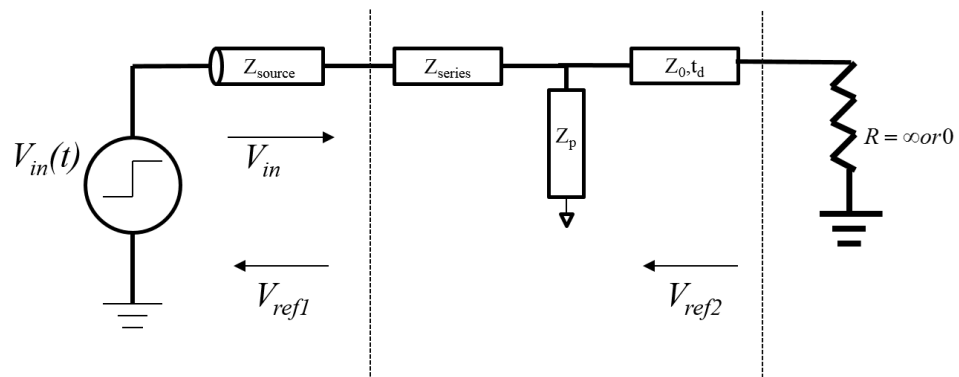
(b)

Figure 5. A transmission line in between discontinuity and termination in the 1X-Reflection fixture design (a) design requirement; (b) reflected waveforms from discontinuities.

The length of the transmission line segment is determined by the two reflected waveforms at the discontinuities, as Figure 5 (b) depicts. As derived in [44], the length of this transmission line is determined by timescale as well as the effective dielectric constant as:

$$Length > \frac{v_c T_{scale}}{2\sqrt{\varepsilon_{eff}}} \tag{7}$$

The timescale T_{scale} is defined as the stabilization time of fluctuated voltage caused by the first reflected TDR waveform. The algorithm requires the T_{scale} stabilizes before the center of the first and second reflected TDR waveform as described in (7). The 2X-thru de-embedding is originated from (8) and (9):

$$S_{11}^{2X} = S_{11}^{1X} + \frac{\left(S_{21}^{1X}\right)^2 S_{22}^{1X}}{1-\left(S_{22}^{1X}\right)^2} \tag{8}$$

$$S_{12}^{2X} = S_{21}^{2X} = \frac{\left(S_{21}^{1X}\right)^2}{1-\left(S_{22}^{1X}\right)^2} \tag{9}$$

The relationships between proposed 1X-reflection SFD and original 2X-thru SFD are able to be connected by rewriting (8) and (9) as (10) and (11):

$$S_{11}^{2X} + S_{21}^{2X} = S_{11}^{1X} + \frac{\left(S_{21}^{1X}\right)^2}{1-S_{22}^{1X}} = Open \tag{10}$$

$$S_{11}^{2X} - S_{21}^{2X} = S_{11}^{1X} + \frac{\left(S_{21}^{1X}\right)^2}{-1-S_{22}^{1X}} = Short \tag{11}$$

Eq. (10) and (11) have the exact format as (1) and are able to be characterized as open and short. As the TCCR in the 1X-reflection SFD only requires T_{scale} to stabilize before the termination, the requirement of length of the transmission line segment is half of (7).

2.4. PASSIVITY RULE

Passivity means a system does not generate energy. In the fixture characterization procedure of de-embedding, S-parameters are used to represent the physical components of the connectors, adaptors, cables, and transmission line, none of which generate energy. Therefore, if the characterized S-parameters are shown to be non-passive, either the VNA was not calibrated correctly or the underlying assumption of the fixture characterization is wrong. The rule of passivity in the 2X-thru was discussed in [44] and defined in (12). By taking advantage of (10)-(12), the passivity rule of the 1X-reflection SFD is further derived in (13).

$$\left| \frac{S_{11}^{2X}}{S_{21}^{2X}} \right| = \left| \frac{S_{22}^{2X}}{S_{21}^{2X}} \right| < 1 \tag{12}$$

$$\left| S_{21}^{1X} \right| > \sqrt{\left(\left| S_{11}^{1X} \right| \right) \times \left(1 + \left| S_{22}^{1X} \right| \right)} \tag{13}$$

2.5. MULTI-PORT 1X-REFLECTION SFD

In [50], the methodology of four-port fixture characterization and de-embedding was reviewed first, followed by eight-port fixture characterization and de-embedding derivation. In the eight-port fixture characterization, the concept of second-order mixed-

mode S-parameters matrices was proposed. The idea in [50] is valid to extend to fixture characterization with any even number of ports. The requirement of using mixed-mode S-parameters to perform the fixture characterization is the balanced design. Such a theory is also suitable for the 1X-reflection SFD.

By using a 1X-reflection calibration pattern of 'open' as depicted in the Figure 6, the TCCR is performed on the first order differential mode and common mode of such fixture separately. Such fixtures actually have four ports, in which Port 1 and 3 are the physical ports with incident and reflect waves, while Port 2 and 4 have open termination.

Fixture A
(1st order differential mode and common mode)
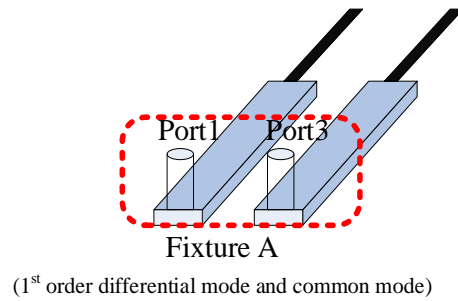
Figure 6. Example of a two-port 1X-reflection calibration pattern.

The single-ended S-parameter matrix of this 1X-reflection calibration pattern is characterized as (12-1), and simplified as (12-2):

$$
\begin{bmatrix} b_1 \\ 0 \\ b_3 \\ 0 \end{bmatrix} = \begin{bmatrix} S_{11} & 0 & S_{13} & 0 \\ 0 & 0 & 0 & 0 \\ S_{31} & 0 & S_{33} & 0 \\ 0 & 0 & 0 & 0 \end{bmatrix} \times \begin{bmatrix} a_1 \\ 0 \\ a_3 \\ 0 \end{bmatrix}
\tag{12-1}
$$

$$\begin{bmatrix} b_1 \\ b_3 \end{bmatrix} = \begin{bmatrix} S_{11} & S_{13} \\ S_{31} & S_{33} \end{bmatrix} \begin{bmatrix} a_1 \\ a_3 \end{bmatrix} \tag{12-2}$$

In (12-3) and (12-4), single-ended incident and reflect waves are transferred to the

mixed-mode incident and reflect waves through transfer matrix m $= \frac{1}{\sqrt{2}} \begin{bmatrix} 1 & -1 \\ 1 & 1 \end{bmatrix}$. Thus,

when balanced 1X-reflection calibration pattern is designed, the first order differential and

common modes reflection coefficients are calculated in (12-5).

$$\begin{bmatrix} a_{d1} \\ a_{c1} \end{bmatrix} = \frac{1}{\sqrt{2}} \begin{bmatrix} 1 & -1 \\ 1 & 1 \end{bmatrix} \begin{bmatrix} a_1 \\ a_3 \end{bmatrix} + \begin{bmatrix} 0 & 0 \\ 0 & 0 \end{bmatrix} \begin{bmatrix} a_2 \\ a_4 \end{bmatrix} \tag{12-3}$$

$$\begin{bmatrix} b_{d1} \\ b_{c1} \end{bmatrix} = \frac{1}{\sqrt{2}} \begin{bmatrix} 1 & -1 \\ 1 & 1 \end{bmatrix} \begin{bmatrix} b_1 \\ b_3 \end{bmatrix} + \begin{bmatrix} 0 & 0 \\ 0 & 0 \end{bmatrix} \begin{bmatrix} b_2 \\ b_4 \end{bmatrix} \tag{12-4}$$

$$\begin{bmatrix} \Gamma_{dd} & 0 \\ 0 & \Gamma_{cc} \end{bmatrix} = m \times \begin{bmatrix} S_{11} & S_{13} \\ S_{31} & S_{33} \end{bmatrix} \times m^{-1} \tag{12-5}$$

For the higher even number of ports in 1X-reflection applications, the reflection

coefficients are able to be developed by using the idea in [6].

3. VALIDATION OF 1X-REFLECTION SFD BY USING SIMULATION AND MEASUREMENT

In this section, the 1X-reflection SFD algorithm is examined by comparing the

extracted test fixture from calculation and a full-wave simulated golden standard first,

followed by a measurement example on a printed circuit board (PCB). TRL, 2X-thru SFD,

and 1X-reflection SFD calibration patterns are manufactured on the PCB, and results

comparison is conducted. The third example in this chapter is a cable de-embedding

application, which demonstrates the uniqueness of the 1X-reflection SFD that shows the other de-embedding methods are not suitable.

3.1. VALIDATION OF 1X-REFLECTION SFD IN FULL-WAVE SIMULATION

Figure 7 (a) shows the full-wave mode of 1X-reflection SFD calibration pattern terminated with open. The other side of the structure is terminated with a wave port. The simulation result is used to calculate the full S-parameter matrix of this 1X-thru fixture. The TDR response of this calibration pattern is shown in Figure 7 (c). The gold standard $|S_{11}|$ and $|S_{21}|$ of the 1X-thru fixture from the separate simulation are plotted in Figure 7 (b).

(a)   (b)

(c)
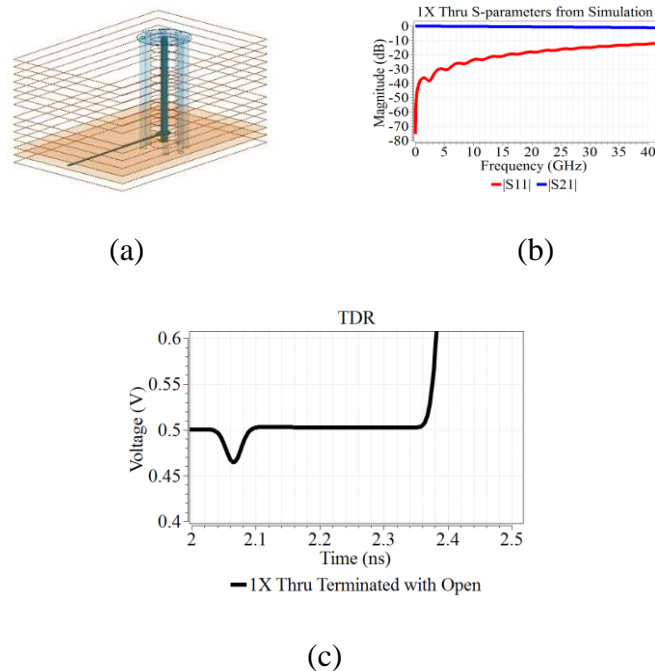
Figure 7. (a) full-wave mode of 1X-reflection; (b) $|S_{11}|$ and $|S_{21}|$ of 1X-thru fixture from simulation; (c) TDR of 1X-reflection terminated with open.

The model satisfied the design criteria in (7) and the passivity rule in (13). Figure 8 shows the 1X-reflection SFD results, compared with the simulation gold standards. Both $|S_{11}|$ and $|S_{21}|$ have less than 1% errors. The inaccuracies are from the processing data in both frequency and time domains, and also from the time domain manipulations.

(a)

(b)

(c)

(d)
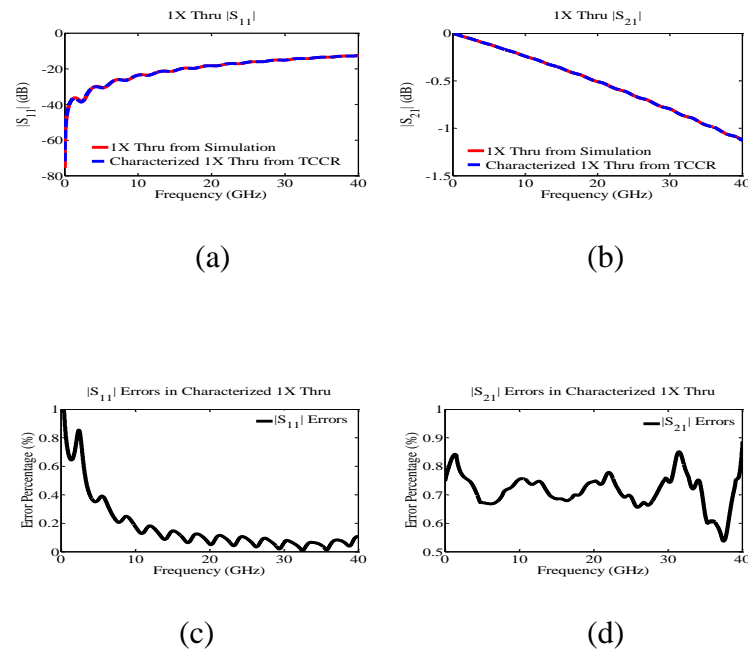
Figure 8. Fixture characterization results verification: (c) Error percentage of $|S_{11}|$; (d) Error percentage of $|S_{21}|$.

3.2. VALIDATION OF 1X-REFLECTION SFD ON A MANUFACTURED TEST COUPON

A test coupon was manufactured to compare the de-embedding results of TRL, 2X-thru SFD and 1X-reflection SFD on the same DUTs. Because of the bandwidth limitation, the TRL requires six calibration standards, indicated in Figure 9 (a). There are two different

DUTs on the coupon, as demonstrated in Figure 9 (b). The Total 1 embedded the DUT 1 of an 8-inch long transmission line, while DUT 2 is an 8 inch long waveguide structure with variable width. Table 2 lists the details of the calibration patterns.

(a)
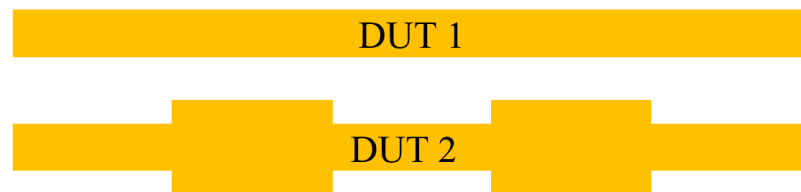
(b)

Figure 9. (a) A manufactured test coupon, with calibration patterns for TRL (highlighted in yellow), 2X-thru (highlighted in blue) and 1X-reflection (highlighted in red). (b) Two different DUTs embedded in the Total 1 and Total 2.

In the original TRL design [7], authors limited a single pair of lines to between $20°$ and $160°$. Thus multiple lines are required in the design to cover the entire frequency range, as Table 2 describes. Mathematically, TRL has no solution when $\alpha = \beta = 0$. In the lossless cases ($\alpha = 0$), the $\beta = 0$ when phase arrives at $0°$ and $\pm 180°$. The expected error at the band edges is approximately 2.92 times greater than at the optimal ($90°$) point. The thru and reflection work for the entire frequency range in the TRL test coupon, and is also suitable for 2X-thru and 1X-reflection de-embedding.

Table 2. Calibration standard details

Trace	Start Frequency	Stop Frequency	Length
Thru	10 MHz	20 GHz	2000 mil
Open	10 MHz	20 GHz	1000 mil
Load	10 MHz	281.2 MHz	1000 mil
Line 1	281.2 MHz	1.44 GHz	3758.4 mil
Line 2	1.44GHz	12.96 GHz	2195.4 mil
Line 3	12.96 GHz	20 GHz	2021.7 mil
Total 1	10 MHz	20 GHz	8000 mil TX-Line
Total 2	10 MHz	20 GHz	8000 mil waveguide
Thru_2	10 MHz	20 GHz	2000 mil
Open_2	10 MHz	20 GHz	1000 mil
Load_2	10 MHz	281.2 MHz	1000 mil
Line 1_2	281.2 MHz	1.44 GHz	3758.4 mil
Line 2_2	1.44GHz	12.96 GHz	2195.4 mil
Line 3_2	12.96 GHz	20 GHz	2021.7 mil
Total 1_2	10 MHz	20 GHz	8000 mil WG
Total 2_2	10 MHz	20 GHz	8000 mil WG

The de-embedded results of TRL, 2X-thru SFD, and 1X-reflection SFD are compared in the Figure 10 (a)-(d), where (a) and (b) are $|S_{11}|$ and $|S_{21}|$ of DUT 1, and (c) and (d) are $|S_{11}|$ and $|S_{21}|$ of DUT 2.
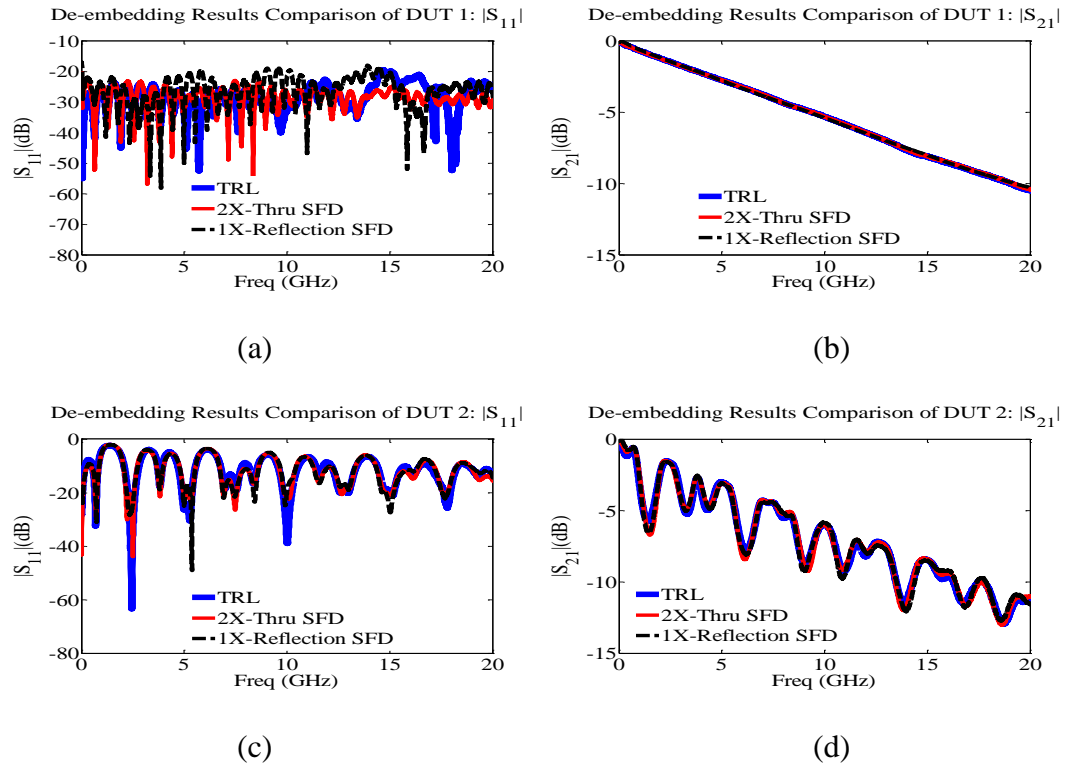
Figure 10. De-embedded results comparison: (a) $|S_{11}|$ of DUT 1; (b) $|S_{21}|$ of DUT 1; $|S_{11}|$ of DUT 2; $|S_{21}|$ of DUT 2.

The error correction feature of 1X-reflection de-embedding mitigates the de-embedding errors due to the manufacturing variations by substituting the major discrepancies of time domain 1X-reflection before the TCCR procedure. The error correction feature is also able to be extended to the 2X-thru SFD and the classical SOLT and TRL. The detail of error correction on de-embedding will be discussed in a separate paper. Figure 11 shows the TDR characteristic impedance differences of 1X-reflection standard and the actual to-be-removed fixtures in the Total 1 and 2.
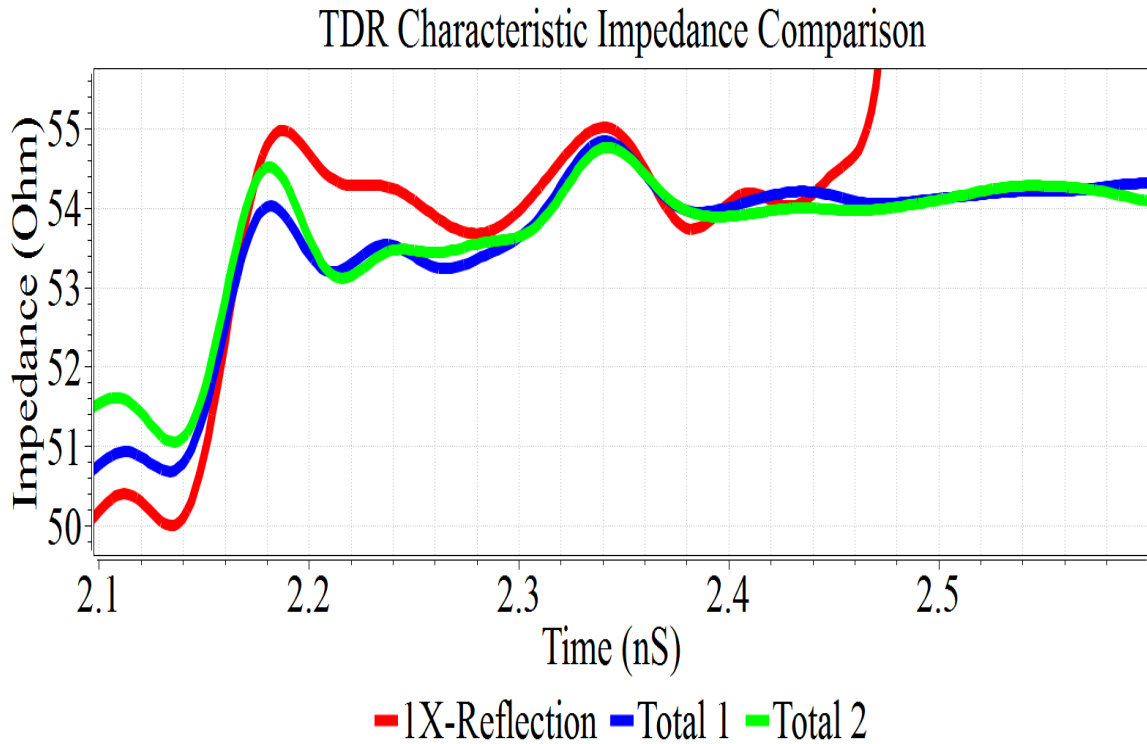
Figure 11. The characteristic impedance of 1X-reflection and the actual 1X- fixtures in the Total 1 and 2.

The TDR characteristic impedance results of 1X-reflection SFD with and without the fixture error correction are compared in Figure 12 (a) and (b) for DUT 1 and DUT 2, respectively. There is a 2 ns 50 Ohm ideal transmission line delay in front of the actual DUT. As observed, without fixture error correction, the de-embedded DUT 1 and DUT 2 have a non-causal time-domain response which is created by the de-embedding procedure when there are manufacturing variations. As a consequence, with the enforced fixture error correction, the non-casual effect is removed.
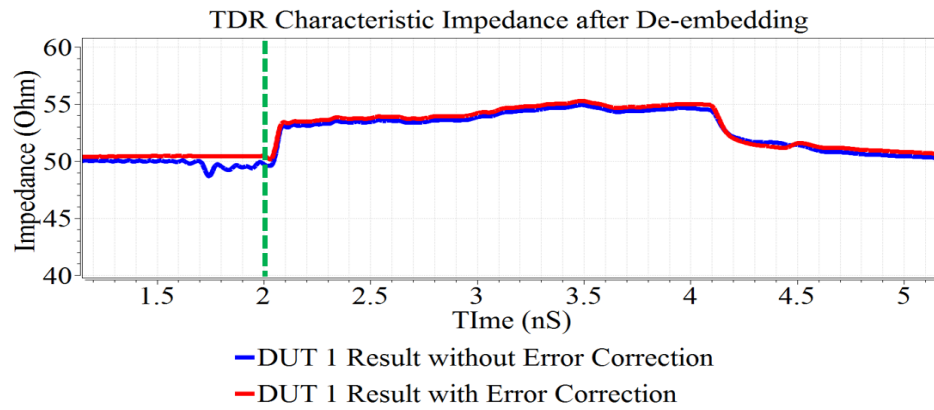
(a)
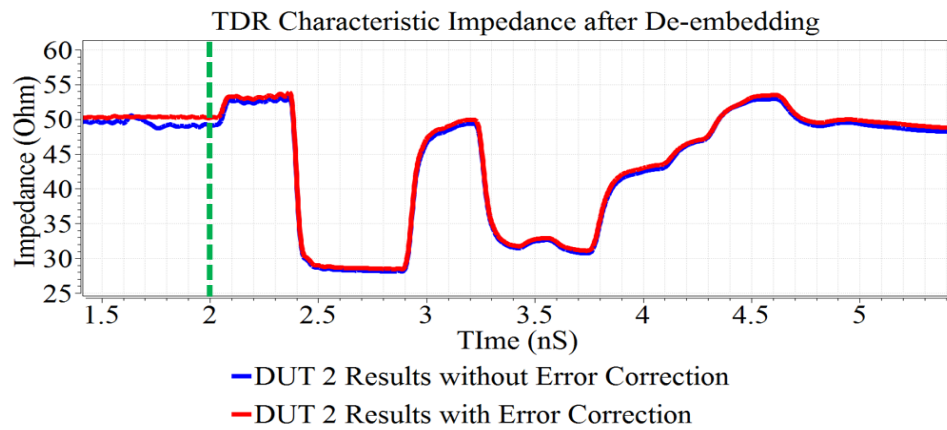
(b)
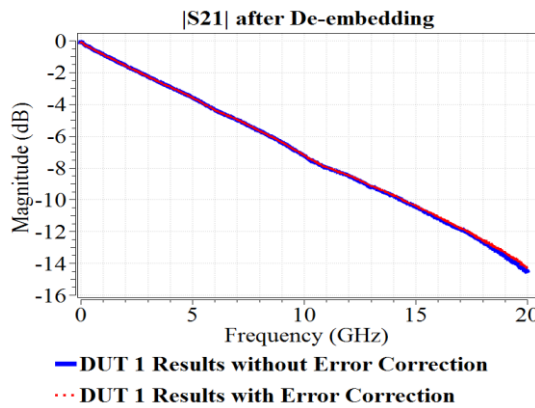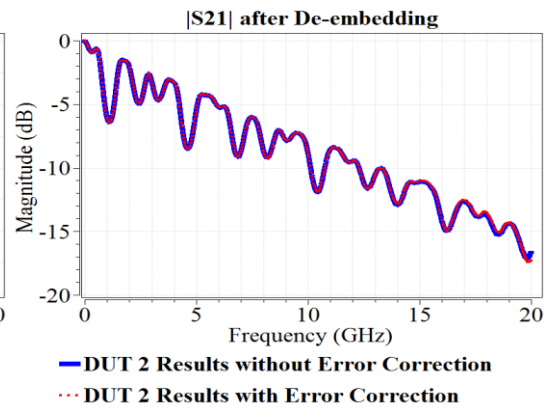
(c)   (d)

Figure 12. TDR characteristic impedance results of 1X-reflection de-embedding with and without the fixture error correction: (a) DUT 1; (b) DUT 2; (c) DUT 1; (d) DUT 2.

3.3. 1X-REFLECTION SFD ON THE USB-C CABLE ASSEMBLY DE-EMBEDDING APPLICATION

Using the exact same test fixtures on the calibration pattern and the total de-embedding structure twice will eliminate the variations from manufacturing. One example is the plug-in de-embedding application reuses the test fixtures in the fixture characterization stage and the de-embedding stage. The 2X-thru SFD requires symmetric design of test fixtures, so it is not suitable for the plug-in de-embedding applications as the adaptors are usually male mount with female.

To quantify the electrical performance of USB-C cable assembly, plug-in de-embedding is required. USB-C cable has two rotationally symmetrical 24-pin USB connectors at each end. The latest USB 3.2 protocol with 20 Gbps data rate and Thunderbolt 3 standard with 40 Gbps top speed are based on USB-C system. In addition, USB-C system also supports power delivery up to 120 W as well as audio and video mode. To achieve these features, four pairs of high-speed channels and several low-speed channels for low-speed communication and power delivery are required. To maintain the quality of signal integrity and power delivery performance, USB-C standard listed specifications on losses and couplings for each channel. Because missing of coaxial ports in USB-C connectors, the plug-in de-embedding is required to remove the test fixture effect.

1X-Refelection SFD is designed and manufactured to serve as the test fixture to provide the connection between the VNA coaxial ports and the USB-C cable assembly. In the fixture characterization stage, the USB-C on-board connectors are left open while in

the measurement of Total, the USB-C cable assembly is plugged-in the USB-C on board connectors on both sides.

(a)

(b)

(c)
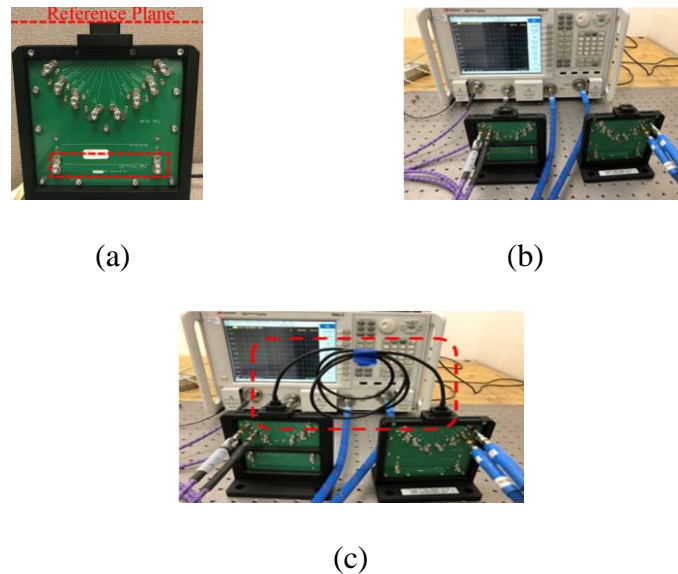
Figure 13. (a) 1X-Reflection SFD calibration board; (b) 1X-Reflection measurement for left and right fixtures; (c) the measurement of Total.

Figure 13 depicts the 1X-reflcetion SFD calibration board and measurement set-up. The reference plane of de-embedding is indicated in Figure 13 (a). The 1X-reflection measurements are plotted in Figure 13 (b), and the total measurement is in Figure 13 (c) with the USB-C cable assembly marked in the red box.

An additional single-ended 2X-thru SFD calibration pattern, marked in the red dashed box of Figure 13 (a) is also routed on board, serves as a comparison. To save on the design space, the 2X-thru calibration pattern is routed as a single-ended straight line. Despite the error correction function in the 2X-thru SFD tool is able to reduce such

inaccuracy introduced by fixture variations dramatically, a better 2X-thru fixture design is more favorable. The better 2X-thru calibration standard should have the exact test fixtures as in the total and cascaded as in the mirror flipped test fixtures indicated in Figure 14. In the test fixture routing design, each trace fan-out immediately after the USB-C receptacle. However, such 2X-thru calibration standard in Figure 14 is very area consuming, and suffers from manufacturing variations as well.
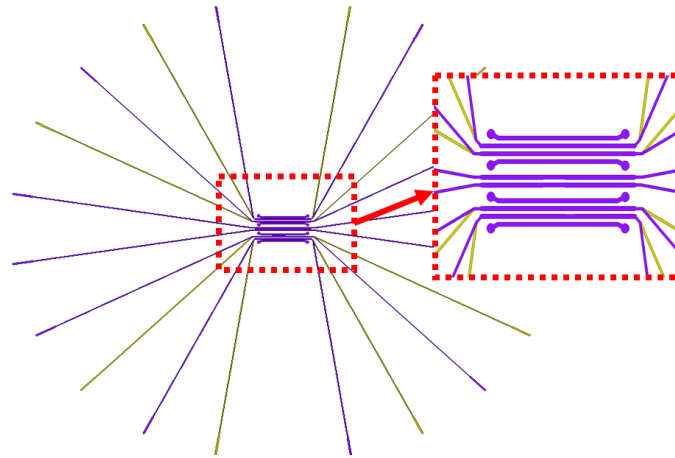
Figure 14. A better 2X-Thru calibration pattern.

By reusing the test fixtures, 1X-reflection SFD has no issue of manufacturing variations. The procedure of 1X-reflection SFD on such USB-C cable assembly application is: 1) four-port electrical calibration (E-Cal) is performed first to remove the effect of coaxial cables; 2) 1X-refelection calibration standards are measured in left and right fixtures, respectively; 3) 1X-thru fixture is constructed; 4) The total of each differential

channel is measured by plugging in the USB-C cable assembly; 5) The de-embedding is performed.

The de-embedded results of 1X-reflection SFD, 2X-thru SFD without error correction, and 2X-thru with error correction are compared in Figure 15. Because the test fixtures are reused, the error correction is not necessary.

(a)   (b)

(c)
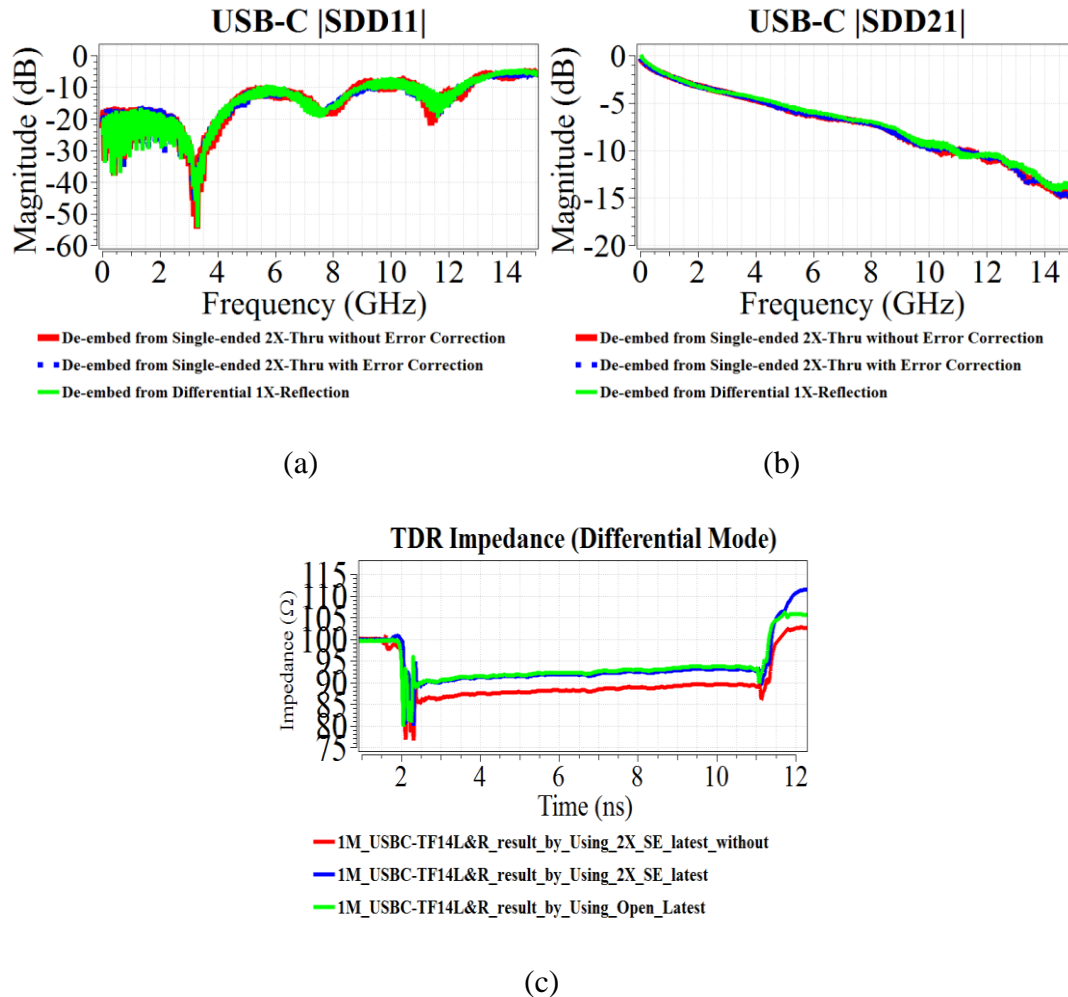
Figure 15. De-embedded results of one differential pairs in USB-C cable: (a) $|S_{dd11}|$; (b) $|S_{dd21}|$; (c) differential TDR impedance comparison.

With error correction, the 2X-thru SFD has almost identical results as the 1X-reflection SFD. The TDR impedance comparison indicates that without error correction in the 2X-thru SFD, the result has non-causal and impedance inaccuracy issues.

REFERENCES

J. Song, F. Ling, G. Flynn, W. Blood, and E. Demircan, "A De-embedding Technique for Interconnects," in *Electronic Performance Electronic packaging*, 2001, pp.129-132.

Luuk F. Tiemeijer, R .J. Havens, " A Calibrated Lumped-Element De-embedding Technique for On-Wafer RF Characterization of High-Quality Inductors and High-Speed Transistors," in *IEEE Trans. On Electron Devices, vol. 50,* pp.822-829, March 2003

A. Mangan, S.P. Voinigescu, M. Yang, and M. Tazkauanu, " De-embedding Transmission Line Measurement for Accurate Modeling of IC Designs," in *IEEE Trans. On Electron Devices*, vol. 53, pp.235-241, Feb. 2006.

R. Lane, "De-embedding Device Scattering Parameters," *Microwave Journal*, vol. 27, pp. 149-156, Aug. 1984.

G. F. Engen, "Calibration technique for automated network analyzers with application to adapter evaluation," *IEEE Trans. Microwave Theory and Technology*, vol. 22, pp. 1255–1260, Dec. 1974.

R. W. Beatty, G. F. Engen, and W. J. Anson, "Measurement of reflections and losses of waveguide joints and connectors using microwave reflect-meter techniques." *IRE Trans. Instrum.*, vol. 9, no. 2, pp. 219–226, Sep.1960.

J. Martens, "LRM: A quantitative look at reference impedance contradictions and other uncertainty impacts," *69th ARFTG meeting digest*, Honolulu, June 2007.

K. Silvonen, Ning Hua Zhu, "A 16-Term Error Model Based on Linear Equations of Voltage and Current Variables," *IEEE Trans. Microwave Theory and Technology*, vol. 54, pp. 1464–1469, April 2006.

Bichen Chen, Xiaoning Ye, Bill Samaras, Jun Fan., "A novel de-embedding method suitable for transmission-line measurement," in *2015 Asia-Pacific Symposium on Electromagnetic Compatibility (APEMC).*

Bichen Chen, Xiaoning Ye, Qiaolei Huang, Shuai Jin, Jun Fan., "Thru-Line De-embedding (TLD), an Accurate and Simplified Fixture Removal Method with Self-validating Line Standard," *DesignCon, 2017.*

Yoon, Changwook, etc.. "Design criteria and error sensitivity of time domain channel characterization (TCC) for asymmetry fixture de-embedding." in *IEEE Transactions on Electromagnetic Compatibility.* vol. 57,no. 4,pp.108-113, Aug.2015

Chunyu Wu, Bichen Chen, Tsiklauri Mikheil, Xiaoning Ye, Jun Fan., " error bounds analysis of de-embedded results in 2x Thru de-embedding methods" in *Electromagnetic Compatibility (EMC),* 2017 *IEEE International Symposium.*

Bichen Chen, Mikheil Tsiklauri, Chunyu Wu, Shuai Jin, Jun Fan, Xiaoning Ye, Bill Samaras., "Analytical and numerical sensitivity analyses of fixtures de-embedding," in *Electromagnetic Compatibility (EMC), 2016 IEEE International Symposium.*

Lingyun Ye, Caixia Li, Xinglin Sun, Shuai Jin, Bichen Chen, Xiaoning Ye, Jun Fan., "Thru-Reflect-Line Calibration Technique: Error Analysis for Characteristic Impedance Variations in the Line Standards," *IEEE Transactions on Electromagnetic Compatibility*, vol.PP, Dec. 2016.

Changwook Yoon, Bichen Chen, Xiaoning Ye, Bill Samaras, Jun Fan., "Advanced On-Chip SOL Calibration Method for Unknown Fixture De-embedding," *Journal of Semiconductor Technology and Science*, Vol.17, no.4,AUG,2017

Hietala V., "Determining Two-Port S-Parameters from a One-Port Measurement Using a Novel Impedance-State Test Chip," *IEEE Microwave Symposium Digest*, 1999, pp.1639-1642.

Bichen Chen, Jiayi He, Xinglin Sun,Yuandong Guo,Shuai Jin,X.Ye,Jun Fan, "Differential S-parameter de-embedding for 8-port network," *Electromagnetic Compatibility (EMC), 2018 IEEE International Symposium.*

Lingyun Ye, Caixia Li, Xinglin Sun, Shuai Jin, Bichen Chen, Xiaoning Ye, Jun Fan., "Thru-Reflect-Line Calibration Technique: Error Analysis for Characteristic Impedance Variations in the Line Standards," *IEEE Transactions on Electromagnetic Compatibility*, vol.PP, Dec. 2016.

Changwook Yoon, Bichen Chen, Xiaoning Ye, Bill Samaras, Jun Fan., "Advanced On-Chip SOL Calibration Method for Unknown Fixture De-embedding," *Journal of Semiconductor Technology and Science*, Vol.17, no.4,AUG,2017

Hietala V., "Determining Two-Port S-Parameters from a One-Port Measurement Using a Novel Impedance-State Test Chip," *IEEE Microwave Symposium Digest*, 1999, pp.1639-1642.

Bichen Chen, Jiayi He, Xinglin Sun,Yuandong Guo,Shuai Jin,X.Ye,Jun Fan, "Differential S-parameter de-embedding for 8-port network," *Electromagnetic Compatibility (EMC), 2018 IEEE International Symposium*.

III. THRU-LINE DE-EMBEDDING (TLD), AN ACCURATE AND SIMPLIFIED FIXTURE REMOVAL METHOD WITH VALIDATION LINE STANDARD

B.Chen

Department of Electrical Engineering

Missouri University of Science and Technology

Rolla, Missouri 65409–0050

Tel: 347–856–7895

Email: bcpr8@mst.edu

ABSTRACT

Accurate high-frequency measurements of multi-ports channels are critical for all high-speed parallel and serial links. As numerical models only provide estimations of electrical behaviors, validations from measurements on test vehicles or real systems are critical to improving model accuracy and design optimization.

1. INTRUDUCTION

Due to measurement limitations, devices under test (DUTs) commonly require test fixtures to be inserted between the DUT and pre-requisite interface of equipment for measurements. However, the discontinuities introduced by test fixtures are usually an unavoidable challenge for engineers, and de-embedding is a necessary procedure to obtain the scattering parameters (S-parameters) of a DUT. Figure 1 shows some typical passive

channel components that need to be de-embedded such as pads on ICs, bond-wire, through-silicon-vias (TSV), traces on ICs/PKGs/PCBs, vias in PKGs/PCBs, connectors, and cables.
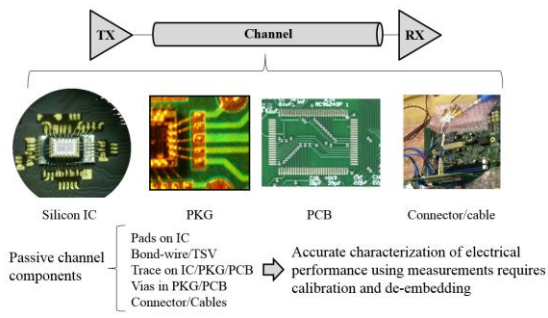
Figure 1. Calibration and de-embedding are required for DUT measurement

The general de-embedding procedure is illustrated in Figure 2. First-tier calibration is conducted to move reference plane to Reference Plane 2, located at end of cables, using electrical calibration kits (E-Cal) or mechanical calibration kits. Second-tier calibration is then conducted to de-embed the error boxes, moving the reference plane to Reference Plane 3 at the interface of DUT.
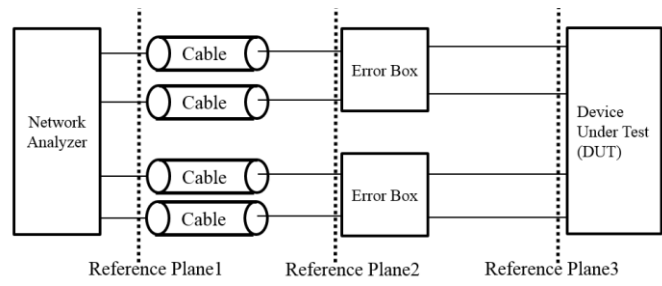
Figure 2. A typical de-embedding diagram

Commercially available second-tier calibration and de-embedding techniques such as the classic thru-reflect-line (TRL), load-reflect-match (LRM), line-reflect-line (LRL), thru-reflect-match (TRM) [1], and short-open-load-thru (SOLT)[2], as well as the novel 2X–thru [3]-[6] are widely used in characterizing electrical performances of DUTs. TRL calibration is performed by using the zero length thru, reflect (short, or open), and line standards, while LRM, LRL, and TRM are the derivatives of TRL. There are certain restrictions in the TRL calibration family, which include: 1) characteristic impedances and propagation constants among the thru and line standards are required to be identical; 2) broad-frequency coverage requires multiple line standards. The new 2X-thru method dramatically reduces the complexity of fixture de-embedding by using a zero length thru standard only. Despite the simplicity of the method, the disadvantages of 2X-thru include: 1) lack of additional validation standard to verify the de-embedding procedure; 2) the typical requirement of a proprietary algorithm to process data in both the frequency and time domains, which introduces approximation errors.

The TLD method in this paper addresses the issues mentioned above by utilizing a zero length thru standard, and an additional non-zero length line standard to accurately remove the fixture effects, as well as to provide validation and error quantification for the de-embedding procedure. Compared to the traditional TRL family, the TLD method reduces the number of calibration structures, yet maintains the accuracy of de-embedded results without multiple line and reflect standards. While comparing to 2X-thru method, an additional structure of non-zero length is needed. The non-zero length line serves two purposes: 1) it allows the TLD algorithm to perform solely in the frequency domain and eliminates the requirement of data processing in both the frequency and time domains as

in the 2X-thru de-embedding methods; 2) it also serves as a validation and error quantification standard to verify the test fixtures and de-embedded results. Since the non-zero length structure is a transmission line, any non-transmission line behavior of the extracted non-zero length line standard is attributed to either poorly designed fixture components or poorly manufactured lead-in transmission line traces. Thus, by examining the extracted results of this line standard and comparing with fitted transmission line behavior from the advanced root-omega method (ARO), it is easy to determine the usable bandwidth of the de-embedding procedure. In addition, the error bounds of de-embedding results in usable bandwidth are derived to quantify the maximum and minimal magnitude errors of de-embedding. The TLD's results of non-zero length line are extremely suitable for other signal integrity applications such as material extractions [7]- [9].

2. THE THRU-LINE DE-EMBEDDING (TLD) ALGORITHM, VALIDATIONTIONS AND DISCUSSIONS

TRL was interpreted and implemented in various approaches [1]-[3]. A recent publication [4] in 2016 derived TRL method from an innovative way that gives rise to a physical explanation. Unlike [1]-[4], the TLD method in this paper is obtained in a more straightforward fashion by solving independent equations in the frequency domain. The independent equations are then characterized as one-port, SOL-like formulas, to solve the unknown parameters in the test fixtures. Simulations and measurements are performed to verify the derivations. Finally, in this session, the reasons that one non-zero length line is sufficient to extract the test fixtures, validations, and error quantifications are explained.

2.1. DERIVATIONS OF THE TLD ALGORITHM

In this work, TLD only requires a zero length thru standard, and a non-zero length line standard to accurately remove the fixtures components under the assumption of symmetric test fixtures design. Figure 3 depicts a zero length thru standard (a), a non-zero length line standard (b), and the total structure (c) in which fixture effects need to be removed.

(a)   (b)

(c)
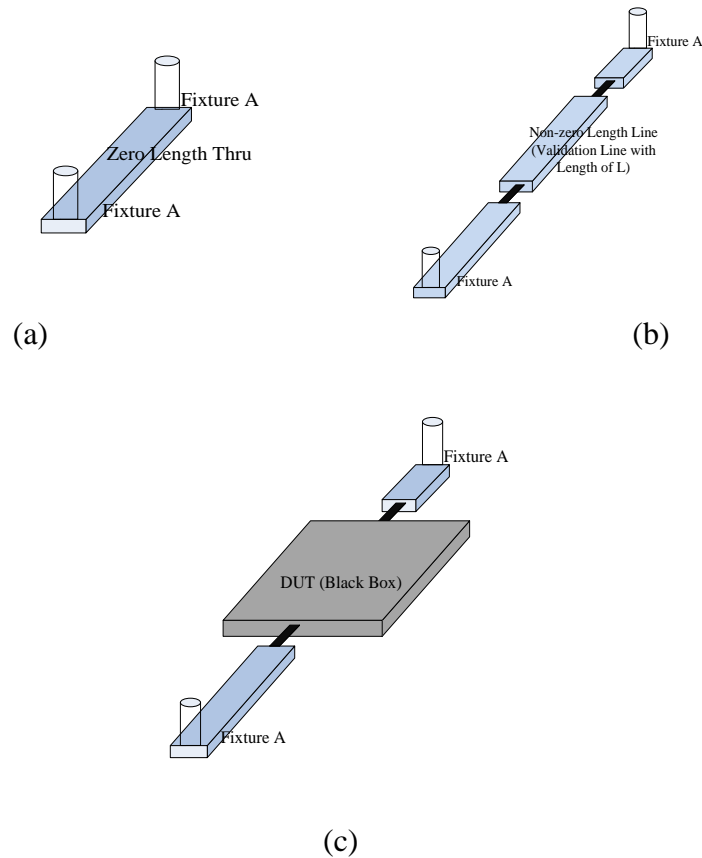
Figure 3. (a) Zero length thru standard; (b) non-zero length line standard; (c) total structure.

Assuming symmetric design of test fixtures, the two-port network of zero length thru, non-zero length line and total can be described by using the concept of transfer

scattering parameters (T-parameters) in (1) to (3). The conversions between two-port scattering parameters (S-parameters) and two-port T-parameters are given in (4) and (5).

$$T_{Zero-Length-Thru} = T_{fixA} \times \overline{T}_{fixA} \tag{1}$$

$$T_{Non-zero-Length-Line} = T_{fixA} \times T_L \times \overline{T}_{fixA} \tag{2}$$

$$T_{Total} = T_{fixA} \times T_{DUT} \times \overline{T}_{fixA} \tag{3}$$

$$\begin{bmatrix} T_{11} & T_{12} \\ T_{21} & T_{22} \end{bmatrix} = \frac{1}{S_{21}} \begin{bmatrix} S_{12}S_{21} - S_{11}S_{22} & S_{11} \\ -S_{22} & 1 \end{bmatrix} \tag{4}$$

$$\begin{bmatrix} S_{11} & S_{12} \\ S_{21} & S_{22} \end{bmatrix} = \frac{1}{T_{22}} \begin{bmatrix} T_{12} & (T_{11}T_{22} - T_{12}T_{21}) \\ 1 & \dfrac{-T_{21}}{T_{22}} \end{bmatrix} \tag{5}$$

Eq. (1) can be written as (6)

$$\overline{T}_{fixA} = T_{fixA}^{-1} \times T_{Zero-Length-Thru} \tag{6}$$

Then substitute Eq. (6) into Eq. (2), Eq. (7) is acquired as,

$$T_{Non-zero-Length-Line} \times T_{Zeros-Length-Thru}^{-1} = T_{fixA} \times T_L \times T_{fixA}^{-1} \tag{7}$$

A transmission line with the same characteristic impedance as the non-zero length line standard is placed after the discontinuity in each fixture to make sure only TEM waves propagate into the line standard. In this case, the non-zero length line standard could be described as (8) in terms of the S-parameters with terminations of the actual transmission line characteristic impedance at both ports, and (7) can be written as (9), where $|e^{\gamma l}|$ is

solved when $\gamma \neq 0$. By using renormalization procedures with actual and system characteristic impedances, S-parameters based on system impedance can be calculated.

$$S_L = \begin{bmatrix} 0 & e^{-\gamma l} \\ e^{-\gamma l} & 0 \end{bmatrix} \tag{8}$$

$$\begin{bmatrix} T_{11}^{New} & T_{12}^{New} \\ T_{21}^{New} & T_{22}^{New} \end{bmatrix} = \begin{bmatrix} -\det(fixA) & S_{11}^{fixA} \\ -S_{22}^{fixA} & 1 \end{bmatrix} \times \begin{bmatrix} e^{-\gamma l} & 0 \\ 0 & e^{\gamma l} \end{bmatrix} \times \begin{bmatrix} -\det(fixA) & S_{11}^{fixA} \\ -S_{22}^{fixA} & 1 \end{bmatrix}^{-1} \tag{9}$$

Where $T_{New} = T_{Non-zero-Length-Line} \times T_{Zeros-Length-Thru}^{-1}$

The cascading of (9) is based on system impedance and non-zero length line standard trace characteristic impedance. The right side of fixture A, both sides of the non-zero length line standard, and the left side of fixture $\bar{A}$ are all terminated with the actual impedance of the trace instead of the system impedance. Figure 4 depicts Eq. (9) in a block diagram.
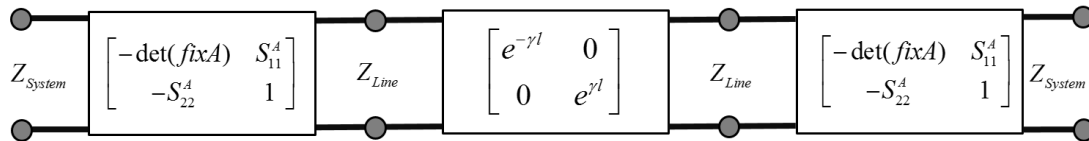
Figure 4. The cascading block diagram of Eq. (9).

S_{11}^{fixA} from (9) is solved by using the same procedures as [1]; however, the solved S_{11}^{fixA} is terminated with Z_0^{System} and Z_0^{Line} on two sides, respectively.

Whenever $Z_0^{System} \neq Z_0^{Line}$ renormalization is required. Z_0^{Line} acquisition techniques of a transmission line are discussed in [5]-[8]. However, the drawbacks of those methods are either dependence on additional time-domain measurements [5] or the cross-sectional information of traces and the properties of the dielectric materials [6]-[8]. The Z_0^{Line} in this paper is calculated based on time-domain response of S-parameters measurements from both the zero length thru and non-zero length line. Such methodology is documented in [3]. In the zero length thru, the S_{21}^{fixA} and S_{22}^{fixA} are calculated in the frequency domain by Eq. (10) and (11).

$$S_{11}^{Zero-Length-Thru} = S_{11}^{fixA} + \frac{\left(S_{21}^{fixA}\right)^2 S_{22}^{fixA}}{1 - \left(S_{22}^{fixA}\right)^2} \tag{10}$$

$$S_{12}^{Zero-Length-Thru} = S_{21}^{Zero-Length-Thru} = \frac{\left(S_{21}^{fixA}\right)^2}{1 - \left(S_{22}^{fixA}\right)^2} \tag{11}$$

Alternatively, another approach to solving (7) is to use the similarity property of matrices. $T_{NZLL} \times T_{ZLT}^{-1}$ and T_{NEW} are matrices with the same eigenvalues. $T_{NZLL} \times T_{ZLT}^{-1}$ has two reciprocal eigenvalues, which are obtained from measurements. The eigenvalue with a magnitude less than 1 ($\gamma \neq 0$) will be the $|e^{\gamma l}|$ in (8). Additionally, (9) and (10) can be rewritten into (12) and (13).

$$S_{11}^{Zero-Length-Thru} + S_{21}^{Zero-Length-Thru} = S_{11}^{fixA} + \frac{\left(S_{21}^{fixA}\right)^2}{\dfrac{1}{G_A^{Open}} - S_{22}^{fixA}} \tag{12}$$

$$S_{11}^{Zero-Length-Thru} - S_{21}^{Zero-Length-Thru} = S_{11}^{fixA} + \frac{\left(S_{21}^{fixA}\right)^2}{\dfrac{1}{G_A^{Short}} - S_{22}^{fixA}} \quad (13)$$

Eq. (12) and (13) are equivalent to the 'Open' and 'Short' standards in the one-port SOL calibration equations, where $S_{11}^{ZLT} + S_{21}^{ZLT}$ is the measured 'Open' coefficient G_M^{Open} and $S_{11}^{ZLT} - S_{21}^{ZLT}$ is the measured 'Short' coefficient G_M^{Short}. The G_A^{Open} and G_A^{Short} coefficients are 1 and -1, respectively, in the TLD method.

The alternative expressions in the TLD method presented here show that by using the assumption of symmetric and reciprocal S-parameters in the zero length thru standard, S_{21} and S_{22} of the test fixtures can be solved in the same manner as the 'Open' and 'Short' in the one-port SOL calibration. The S_{11}^{fixA} is solved from TRL equations in [51]. The electrical performance of validation transmission line is acquired either by the TRL or eigenvalue method. The TLD procedures derived in this paper provide a more practical method for implementation during design and measurement stages. Mathematically, TLD is a hybrid of SOL and TRL.

2.2 TLD VERIFICATION

The simulation verification is studied first to verify the mathematical expressions in the above section. In the first example, Fixture A is a 1" transmission line with 1 pf and 0.3 nH of parasitic (schematic is embedded in Figure 5. (c)), while the non-zero length line standard is an 8" transmission line. S -parameters of zero-length thru, line standard, and line standard with fixture are all calculated directly through ADS. These S -parameters are used for the TLD de-embedded study. The S- parameters of line standard are calculated

through the proposed TLD algorithm, using the S-parameter of zero-length thru and line standard with fixture. The results are then compared to the directly simulated cases, and the comparisons are shown in Figure 5. (a) and (b). The results of the extracted fixture A's S-parameters and the golden standards (simulated directly) are compared in Figure 5. (c) and (d). The results indicate that the TLD method could accurately recover the Fixture A's S-parameters.
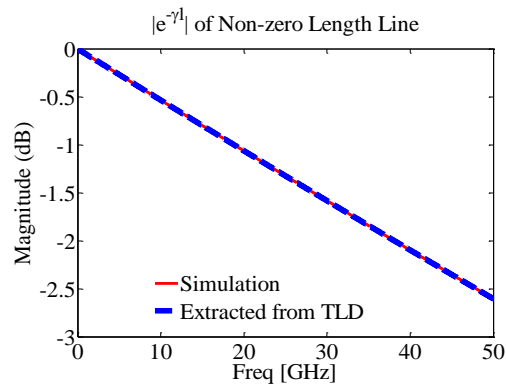
(a)
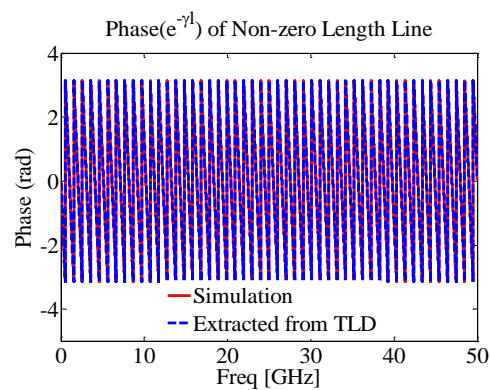
(b)

Figure 5. (a) Non-zero length Line $|e^{\gamma l}|$comparison; (b) Non-zero length Line transmission phase comparison; (c) Fixture A $|S_{11}|$ comparison (schematic is embedded); (d) Fixture A $|S_{21}|$ comparison.
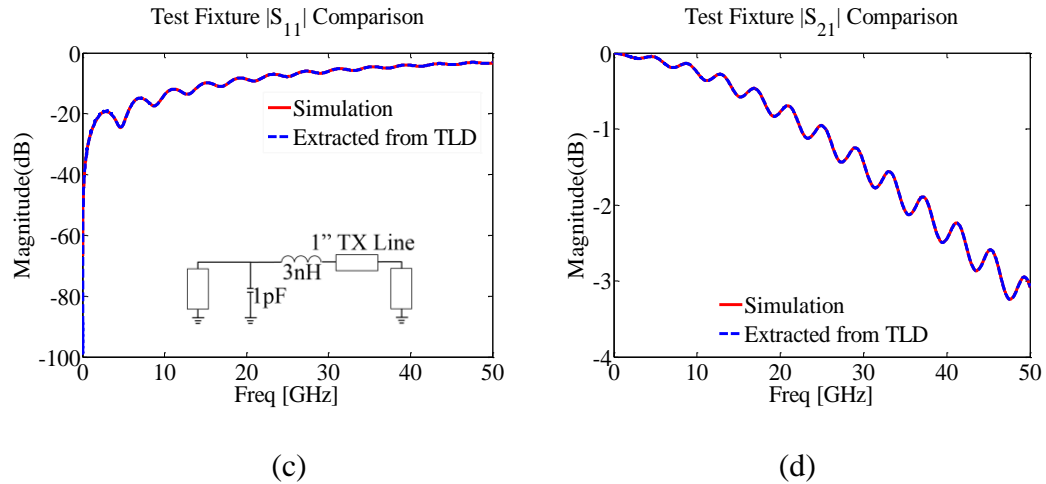
Figure 5. (a) Non-zero length Line $|e^{\gamma l}|$comparison; (b) Non-zero length Line transmission phase comparison; (c) Fixture A $|S_{11}|$ comparison (schematic is embedded); (d) Fixture A $|S_{21}|$ comparison.(cont.)

2.3. NUMBER OF LINES DISCUSSION

In the TRL design [1] and [9], authors limited a single pair of lines to between 20° and 160°. Thus, multiple lines are required in such a design to cover the entire frequency range. Mathematically, (9) has no solution when $\boldsymbol{\alpha = \beta = 0}$. In the lossless cases ($\boldsymbol{\alpha = 0}$), then $\boldsymbol{\beta = 0}$ when the phase arrives at 0° and ±180°. The expected error at the band edges is approximately 2.92 times that at the optimal (90°) point. However, the accuracy increases linearly with both the attenuation factor and the length difference. In general, if the loss is in the PCB manufacture-valid range ($\boldsymbol{\alpha \neq 0}$), the phase difference criterion is irrelevant.

To justify the statement that the increasing attenuation factor is able to decrease inaccuracy of the proposed methodology, a comparison group by using simulations was adopted. The lossless, ultra-low loss, and high loss transmission lines with test fixtures are

simulated separately. Table 1 offers the details of transmission line information in the comparison group. All study cases have same characteristic impedances, transmission phase, and dielectric constant (Dk), but different dissipation factors (Df). The test fixtures are same as those in a previous paragraph as plotted in Figure 5 (c). Noises at -70 dB were injected into the S-parameters to mimic the measurement scenario. The extracted $|S_{11}|$ of the fixtures are compared in Figure 6.

Table 1. Parameters of non-zero length line

	Lossless	Ultra-Low Loss	High Loss
Dk@1 GHz	3.6	3.6	3.6
Df @1GHz	0	0.0005	0.005
Non-zero Length Line	1 inch	1 inch	1 inch
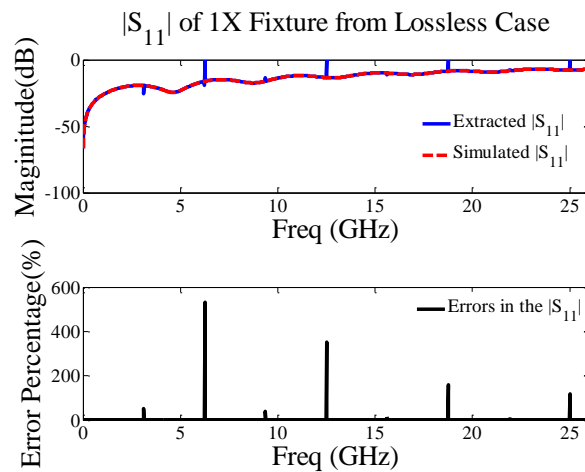
(a)

Figure 6. $|S_{11}|$ comparison and error percentage of fixture from (a) lossless; (b) ultra-low loss; and (c) high loss.
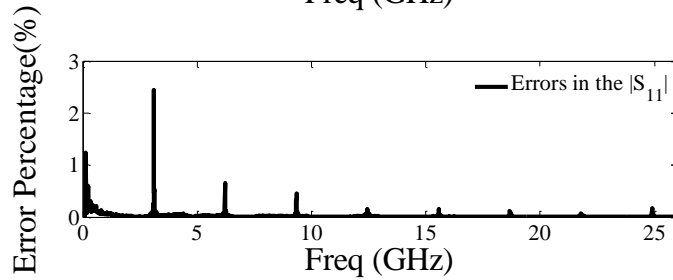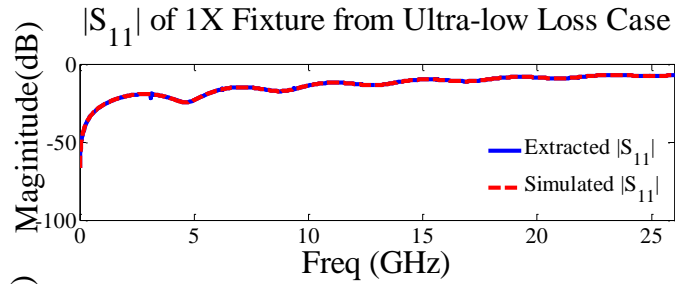
(b)
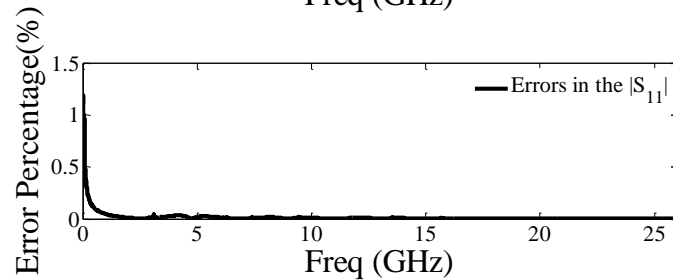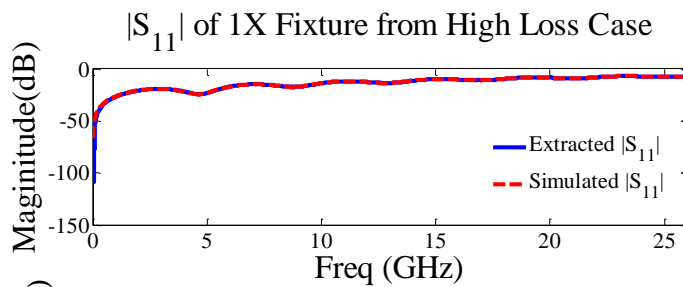
(c)

Figure 6. $|S_{11}|$ comparison and error percentage of fixture from (a) lossless; (b) ultra-low loss; and (c) high loss. (cont.)

As observed from Figure 6, the errors are amplified by the injected noise at 0° and ±180°, but are attenuated by losses drastically. To reduce the measurement noise such as a

sufficient small IF bandwidth, adequate average times in the VNA setting, the errors were also reduced. However, the errors are negligible when the dissipation factor is larger than 0.005, which is still lower than most commercial PCBs dielectric materials.

3. VALIDATION AND ERROR QUANTIFICATION PURPOSE OF NON-ZERO LENGTH THRU

As mentioned in the previous paragraph, in addition to providing equations to solve the test fixtures, the non-zero length line also provided validation and error quantification purposes. Rigorously, the behavior of non-zero length line is a transmission line. The small extracted perturbations come from manufacturing variation and/or measurement. However, if the test fixtures were not well designed, the extracted non-zero length line deviated from transmission line behavior drastically at certain frequencies. The non-zero length line helps to identify the useable frequency range of the test fixtures, as well as the de-embedded results by using both the fitted $|e^{-\gamma l}|$ and solved $|e^{-\gamma l}|$. Furthermore, within the valid frequency range, fixture and de-embedding error bounds due to the non-ideal manufacturing and measurement were calculated.

3.1. FITTING AND TRUNCATION FUNCTION IN $|e^{-\gamma l}|$

Dielectric and conductor loss of transmission line in PCBs were well studied in [6]-[9]. In the inner layer of PCB, the AC conductor loss is proportional to ω^n $(0 < n < 1)$, and the dielectric loss is associated with summation of a function of ω and a function ω^2. The DC conductor loss is a constant K. The method was referred to as "Advanced Root Omega (ARO)" in [20]. The fitting function of $|e^{-\gamma l}|$ is:

$$dB(e^{-\gamma l}) = a\omega^2 + b\omega + c\omega^d + K \tag{14}$$

The initial values and fitting ranges of 'a', 'b', 'c', and 'd' are specified in the Table 2. It is possible that the fitted values are the just boundary values, which means no optimal solution was found in the fitting ranges. As discussed in [20], the quality of the fitting remains relatively high in these cases, except with some exceptions at the ultra-low frequencies.

Table 2. ARO fitting parameters initial values and constraints

Parameter	Initial Value	Fitting Ranges
a	-0.00025	-10~0
b	0.1	0~Inf
c	0.5	0~Inf
d	0.6	0.2~0.8

In [10], the author used two-step fitting to find the optimal solutions. However, the two-step fitting is not the best option when applied to truncation frequency searching. In this work, the ARO uses changeable data lengths to fit. The data length is determined by (16).

$$M_k = M_{k-1} + \frac{N}{2^k}(-1)^{T_{k-1}}, \tag{16}$$

where M_k is the data length in the kth fitting; N is the total length of the original data; T_k is either 0 or 1; and T$_k$= 1 means after k$_{th}$ fitting, fitted data has less than 10% differences, while T$_k$=0 means the opposite.

In order to find the truncation frequency accurately, and efficiently, the binary search algorithm (BSA) was applied. BSA is an efficient search algorithm that finds the truncation frequency within the entire bandwidth. The criteria of valid data is the differences ($|\Delta e^{-\gamma l}|$) between extracted and fitted $|e^{-\gamma l}|$, is less than $|\Delta e^{-\gamma l}{}_{TH}|$:

$$| \Delta e_{TH}^{-\gamma l} |= 0.02 + \frac{0.25}{1+\dfrac{f_n}{5}} \tag{17}$$

BSA compares the $|\Delta e_{TH}^{-\gamma l}|$ to the middle element of the $|\Delta e^{-\gamma l}|$ array; if they are unequal, the half in which the target cannot lie is eliminated and the search continues on the remaining half until it is successful. When the truncation frequency is found through the above procedure, the valid frequency range of test fixtures and the de-embedding is determined.

3.2. SENSITIVITY ANALYSIS AND ERROR BOUNDS CALCULATION OF DE-EMBEDDED RESULTS

De-embedding sensitivity analysis are studies of deviation of de-embedding results due to manufacturing variations in test fixtures, as well as inaccuracies associated with the calibration and measurement process.

The uncertainties of SOLT, TRL, and LRM calibration methods were well studied by Dr. Ulrich Stumper through local sensitivity analysis in [11] and [12]. The analytical

and numerical local sensitivity analyses of general fixture de-embedding was presented in [13] to implement the sensitivity calculation in the first order partial derivative. For example, the local sensitivity coefficient of S_{21}^{DUT}, associated with S_{11}^{fixA}, is defined in (18) as:

$$Sensitivity(S_{21}^{DUT}, S_{11}^{fixA}) = \left| \frac{\partial S_{21}^{DUT}}{\partial S_{11}^{fixA}} \right|_{X^0}. \tag{18}$$

The subscript X^0 represents the partial derivative is only taken at some points where small perturbations happened in manufacturing and measurements. The absolute error of a de-embedded output is defined as the summation of the products of sensitivity coefficients and absolute input errors. In (19), the first-order error for de-embedded $|S_{21}^{DUT}|$ is approximated as:

$$\Delta S_{21}^{DUT} = \frac{\partial S_{21}^{DUT}}{\partial S_{11}^{FixtureA}} \Delta S_{11}^{FixtureA} + \frac{\partial S_{12}^{DUT}}{\partial S_{12}^{FixtureA}} \Delta S_{12}^{FixtureA} + \frac{\partial S_{21}^{DUT}}{\partial S_{21}^{FixtureA}} \Delta S_{21}^{FixtureA} + \frac{\partial S_{21}^{DUT}}{\partial S_{22}^{FixtureA}} \Delta S_{22}^{FixtureA}$$
$$+ \frac{\partial S_{21}^{DUT}}{\partial S_{11}^{FixtureB}} \Delta S_{11}^{FixtureB} + \frac{\partial S_{12}^{DUT}}{\partial S_{12}^{FixtureB}} \Delta S_{12}^{FixtureB} + \frac{\partial S_{21}^{DUT}}{\partial S_{21}^{FixtureB}} \Delta S_{21}^{FixtureB} + \frac{\partial S_{21}^{DUT}}{\partial S_{22}^{FixtureB}} \Delta S_{22}^{FixtureB} \tag{19}$$

The first-order local sensitivity method of de-embedding only allows one parameter change at the de-embedding function each time while keeping the other parameters fixed. It is only suitable to quantify very small errors in the de-embedding.

To quantify errors of the TLD results precisely, a more general error bounds calculation method is required. The proposed error bounds method is to calculate the maximum and minimal complex errors in the test fixtures and de-embedded results. The error includes measurement and instrument imperfections, test fixtures manufacturing variations, and small errors from (9) when the transmission phase of a non-zero length line close to 0° and ±180°.
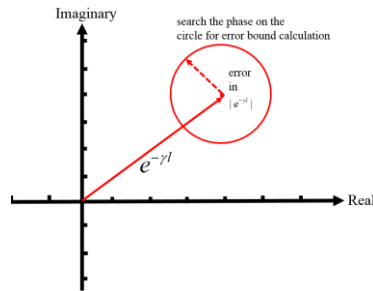
Figure 7. Complex errors combinations of $e^{-\gamma l}$.

Such an error bounds calculation procedure is also associated with the fixture characterization algorithms. In the error bounds calculation of TLD, the $e^{-\gamma l}$ magnitude errors are first calculated in the range of valid frequencies. With a 360° sweeping in the complex plane, the complex errors of $e^{-\gamma l}$ with all possibilities are constructed in Figure 7. Using the complex errors of $e^{-\gamma l}$, the maximum and minimal complex errors of the test fixtures and final de-embedded results are calculated. The maximum error is characterized as up error bounds and the minimal error is the low error bounds.

3.3. IMPLEMENTATION OF FITTING CALCULATION

The ARO, BSA algorithm, and de-embedding error bounds were implemented in two full-wave simulation models first. Case A is a fixture without any signal integrity optimization and case B is a fully optimized fixture. The fixture optimizations in the case B include: 1) 50 Ohm signal via characteristic impedance adjustment; 2) via to trace tear drop transition; 3) add diving board on the adjacent GND planes; 4) back-drilled via stubs

for both GND and signal. Figure 8 (a) depicts the complete optimized structure of one test fixture in the full-wave model, half of the zero length thru standard (0.5"). Figure 8 (b) is the non-zero-length line standard (2.5"). Figure 8 (c) is the actual DUT embedded in the test fixtures.
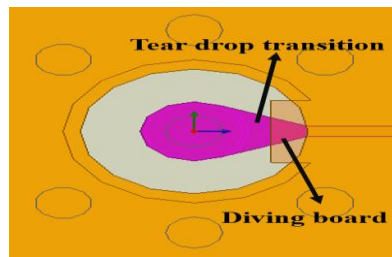

(a)
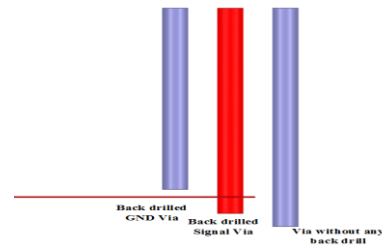
(b)
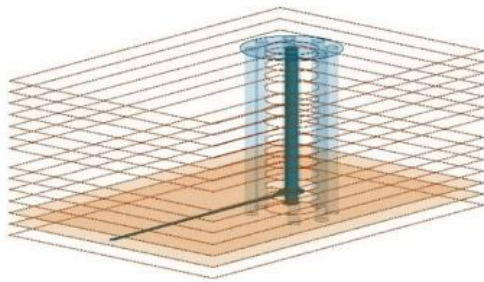
(c)
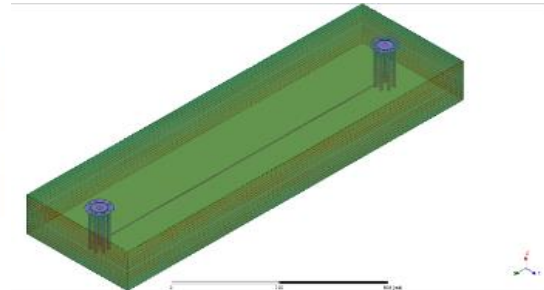
(d)

(e)

Figure 8. (a)Top view of case A; (b) side view of case A;(c) the half of zero length Thru standard; (d) non-zero length Line standard; (e) DUT embedded in the Total.

The ARO algorithm fits the $|e^{-\gamma l}|$ and BSA decides the truncation frequency, as Figure 9 (a) and (b) show the extracted validation lines from optimized and non-optimized fixtures. The truncation frequency of a non-zero length line from non-optimized fixtures is 34.2 GHz, while from the optimized fixtures is 50 GHz. It means with signal integrity optimization works, the valid frequency range of such test fixtures and de-embedded results are extended from 34.3 GHz to 50 GHz. Figure 9 (c) and (d) are the small perturbations between extracted and fitted $|e^{-\gamma l}|$ in percentagewise for non-optimized and optimized fixtures, respectively. (e) and (h) demonstrate error bounds plots of $|S_{11}|$ and $|S_{21}|$ from 10 MHz to 34.2 GHz in the actual DUT after performing de-embedding from non-optimized fixtures. In the optimized fixtures case, the error bounds are from 10 MHz to 50 GHz.
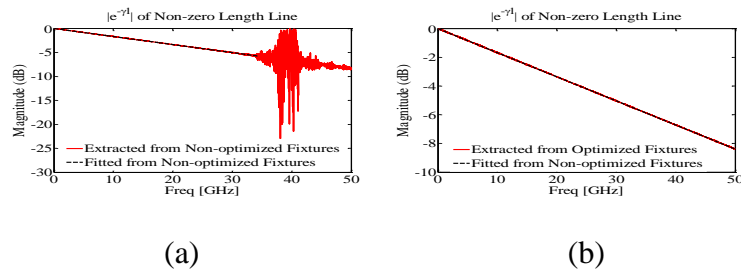
(a)   (b)

Figure 9. (a) Extracted and fitted $\left|e^{\gamma l}\right|$ from non-optimized fixtures; (b) extracted and fitted $\left|e^{\gamma l}\right|$ from optimized fixtures; (c) small perturbations of $|e^{-\gamma l}|$ from non-optimized fixtures ; (d) small perturbations of $|e^{-\gamma l}|$ from optimized fixtures; (e) error bounds of de-embedded $|S_{11}|$ from non-optimized fixtures; (f) error bounds of de-embedded $|S_{21}|$ from non-optimized fixtures; (g) error bounds of de-embedded $|S_{11}|$ from optimized fixtures; (h) error bounds of de-embedded $|S_{21}|$ from optimized fixtures.

Figure 9. (a) Extracted and fitted $\left|e^{\gamma l}\right|$ from non-optimized fixtures; (b) extracted and fitted $\left|e^{\gamma l}\right|$ from optimized fixtures; (c) small perturbations of $\left|e^{-\gamma l}\right|$ from non-optimized fixtures ; (d) small perturbations of $\left|e^{-\gamma l}\right|$ from optimized fixtures; (e) error bounds of de-embedded $\left|S_{11}\right|$ from non-optimized fixtures; (f) error bounds of de-embedded $\left|S_{21}\right|$ from non-optimized fixtures; (g) error bounds of de-embedded $\left|S_{11}\right|$ from optimized fixtures; (h) error bounds of de-embedded $\left|S_{21}\right|$ from optimized fixtures.(cont.)

A test coupon was built with different test fixtures shown in Figure 10 (a). One has a poor fixture design with a via stub length of 51 mil (case C), while the other has a better fixture design with a via stub length of 10 mil (case D), as indicated in Figure 10 (b). The zero length thru, the non-zero length lines, and the total are all differential transmission

lines of 2", 5", and 10" in layer 3 and layer 4, respectively. The DUTs in the case C and case D are identical 8" long transmission line. The GSSG microprobes are used in the measurement, as shown in Figure 10 (c).
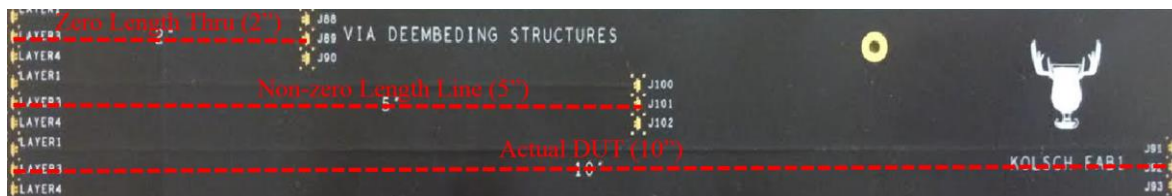
(a)
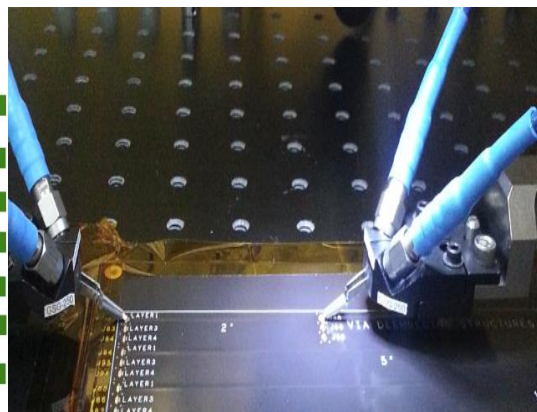
(b)   (c)

Figure 10. (a) A test coupon with marked TLD standards; (b) stack up information of the test coupon; (c) GSSG microprobes are used in the measurement.

The truncation frequencies calculated from the BSA are 15.12 GHz for case C 20.03 GHz for case D within the valid frequency range, the perturbations between extracted and fitted $|e^{\gamma l}|$ from measurements are relatively larger than those values from the full-wave simulations. Such discrepancies in the measurement are from the random noise, and

manufacturing variations of the test fixtures. Figure 11 are the results of TLD, ARO, BSA, and the error bounds on the de-embedded results.

Figure 11. (a) Extracted and fitted $|e^{\gamma l}|$ from case C; (b) extracted and fitted $|e^{\gamma l}|$ from case D; (c) small perturbations of $|e^{-\gamma l}|$ from case C; (d) small perturbations of $|e^{-\gamma l}|$ from case D; (e) error bounds of $|S_{11}|$ from case C; (f) error bounds of $|S_{21}|$ from case C; . (g) Error bounds of $|S_{11}|$ from case D; (h) error bounds of $|S_{21}|$ from case D.

(g) (h)
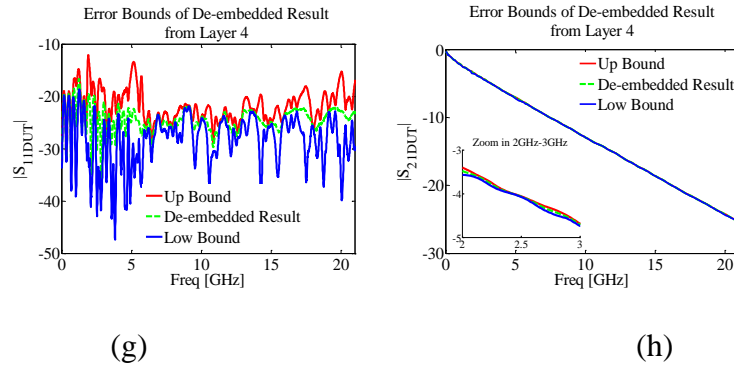
Figure 11. (a) Extracted and fitted $|e^{\gamma l}|$ from case C; (b) extracted and fitted $|e^{\gamma l}|$ from case D; (c) small perturbations of $|e^{-\gamma l}|$ from case C; (d) small perturbations of $|e^{-\gamma l}|$ from case D; (e) error bounds of $|S_{11}|$ from case C; (f) error bounds of $|S_{21}|$ from case C; . (g) Error bounds of $|S_{11}|$ from case D; (h) error bounds of $|S_{21}|$ from case D. (cont.)

REFERENCES

G. F. Engen and C. A. Hoer, "Thru-Reflect-Line: an improved technique for calibrating the dual six-port automatic network analyzer," in *Microwave Theory and Techniques, IEEE Transactions on*, vol. 27, pp.987-993, 1979.

H. Cho and D. Burk, "A three step method for the de-embedding of high frequency S-parameter measurements," in *IEEE Trans. Electron Devices*, vol. 38, pp. 1371–1375, June 1991

Yoon, Changwook, etc. "Design criteria and error sensitivity of time domain channel characterization (TCC) for asymmetry fixture de-embedding." in *IEEE Transactions on Electromagnetic Compatibility*. vol. 57,no. 4,pp.108-113, Aug.2015

Bichen Chen, Xiaoning Ye, Bill Samaras,Jun Fan, "A novel de-embedding method suitable for transmission-line measurement," *IEEE Asia-Pacific Symposium on Electromagnetic Compatibility,* May 25-29, 2015

Chunyu Wu, Bichen Chen, Tsiklauri Mikheil, Xiaoning Ye, Jun Fan., "Error bounds analysis of de-embedded results in 2x Thru de-embedding methods" in *Electromagnetic Compatibility (EMC),* 2017 *IEEE International Symposium.*

Xiaoning Ye, Jun Fan, Bichen Chen, James L. Drewniak, Qinghua Bill Chen, "Accurate characterization of PCB transmission lines for high speed interconnect" in *2015 Asia-Pacific Symposium on Electromagnetic Compatibility (APEMC).*

L. Hua, Bichen Chen, Shuai Jin, M. Koledintseva, J. Lim, K. Qiu, R. Brooks, Ji Zhang, K. Shringarpure and J. Fan. "Characterization of PCB Dielectric Properties Using Two Striplines on the Same Board." *Electromagnetic Compatibility, 2014 IEEE International Symposium on, Raleigh, NC, 4-8 Aug. 2014, pp. 809 – 814.*

Shuai Jin, Xiang Fang, Bichen Chen, Han Gao, Xiaoning Ye, Jun Fan., "Validating the transmission-line based material property extraction procedure including surface roughness for multilayer PCBs using simulations" in *Electromagnetic Compatibility (EMC), 2016 IEEE International Symposium.*

S. Jin, Bichen Chen, X. Fang, H. Gao and J. Fan., "Improved "Root-Omega" method for transmission-line based material property extraction for multilayer PCBs," *IEEE Trans. On Electromagnetic Compatibility.* Vol. 59, no. 4, pp1356-1367, March 2017.

M. B. Steer, S. B. Goldberg, G. Rinne, P. D. Franzon, I. Turlik, and J. S. Kasten, "Introducing the through-line deembedding procedure," in *IEEE MTT-S Int. Microw. Symp*. Dig., Jun. 1992, pp. 1455–1458.

Lingyun Ye, Caixia Li, Xinglin Sun, Shuai Jin, Bichen Chen, Xiaoning Ye, Jun Fan., "Thru-Reflect-Line Calibration Technique: Error Analysis for Characteristic Impedance Variations in the Line Standards," in *Electromagnetic Compatibility, IEEE Transactions on ,* vol.PP,Dec. 2016.

M. Wojnowski, V. Issakov, G. Sommer, and R. Weigel,"Multimode TRL calibration technique for characterization of differential devices," *IEEE Trans. Microw. Theory Techn*., vol. 60, no. 7, pp. 2220–2247, Jul. 2012.

P. Souzangar and M. Shahabadi, "Numerical multimode thru-line (TL) calibration technique for substrate integrated waveguide circuits," *J. Electromagn. Waves Appl*., vol. 23, no. 13, pp. 1785–1793, 2009.

Kimberley W. Eccleston. "New Interpretation of Through-Line Deembedding," *Microw. Theory Techn.*, vol. 64, no. 11, pp. 3887–3893, Nov. 2016.

J. Zhang, et al., "Causal RLGC(f) models for transmission lines from measured S-parameters," *IEEE Trans. Electromagnetic Compatibility*, vol. 52, no. 1, Feb. 2010, pp 189-198.

M. J. Degerstrom, B. K. Gilbert, and E. S. Daniel, *"Accurate resistance, inductance, capacitance, and conductance (RLGC) from uniform transmission line measurements,"* *IEEE EPEP Conf.* 2008, pp. 77-80.

S. Jin, D. Liu, Bichen Chen, K. Qiu, J. Lin, R. Brooks, and J. Fan., "Analytical Equivalent Circuit Modeling for BGA in High-Speed Package, " *IEEE Trans. On Electromagnetic Compatibility*, vol.PP, 2017.

S. Jin, D. Liu, Y. Wang, Bichen Chen and J. Fan., "Equivalent Inductance Extraction for Power/Ground Parallel Plate by Modal Based Methodology, " *IEEE Trans. On Electromagnetic Compatibility*, 2017.

R. B. Marks, "A multiline-method of network analyzer calibration," *IEEE Trans. Microw. Theory Tech.,* vol. 39, no. 7, pp. 1205–1215, Jul. 1991.

Xiaoning Ye, M.Balogh, "physics-based fitting to improve PCB loss measurement accuracy" in *Electromagnetic Compatibility and Signal/Power Integrity (EMCSI), 2017 IEEE International Symposium*

U. Stumper, "Uncertainty of VNA S-parameter measurement due to non-ideal TRL calibration items*," IEEE Trans. Instr. and Meas.*, vol. 54, pp. 676-679, Apr. 2005.

U. Stumper, "Influence of non-ideal calibration items on S-parameter uncertainties applying the SOLR calibration method," *IEEE Trans. Instr. and Meas.*, Vol. 58, pp. 1158-1163, Apr. 2009

Lingyun Ye, Caixia Li, Xinglin Sun, Shuai Jin, Bichen Chen, Xiaoning Ye, Jun Fan., "Thru-Reflect-Line Calibration Technique: Error Analysis for Characteristic Impedance Variations in the Line Standards," in *Electromagnetic Compatibility, IEEE Transactions on ,* vol.PP,Dec. 2016.

M. Wojnowski, V. Issakov, G. Sommer, and R. Weigel,"Multimode TRL calibration technique for characterization of differential devices," *IEEE Trans. Microw. Theory Techn*., vol. 60, no. 7, pp. 2220–2247, Jul. 2012.

P. Souzangar and M. Shahabadi, "Numerical multimode thru-line (TL) calibration technique for substrate integrated waveguide circuits," *J. Electromagn. Waves Appl.*, vol. 23, no. 13, pp. 1785–1793, 2009.

Kimberley W. Eccleston. "New Interpretation of Through-Line Deembedding," *Microw. Theory Techn.*, vol. 64, no. 11, pp. 3887–3893, Nov. 2016.

J. Zhang, et al., "Causal RLGC(f) models for transmission lines from measured S-parameters," *IEEE Trans. Electromagnetic Compatibility*, vol. 52, no. 1, Feb. 2010, pp 189-198.

L. Hua, Bichen Chen, Shuai Jin, M. Koledintseva, J. Lim, K. Qiu, R. Brooks, Ji Zhang, K. Shringarpure and J. Fan. "Characterization of PCB Dielectric Properties Using Two Striplines on the Same Board." *Electromagnetic Compatibility, 2014 IEEE International Symposium on, Raleigh, NC, 4-8* Aug. 2014, pp. 809 – 814.

Bichen Chen, Xiaoning Ye, Bill Samaras,Jun Fan, "A novel de-embedding method suitable for transmission-line measurement," *IEEE Asia-Pacific Symposium on Electromagnetic Compatibility,* May 25-29, 2015

Chunyu Wu, Bichen Chen, Tsiklauri Mikheil, Xiaoning Ye, Jun Fan., "Error bounds analysis of de-embedded results in 2x Thru de-embedding methods" in *Electromagnetic Compatibility (EMC),* 2017 *IEEE International Symposium.*

SECTION

2. CONCLUSIONS

This dissertation presented the 2XTD, 1XRD, and Thru-Line De-embedding method (TLD) by deriving the algorithm in a more straightforward way. The reported derivation combined the ideas from both TRL and 1-port SOL under the assumption of symmetric fixtures design. The algorithms are verified through simulations and measurements. Compare with the traditional TRL methods, the TLD method presented here reduced calibration patterns to a zero-length Thru standard and a non-zero-length Line standard. Meanwhile, by assuming known behavior of the insertion loss curve of the transmission line, the TLD method also provides useful bandwidth prediction of final de-embedded results as well as quality checks of fixtures design.

VITA

Bichen Chen, was born in Nanjing, Jiangsu Province, P.R. China. In May 2009, he received his Bachelor of Science, Electrical Engineering in Southeast University, P.R. China. Shortly after his graduation from Southeast, he started to pursuit of his M.S degree in the Electrical Engineering at Tandon School of New York University.

In May 2013, he enrolled at the Missouri University of Science and Technology to pursue his Ph.D degree in Electrical Engineering at the Electromagnetic Compatibility (EMC) Laboratory. His research interests included signal integrity in high speed digital systems, power distributed network modeling, RF interference and high-speed package modeling. In July 2019, he received his Ph.D degree in Electrical Engineering from Missouri University of Science and Technology.

Bichen joined Facebook, Inc., as a network hardware engineer after the completion of his Ph.D degree.